SafeG

(Project Number: 945 041)
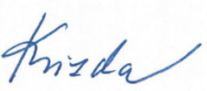
DELIVERABLE D5.4

Results of the thermal-hydraulics benchmark

Lead Beneficiary: VUJE, a.s.

Due date: 31/01/2024　　　　　　　　　　　　　　　Released on: 30/04/2024

Authors:	Boris Kvizda, Miriama Lacková, Tomáš Melichar, Zalán Csekei, Bendegúz Kopp, Jan Pokorný, Daniel Kříž, Tamás Varju, Gergely Imre Orosz, Martin Kratochvíl, Chandae Jeong, Miroslav Gleitz, Štěpán Hrouda, Ján Remiš, Jan Komrska

For the Lead Beneficiary	Reviewed by Work package Leader	Approved by Coordinator
Boris Kvizda	**Eugene Shwageraus**	**Boris Kvizda**

Start date of project:　　　　**01/10/2020**　　　　　　Duration: **48 Months**
Project Coordinator:　　　　　**Boris Kvizda**
Project Coordinator Organisation:　**VUJE, a. s.**　　　　VERSION: 1.1

Version control table

Version number	Date of issue	Author(s)	Brief description of changes made
0.1	22/04/2024	Boris Kvizda, Miriama Lacková, Tomáš Melichar, Zalán Csekei, Bendegúz Kopp, Jan Pokorný, Daniel Kříž	1st Draft
1.0	25/04/2024	Boris Kvizda, Tamás Varju, Bendegúz Kopp	Revision of 1st draft based on the comments from all authors.
1.1	30/04/2024	Slavomír Bebjak Michaela Velčková	Revision by MST Final version

Project information

Project full title:	Safety of GFR through innovative materials, technologies and processes
Acronym:	SafeG
Funding scheme:	Research and innovation action
ECGA number:	945041
Programme and call	Horizon 2020 Framework Programme for Research and Innovation (2014-2020) NFRP-2019-2020 (Nuclear Fission and Radiation Protection Research)
Coordinator:	Boris Kvizda
EC Project Officer:	Cristina Fernandez Ramos
Start date – End date:	01/10/20 – 30/09/2024 i.e. 48 months
Coordinator contact:	+421 33 599 1172, boris.kvizda@vuje.sk
Administrative contact:	+420 602 771 784, jakub.heller@evalion.cz
Online contacts (website):	www.safeg.eu

Copyright

EXECUTIVE SUMMARY

A thermal-hydraulic modelling benchmark is organized within the SafeG project. The whole activity was divided into two separate parts the TH system code benchmark and the CFD benchmark. The benchmarks were described in the previous deliverable D5.3 – Definition of the thermal-hydraulic benchmark. In this document, results of both benchmark are presented and evaluated.

This document is prepared in compliance with the template provided by the Commission in Annex 1 of the Guidelines on Data Management in Horizon 2020.

CONTENT

LIST OF TABLES

LIST OF FIGURES

LIST OF ACRONYMS AND ABBREVIATIONS

ACC	-Accumulator tank
APROS	Finish TH system code developed Fortum and VTT
ASME	American Society of Mechanical Engineers
BME	Budapest University of Technology and Economics
CATHARE2	French TH system code developed by CEA
CEA	The French Alternative Energies and Atomic Energy Commission
CFD	Computational fluid dynamics
CTU	Czech Technical University in Prague
CVR	Research Centre Řež (Czech Republic)
DAE	Differential Algebraic Equations
DHR	Decay Heat Removal
DYMOLA	Dynamic Modeling Laboratory
EC	European Commision
GA	Grant Agreement
EK	Centre for Energy Research in Hungary
ESFAS	Engineered Safety Features Actuation System
FFTBM	Fast Fourier Transformation Based Method
FSA	Finite State Automata
GA	Grant Agreement
GFR	Gas Fast Reactor
GUI	Graphical User Interface
HS	Heat Structure
HTC	Heat transfer coefficient
HTS	Heat exchanger tubeside
HX	Heat Exchanger
I.C.	Primary circuit
II.C	Secondary circuit
III.C	Tertiary circuit
ID	Internal diameter
ITF	Integral Test Facility
LOCA	Loss Of Coolant Accident
LWR	Light Water Reactor
OD	Outer diameter
ODE	Ordinary Differential Equations
PHX	Primary Heat Exchanger
PIV	Particle Image Velocimetry
R&D	Research and Development
RPV	Reactor Pressure Vessel
RTS	Reactor Trip System
RV	Reactor Vessel
SG	Steam generator
SHX	Secondary Heat Exchanger
SS	Steady State
TH	Thermal Hydraulic
TR	Transient
UJV	Ústav Jaderného Výzkumu (UJV) Řež
UNIPI	University of Pisa
VTT	Technical Research Centre of Finland
WP	Work Package

1 THERMAL HYDRAULIC BENCHMARK

1.1 Introduction

In this document the work done within the SafeG project Work Package 5, Task 5.2 is summarized. It contains the comparison and assessment of the numerical results of the thermal hydraulic benchmark of S-Allegro experimental facility. The activity was focused on development of the brand new TH models using the computational tools utilized in the R&D of ALLEGRO Gas Fast Reactor demonstrator.

The purpose of the benchmark was primarily educational, but it is intended that the developed S-Allegro models will be further used in ALLEGRO related R&D activities. A number of young professionals have been involved in this activity increasing their modeling and computational skills.

The data for the benchmarking were obtained from existing Integral Test Facility (ITF) the S-Allegro is operated by CVR in Pilsen Czech Republic. Various computational tools have been used including APROS, RELAP5 and DYMOLA.

The benchmarking activity have been divided into following consecutive steps:

1. Collection of the relevant experimental data from the S-Allegro ITF.

2. Definition of the Thermal Hydraulic benchmark. It was published in D5.3 [5]   including design database of the key S-Allegro components (systems) and selected experimental data.

3. Development of the S-Allegro TH models.

4. The TH benchmark exercise:

   - **Phase I:** The validation and verification of the models of key S-Allegro components. Specifically the Primary Heat Exchanger (PHX) and the Secondary Heat Exchanger (SHX). The four steady states have been measured on S-Allegro ITF denominated as SS#1 to SS#4). The aim was to qualify the PHX and SHX models and to reduce large discrepancies among participants.

   - **Phase II:** The comparison of the steady state conditions SS_2306-01 and SS_2306-02. For this purpose two steady state conditions have been measured on S-Allegro denominated as SS_2306-01 and SS_2306-02. The SS_2306-01 was considered as open benchmark where all the data have been made available to all participants and the SS_2306-02 considered as semi-blind benchmark where only the boundary conditions have been released to the participants. The data have been collected during S-Allegro operation in June 2023. The facility was in the configuration with completely disconnected DHR loop, therefore only primary, secondary and tertiary loops were in operation.

   - **Phase III:** The simulation of two transients TR_2306-01 and TR_2306-02. The transient TR_2306-01 was launched from the initial conditions SS_2306-01. As the boundary condition the primary blower speed was reduced and the heating power dropped from 210kW to 99kW within 50 s. Later the heating power recovered back to 210kW. Similarly, the transient event TR_2306-02 was initiated from SS_2306-02 conditions. In this case the heating power was slowly increased by the automatic control system. Later it dropped to zero power and recovered. Since then the power was controlled automatically until the end of transient (10 000 s).

5. The results of the TH benchmark were compared with the measurement and have been evaluated from qualitative and quantitative point of view.

1.2 S-Allegro demonstrator

In this chapter a short description of S-Allegro Integral Test Facility (ITF) is given. More comprehensive description of the ITF is published in the D5.3 [5] .

S-Allegro is a large scale experimental facility operated by CVR in Pilsen, Czech Republic. The purpose of the facility is to support the development of the GFR demonstrator ALLEGRO. For this reason, S-Allegro is designed as an electrically heated full pressure scale down model of ALLEGRO demonstrator. Therefore the layout of the main loops and the key components (including main heat exchanger, secondary-to-tertiary heat exchanger, DHR system and main blowers in primary and secondary loops) are similar to what is expected in the design of ALLEGRO GFR demonstrator.

The S-Allegro is design for investigation of operational states and transient processes of ALLEGRO GFR demonstrator e.g. core power transients, blower trips, small and medium LOCAs, transition sequences to DHR, gas injection in post LOCA situations etc. Another very important goal of S-Allegro is to test GFR specific systems and components like blowers, isolation devices, heat exchangers, GFR specific instrumentation and heat removal strategies (DHR) in accident situations.

Further purpose of ITF is production of data for the validation of thermal hydraulic models and codes and CFD models. The layout of the facility is shown in Figure 1-1.

It is composed of the primary helium circuit (I.C) with the reactor vessel (RV), secondary helium circuit (II.C), tertiary water circuit (III.C) and DHR circuit that is also connected to the RV.
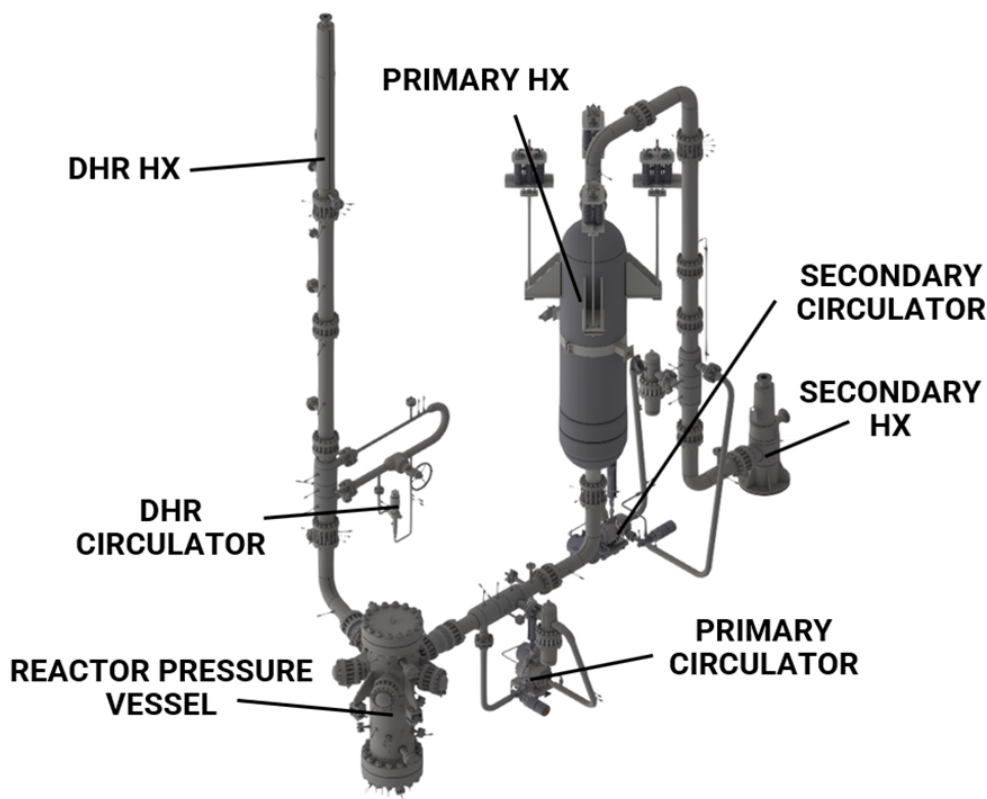
Figure 1-1: S-Allegro facility general layout.

The S-Allegro power (1.05 MW) is scaled down by ratio 1/75 and it is a full pressure device. Nominal design parameters are summarized in Table 1-1. It is worth to say that in this stage of the ALLEGRO project the design parameters have not been reached in S-Allegro ITF. The values represents design values.

Table 1-1: Nominal design parameters

Sensor	Parameter	Value	Unit
T132	He temperature – outer leg I.C – PHX outlet	445	°C
T131	He temperature – outer leg I.C	450	°C
T900	He temperature – inner leg I.C – RV outlet	850	°C
F101	He mass-flow rate – inner leg I.C (differential pressure Torbar)	0.5	kg/s
P101	He pressure – inner leg I.C (Cerabar S PMP71)	7	MPa
T633	He temperature – outer leg II.C – PHX inlet	360	°C
T631	He temperature – outer leg II.C – SHX outlet	365	°C
T601	He temperature – inner leg II.C – PHX outlet (differential pressure Torbar)	820	°C
F601	He mass-flow rate – inner leg II.C (differential pressure Torbar)	0.445	kg/s
P604	He pressure in the P HX – II.C (Cerabar S PMP71)	6.5	MPa
POW	Heating power	1050	kW
P991	Water inlet pressure (Cerabar PMP11)	0.5	MPa
T991	Water inlet temperature (Pt100)	30	°C
T962	Water temperature – SHX outlet	45	°C
F952	Water flow rate in DHR HX (Promag 10L80)	17	kg/s

For this benchmark purpose, several sensors were selected that are relevant for the comparison with the experiments. The layout of the instrumentation is shown in Figure 1-3, the layout of the temperature sensors at the outlet of the heating core is in Figure 1-2. The list of benchmark relevant instrumentation sensors including accuracy is shown in Table 1-2.
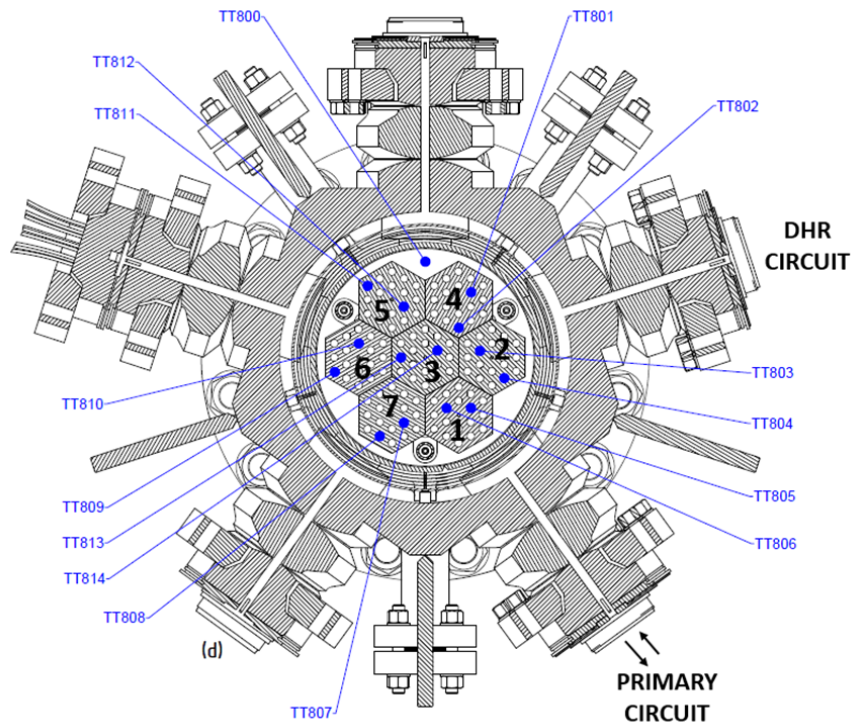
Figure 1-2: Temperature sensors at the outlet of the heating core
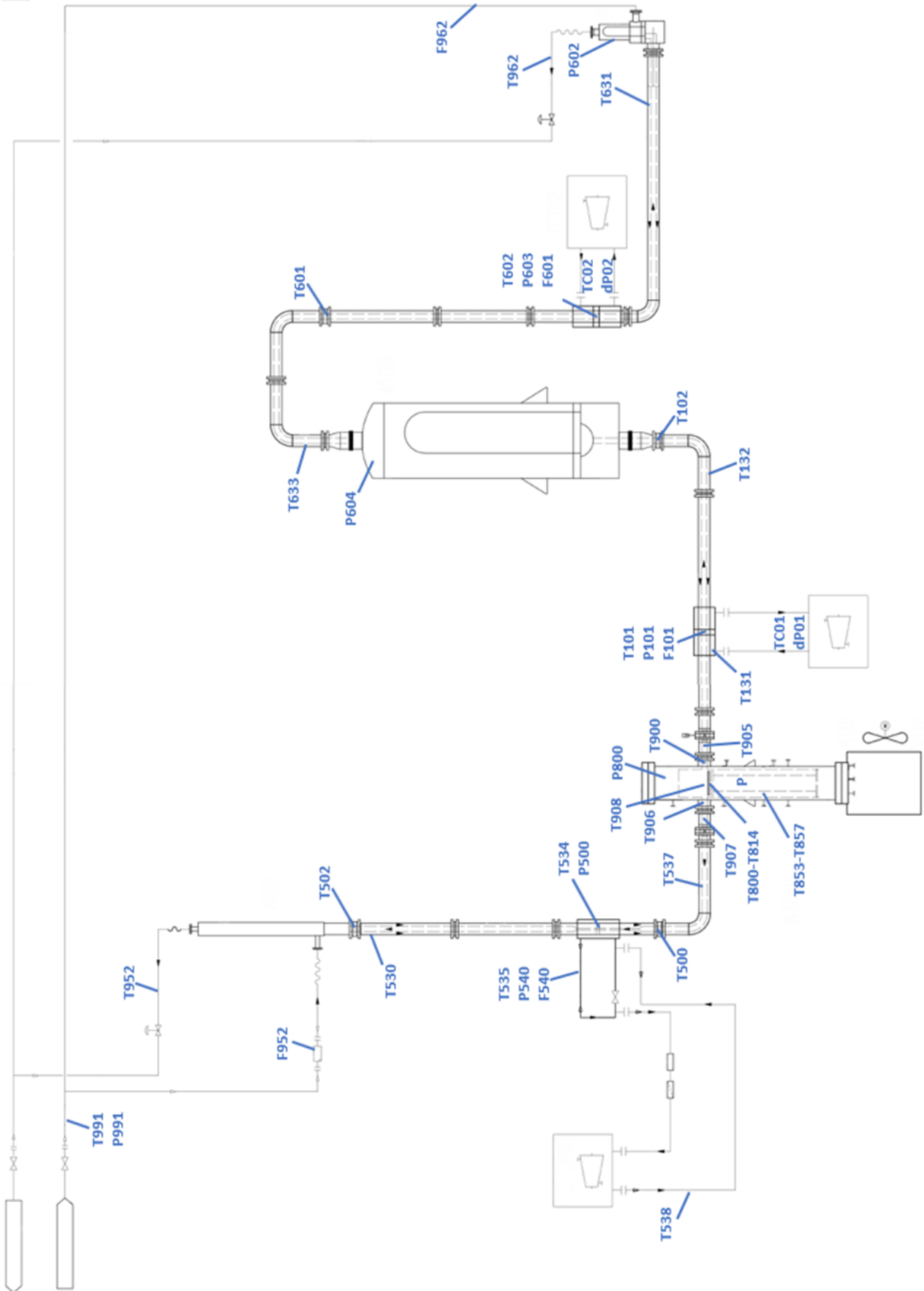
Figure 1-3: Instrumentation layout

Table 1-2: List of relevant S-Allegro instrumentation.

Sensor	Accuracy	Description
T101	0.4 % + 0.5 °C	He temperature – inner leg I.C
P101	0.25 %	He pressure – inner leg I.C (Cerabar S PMP71)
F101	2.5 % (total)	He mass-flow rate – inner leg I.C (differential pressure Torbar)
T131	0.4 % + 0.5 °C	He temperature – outer leg I.C
T132	0.4 % + 0.5 °C	He temperature – outer leg I.C – PHX outlet
T102	0.4 % + 0.5 °C	He temperature – inner leg I.C – PHX inlet
TC01	-	Primary blower speed
dP01	0.05 %	Primary blower PR (Deltabar S PMD 75)
T900	0.4 % + 0.5 °C	He temperature – inner leg I.C – RV outlet
T905	0.4 % + 0.5 °C	He temperature – inner leg I.C – RV outlet
T853-857	0.4 % + 0.5 °C	He temperature – RV downcomer (circumferentially)
T800-814	0.4 % + 0.5 °C	He temperature – outlet of the heating sections
T908	0.4 % + 0.5 °C	He temperature – above the hydraulic resistor
P800	0.25 %	He pressure in the RV - outer leg (Cerabar S PMP71)
POW	0.5 %	Heating power
P604	0.25 %	He pressure in the PHX – II.C (Cerabar S PMP71)
T633	0.4 % + 0.5 °C	He temperature – outer leg II.C – PHX inlet
T601	0.4 % + 0.5 °C	He temperature – inner leg II.C – PHX outlet (differential pressure Torbar)
T602	0.4 % + 0.5 °C	He temperature – inner leg II.C
P603	0.25 %	He pressure – inner leg II.C (Cerabar S PMP71)
F601	2.5 % (total)	He mass-flow rate – inner leg II.C (differential pressure Torbar)
TC02	-	Secondary blower speed
dP02	0.05 %	Secondary blower PR (Deltabar S PMD 75)
T631	0.4 % + 0.5 °C	He temperature – outer leg II.C – SHX outlet
P602	0.25 %	He pressure – SHX (Cerabar S PMP71)
T962	0.4 % + 0.5 °C	Water temperature – SHX outlet
F962		Water flow rate in SHX (Promag 10L80)
T906	0.4 % + 0.5 °C	He temperature – inner leg DHR – RV outlet
T907	0.4 % + 0.5 °C	He temperature – inner leg DHR – RV outlet
T537	0.4 % + 0.5 °C	He temperature – outer leg DHR
T500	0.4 % + 0.5 °C	He temperature – inner leg DHR
T534	0.4 % + 0.5 °C	He temperature – inner leg DHR
P500	0.25 %	He pressure – inner leg DHR (Cerabar S PMP71)
T535	0.4 % + 0.5 °C	He temperature – outer leg DHR – DHR blower
P540	0.25 %	He pressure – outer leg DHR – DHR blower (Cerabar S PMP71)
F540	2.5 % (total)	He mass-flow rate – outer leg DHR – DHR blower (differential pressure Deltatop)
T538	0.4 % + 0.5 °C	He temperature – outer leg DHR – DHR blower outlet
T530	0.4 % + 0.5 °C	He temperature – outer leg DHR – DHR HX outlet
T502	0.4 % + 0.5 °C	He temperature – inner leg DHR – DHR HX inlet
T952	0.13 °C	Water temperature – inner leg DHR – DHR HX outlet (Pt100)
F952	0.5 %	Water flow rate in DHR HX (Promag 10L80)
T991	0.13 °C	Water inlet temperature (Pt100)
P991	0.25 %	Water inlet pressure (Cerabar PMP11)

1.3 DEFINITION OF TH BENCHMARK

This section contains the data measured on S-Allegro ITF for the code to ITF benchmarking activities. There have been three groups of measured S-Allegro data used for the benchmarking activities described in this chapter.

1.3.1 Steady state data on the primary (PHX) and secondary (SHX) heat exchangers

The data were collected during the startup tests of S-Allegro ITF. As the PHX and SHX components are the most complex ones in S-Allegro ITF there have been four steady states measured (SS#1-4) aiming to qualify the PHX and SHX TH models. The data can be seen in the following table.

Table 1-3: Data for the PHX and SHX benchmarking

Sensor	Unit	SS#1	SS#2	SS#3	SS#4
T101	°C	145.4	133.1	169.9	280.3
T102	°C	141.8	129.6	164.9	273.3
P101	MPa	3.11	3.04	3.25	3.58
F101	kg/s	0.223	0.247	0.222	0.245
T132	°C	79.0	57.2	63.9	141.1
F601	kg/s	0.197	0.497	0.499	0.192
P604	MPa	3.14	3.0	3.05	3.71
T601	°C	44.1	48.6	53.4	69.5
T633	°C	117.9	84.2	99.8	230.9
T602	°C	117.1	82.3	101.4	223.2
T631	°C	40.4	45.2	50.1	60.4
F962	kg/s	2.79	2.76	2.8	3.61
P991	MPa	0.58	0.57	0.57	0.56
T962	°C	27.0	31.3	32.5	32.3
T991	°C	20.4	22.7	21.8	21.6

1.3.2 Steady state data for open benchmark (SS_2306-01) and semi-blind benchmark (SS_2306-02)

The data have been collected during S-Allegro operation in June 2023. The facility was in the configuration with completely disconnected DHR loop, therefore only primary, secondary and tertiary loops were in operation. Two steady-state conditions were selected for this activity. The first SS_2306-01 (Table 1-4) is presented as open and all the relevant measured values have been provided to the benchmark participants. These data were also used to qualify the computational models. The second steady-state SS_2306-02 (Table 1-5) is partially blind and only selected values have been provided to the participants.

Table 1-4: Open benchmark measured data (SS_2306-01)

Sensor	Value	Unit
T101	361.3	°C
P101	52.631	bar
F101	0.25	kg/s
T131	166.5	°C
T132	159.2	°C
T102	352.1	°C
TC01	25288	rpm
dP01	18.1	kPa
T900	370.1	°C
T905	367.3	°C
T853-857	169.5 170.2 169.2 170.3 171.2	°C
T908	361.3	°C
POW	249.6	kW
T633	96.3	°C
T601	281.4	°C
T602	274.3	°C
P603	39.958	bar
F601	0.25	kg/s
TC02	23216	rpm
dP02	9.83	kPa
T631	80.9	°C
T962	42.2	°C
F962	10.0	m³/hod
T991	20.7	°C
P991	4.94	bar

Table 1-5: Semi-blind benchmark measured data (SS_2306-02)

Sensor	Value	Unit
T101	226.1	°C
*)P101	44.801	bar
*)F101	0.25	kg/s
T131	107.3	°C
T132	102.2	°C
T102	220.7	°C
*)TC01	26759	rpm
*)dP01	21.5 kPa	kPa
T900	230.6	°C
T905	229.2	°C
T853-857	106.7 108.3 106.4 108.4 108.8	°C
T908	222.0	°C
*)POW	151.6	kW
T633	66.9	°C
T601	177.8	°C
T602	178.2	°C
*)P603	34.992	bar
*)F601	0.25	kg/s
*)TC02	24027	rpm
*)dP02	10.5 kPa	kPa
T631	58.1	°C
T962	33.4	°C
*)F962	10.0	m³/hod
*)T991	20.7	°C
*)P991	4.89	bar

*) Provided to all participants

1.3.3 The transient data for the open benchmark (TR_2306-01) and blind benchmark (TR_2306-02)

The TR_2306-01 was initiated from the SS_2306-01 initial conditions. The participants have taken the SS_2306-01 and two time-dependent values of heating power (POW) and primary blower speed (TC01) as the boundary conditions of the open benchmark simulation. The time dependence of the POW and TC01 parameters are depicted in the Figure 1-4 and Figure 1-5 respectively.

Other boundary conditions corresponding to the speed of secondary blower (TC02), tertiary feed water flowrate (F962) and feed water temperature (T991) can be considered constant during the whole transient.
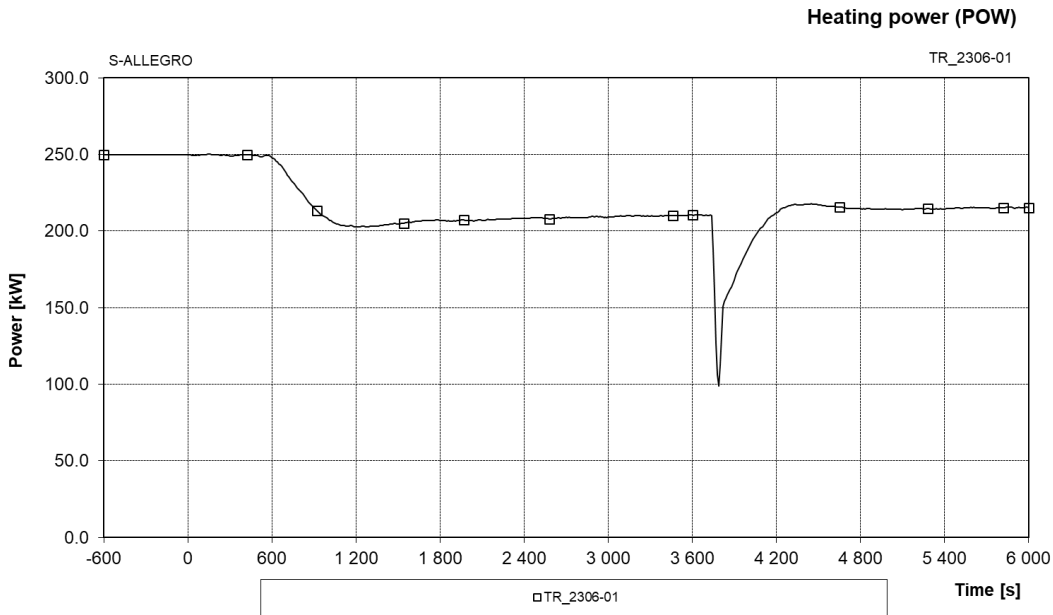
Heating power (POW)

Figure 1-4: Heating power (POW) – TR_2306-01

Primary blower speed (TC01)
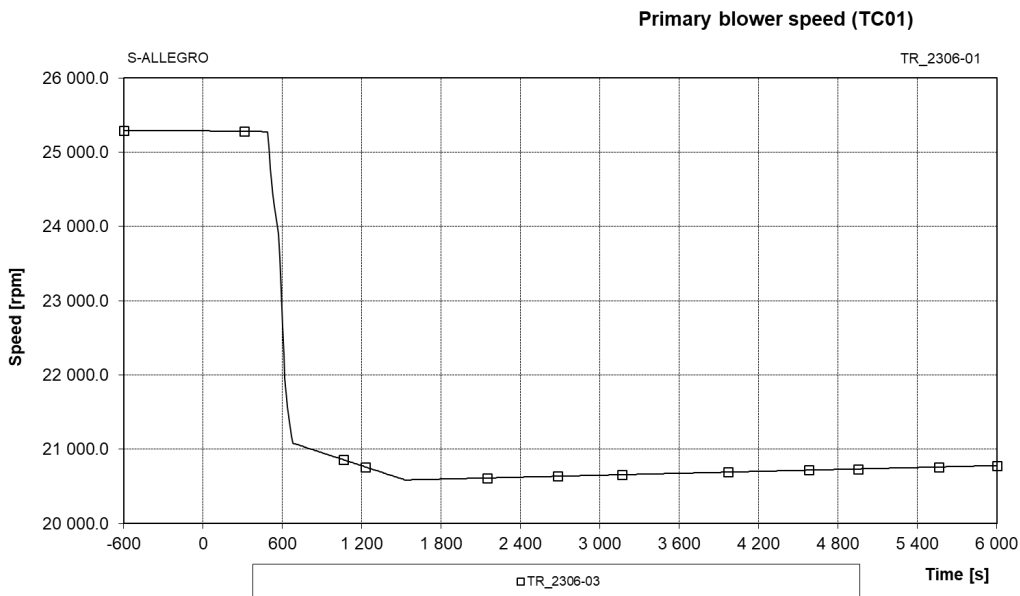
Figure 1-5: Primary blower speed (TC01) – TR_2306-01

At 460 s, the primary blower speed was reduced, resulting in mass-flow rate drop from 0.25 kg/s to 0.2 kg/s in approximately 310 s. The second event was initiated in time 3740 s, when heating power dropped from 210 kW to 99 kW (non-intentionally) within 50 s and then recovered to 210 kW.

The transient TR_2306-02 was initiated from the SS_2306-02 conditions. The participants have taken the SS_2306-02 and time-dependent value of heating power (POW) as the boundary conditions of the blind benchmark simulation. The time dependence of the POW parameter is depicted in the Figure 1-6. Other boundary conditions corresponding to the speed of primary blower (TC01), the secondary blower (TC02), tertiary feed water flowrate (F962) and feed water temperature (T991) can be considered constant during the whole transient.

The heating power was slowly increased by the automatic control system between 370 s to 2880 s. At 2880 s, heating power sharply dropped to zero then increased again and further controled automatically. The duration of the whole transient is 10000 s.
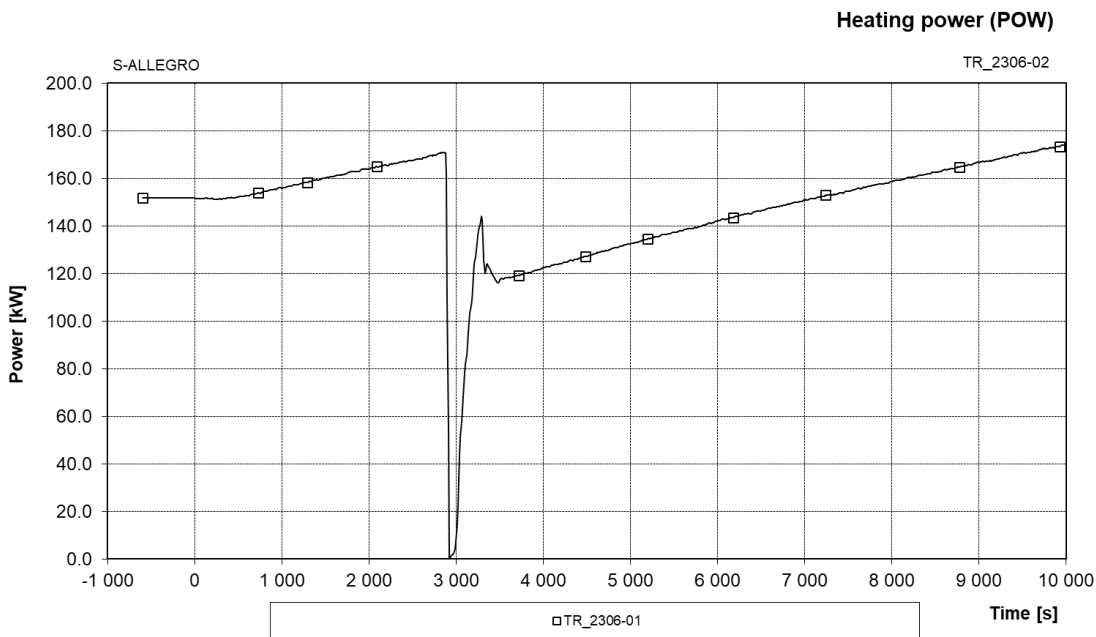
Figure 1-6: Heating power (POW) – TR_2306-02

1.4 Method

In the S-Allegro benchmark the criteria of acceptability for the quality of the TH models are followed according to the qualification procedure developed in the University of Pisa [7] . The procedure is rather extensive and the portion of the work is beyond the scope of the SafeG man power allocated. Therefore, only fraction of the steps have been performed within this task.

1.4.1 Steady state evaluation

The basic idea was to compare steady state values of the relevant parameters calculated by the TH code with the corresponding measured values at S-Allegro ITF. The method, however, does not simply compares calculated values with corresponding measured values but in addition it specifies the criterion of acceptability defining the acceptable range of the evaluated calculated parameter.

The calculated error (°) is defined as the ratio between the reference (measured) and calculated value according to the following formula:

$$Error = \frac{|(reference\ value\ \pm\ accuracy) - calculated\ value|}{(reference\ value\ \pm\ accuracy)}$$

In other words the calculated "Error" also includes the accuracy (°°) of the measurement device (sensor) as the methodology can be used for nodalization qualification of experimental facilities too. The "accuracy" of the S-Allegro instrumentation sensors used for the calculation are listed in Table 1-2. In general the participants followed the criteria of acceptability (Table 1-6) for the selected key steady state parameters.

The comparison includes calculated Errors [%] with respect to the reference values and also the objective judgment indicating either:

- E-Excellent - calculated Error is within the range of acceptability,

- M-Minimal - calculated Error is outside the range of acceptability but the reason is well understood

- U-Unqualified - calculated Error is outside the range of acceptability but the reason is unknown or not understood.

Table 1-6: Criteria of acceptability for nodalization qualification.

	Quantity	Acceptable Error (°)	Accuracy (°°)
1	Primary circuit volume	1 %	-
2	Secondary circuit volume	2 %	-
3	Non-active structures heat transfer area (overall)	10 %	-
4	Active structures heat transfer area (overall)	0.1 %	-
5	Non-active structures heat transfer volume (overall)	14 %	-
6	Active structures heat transfer volume (overall)	0.2 %	-
7	Volume vs. height curve (i.e. "local" primary and secondary circuit volume)	10 %	-
8	Component relative elevation	0.01 m	-
9	Axial and radial power distribution	1 %	-
10	Flow area of components like valves, pumps, orifices	1 %	-
11	Generic flow area	10 %	-
(*)			
12	Primary circuit power balance	2 %	0.5 %
13	Secondary circuit power balance	2 %	0.5 %
14	Absolute pressure (PRZ, SG, ACC)	0.1 %	0.5 %
15	Fluid temperature	0.5 % (**)	0.5 %
16	Rod surface temperature	10 K	0.5 %
17	Pump (Blower) velocity	1 %	0.5 %
18	Heat losses	10 %	-
19	Local pressure drops	10 % (+)	0.5 %
20	Mass inventory in primary circuit	2 % (++)	-
21	Mass inventory in secondary circuit	5 % (++)	-
22	Flow rates (primary and secondary circuit)	2 %	1 %
23	Bypass mass flow rate (total)	10 %	1 %
24	Pressurizer level (collapsed)	0.05 m	1 %
25	Secondary side or down comer level	0.1 m (++)	1 %

Notes)

(*) With reference to each of the quantities below, following a one hundred seconds "transient-steady-state" calculation, the solution must be stable with an inherent drift < 1% / 100 s.

(**) And consistent with power error

(+) Of the difference between maximum and minimum pressure in the loop

(++) And consistent with other errors

1.4.2 On-transient evaluation

On transient evaluation was based on a visual observation and a subjective judgement of the results. There are obviously an analytical methods available to quantify accuracy of the TH models and simulations, such as Fast Fourier Transformation Based Method (FFTBM) but for the purpose of this study it was not used due to lack of resources as the whole exercise was focused mainly on the development of the models from scratch and to run steady state and on-transient simulations. In future activities we are planning to use a FFTBM to quantify accuracy of the simulations and to validate all the developed models for father code validation activities

and also for the similarity analyses between S-Allegro experiments and calculations of same scenarios by existing ALLEGRO models.

1.5 DESCRIPTION OF TH CODES

1.5.1 RELAP5 3D ver. 4.3.4

The RELAP5-3D code is a successor to the RELAP5/MOD3 code1.1-1 which was developed for the Nuclear Regulatory Commission. The RELAP5-3D [1] version contains several important enhancements over previous versions of the code. The most prominent attribute that distinguishes the RELAP5-3D code from the previous versions is the fully integrated, multi-dimensional thermal-hydraulic and kinetic modelling capability. This removes any restrictions on the applicability of the code to the full range of postulated reactor accidents. Enhancements include a new matrix solver for 3D problems, new thermodynamic properties of water, and improved time advancement for greater robustness. The component defines a one, two, or three - dimensional array of volumes and the internal junctions connecting them. The geometry can be either Cartesian (x, y, z) or cylindrical (r, θ, z). The multi-dimensional neutron kinetics model in RELAP5-3D is based on the NESTLE code, which solves the two or four group neutron diffusion equations in either Cartesian or hexagonal geometry using the Nodal Expansion Method and the non-linear iteration technique. The code improvements were validated, generally through comparisons with independent design calculations. A model of the power conversion unit of the GFR was developed and coupled to a reactor model to develop a complete model of the GFR system.

The object oriented architecture of the RELAP-3D code allows to organize various types of components into a complex representation of the TH systems. The code build-in models includes pumps, valves, pipes, active and passive thermal structures including modelling of nuclear fuel with point and kinetics, electrical heaters and tanks (including accumulators). Unlike the RELAP5/MOD3 the RELAP5-3D includes full set of the components and features devoted to the gas cooled system applications such as turbines and compressor models including joined turbomachinery modules. The code includes possibility to model circulation of various types of gases and fluids specific for the GFR such as helium, nitrogen, air and obviously water. The single gas can be defined as a main fluid. The specific fraction of gas can be defined in a specific component. This allows to model more than one gas in a system and allows to model e.g. nitrogen gas inside accumulator tank which is connected to primary system using helium as a main coolant. Moreover it allows mixing gasses of different types e.g. helium and nitrogen and to predict heat transfer and transport under mixed conditions.

The RELAP5-3D allows to model complex trees of logical signals through the system of control variables and trips which allows to manage e.g. actuation of ESFAS and RTS devices. This includes also the modelling and management of classical proportional and proportional-integration controllers.

The code includes also the models for determination of pressure losses for various pipe profiles with smooth or abrupt area change, chocking flow model, branch model, boron mixing and distribution, non-condensable gas transport.

1.5.2 APROS

APROS is a software package originally developed in the early 90's by the Finnish companies Fortum and VTT Technical Research Centre of Finland, with the main goal to simulate transient thermal-hydraulic phenomena in LWR reactors. However, during its 30-year development period, the software evolved into a full-scale modelling and simulation tool for a wide range of industrial processes. Today, APROS version 6.12 (which was used for the S-Allegro benchmark) is suitable for simulation of nuclear power plant transients with various coolant and moderator fluids, chemical reactions and neutronics processes. In addition to the thermal-hydraulic solver, the software also offers the possibility to model instrumentation and control (I&C) systems and electrical equipment.

There are multiple thermal-hydraulic solvers available in the current version of APROS. When building a model, the user may choose the most suitable solver depending on the types of fluids and the number of phases present. In the current benchmark exercise, the goal is to simulate pure Helium, therefore the 3-equation (homogeneous, single-phase) solver was chosen for the BME S-Allegro model. This version of the solver takes the conservation equations for mass, momentum, and energy in one-dimension, discretizes them using nodes (control volumes where state parameters are defined) and branches (defining the flow of mass, momentum and energy between two nodes), and solves them with an iterative process. Additionally, to modelling the flow of the fluid, 1D heat conduction in a solid body is also calculated by employing a similar structure of nodes and branches, allowing the simulation of thermal processes in pipe/tank walls. In order to close this system of equations, quantities like momentum and energy transfer between the fluid and solid bodies around the flow must be calculated. Due to the one-dimensional nature of the code, multi-dimensional phenomena necessary for these calculations (turbulence, boundary layer, heat transfer, or 2D/3D heat conduction) cannot be directly resolved, instead they have to be estimated, usually by empirical formulas [2] .

APROS - unlike most other TH system codes - has completely moved away from the practice of building and manipulating models using an input-deck. Instead, the users must use the graphical interface, where models can be configured on a visual diagram by adding and connecting graphical modules (pipes, tanks, compressors, reactors Etc.) from a predefined list. The user can also create and add so-called "custom user components" to this list in order to easily represent structures that repeat frequently within a model. When a module on the GUI is placed and configured, the underlying network of nodes and branches is automatically created.

Through the GUI, APROS offers a very high level of customizability for the user. All parameters of any components in the model can be monitored in real time during simulation, most of these parameters can even be changed. More importantly however, the user has the option to tune the empirical correlations defined in the code, or to define custom correlations, providing a great freedom when it comes modelling phenomena like hydraulic resistance, heat transfer, or phase changes. To further increase the customizability of the code, APROS has its own scripting language called SCL, which makes it possible to access and manipulate any model parameter (or even entire models and solver configuration options), both during model building and simulation.

1.5.3 DYMOLA

The thermo-hydraulic model of S-Allegro cycle is created in Dymola environment, originally designed in 1978 by Hilding Elmqvist for his PhD thesis. Since 2006, the software is being developed by Dassault Systémes. It is a Modelica based, universal tool for development of numerical models in a wide range of disciplines such as electrical engineering, mechanics, chemistry, energy engineering and others. It is possible to create custom components or whole libraries using Modelica language as same as there are a lot of third-party open-source or commercial libraries, which can be easily implemented. In CVR, the commercial library ClaRa+, developed by XRG Simulation GmbH is being used. The ClaRa+ library contains all the components needed for the pipes and fittings, heat transfer, working fluid transportation and more [11].

Modelica language is being developed since 1996 by Hilding Elmqvist and the Modelica Association, a non-profit organization with seat in Linköping, Sweden. Modelica is a freely available, object-oriented language for modelling of large, complex, and heterogeneous systems. It is suited for multi-domain modelling, for example, mechatronic models in robotics, automotive and aerospace applications involving mechanical, electrical, hydraulic control and state machine subsystems, process-oriented applications and generation and distribution of electric power. Models in Modelica are mathematically described by differential, algebraic and discrete equations. No particular variable needs to be solved for manually. A Modelica tool will have enough information to decide that automatically. Modelica is designed such that available, specialized algorithms can be utilized to enable efficient handling of large models having more than one hundred thousand equations. Modelica is suited and used for hardware-in-the-loop simulations and for embedded control systems. [12]

Dymola respectively Modelica allows to create models by coding as same as by graphical interface (GUI). There are several numerical solvers with constant, even with variable time step in Dymola, which allows solving ODE (Ordinary Differential Equations), DAE (Differential Algebraic Equations) or FSA (Finite State Automata) and more. It is also possible to use some models developed in other software or vice versa via FMI interface.

1.5.4 CATHARE2

The CATHARE thermohydraulics code was originally intended for modelling two-phase flows in PWR, PWR, BWR and BWR reactors, but its toolbox has been extended to include Generation IV power plant calculations.

Several modules for component assembly are available within the CATHARE code. The part of interest for us is the two-phase one-dimensional six-equation model. The mass, momentum and energy conservation equations are written for liquid and gas phase. In the case where non-condensable gases are present in the system, the system of equations can be extended with transport equations.

Equations 1.1 and 1.2 for the mass conservation terms

$$A\frac{\delta a\rho_G}{\delta t} + \frac{\delta Aa\rho_G V_G}{\delta Z} = A\Gamma \tag{1.1}$$

$$A\frac{\delta(1-a)\rho_L}{\delta t} + \frac{\delta A(1-a)\rho_L V_L}{\delta Z} = -A\Gamma \tag{1.2}$$

1.2 and 1.4 on the Navier-Stokes equations with momentum conservation terms

$$A\frac{\delta a\rho_G V_G}{\delta t} + \frac{\delta A\alpha\rho_G V_G}{\delta Z} + A\alpha\frac{\delta P}{\delta Z} = -\chi\tau_{WG} + A[I + \alpha\rho_G g] + f_G\frac{\delta A}{\delta Z} \tag{1.3}$$

$$A\frac{\delta(1-a)\rho_L V_L}{\delta t} + \frac{\delta A(1-\alpha)\rho_L V_L^2}{\delta Z} + A(1-\alpha)\frac{\delta P}{\delta Z}$$
$$= \chi\tau_{WL} + A[-I + (1-\alpha)\rho_L g] + f_L\frac{\delta A}{\delta Z} \tag{1.4}$$

1.5 and 1.6 are the energy conservation terms

$$A\frac{\delta\alpha\rho_G\left(h_G + \frac{1}{2}V_G^2\right)}{\delta t} - A\alpha\frac{\delta P}{\delta t} + \frac{\delta A\alpha\rho_G\left(h_G + \frac{1}{2}V_G^2\right)}{\delta Z} = A[Q_{GI} + a\rho_G V_G g] + \chi Q_{WG} \tag{1.5}$$

$$A\frac{\delta(1-\alpha)\rho_L\left(h_L + \frac{1}{2}V_L^2\right)}{\delta t} - A(1-\alpha)\frac{\delta P}{\delta t} + \frac{\delta A\alpha\rho_L\left(h_L + \frac{1}{2}V_L^2\right)}{\delta Z}$$
$$= A[Q_{LI} + (1-a)\rho_L V_L g] + \chi Q_{WL} \tag{1.6}$$

Since we are working with non-condensing flows in our model, we include a seventh equation in the system of equations.

$$A\frac{\delta a\rho_G X_I}{\delta t} + \frac{\delta Aa\rho_G X_I V_G}{\delta Z} = S_I \tag{1.7}$$

There are seven equations with seven unknown variables, which are $V_G, V_L, p, h_L, h_G, \alpha, X$. These values are loaded into the software and the code solves the upper equations, along with other coupling equations. For single-phase gas refrigerant, e.g. in ALLEGRO, it is possible to switch to a three-equation model to speed up the calculations.

GUITHARE is a visual design program using the CATHARE code. The operators and commands integrated in CATHARE are all included in this software, in a lighter, more user-friendly design. While CATHARE is a one-dimensional thermo-hydraulic code that calculates based on the X coordinate of the nodes and whose input can only be built by manual input, GUITHARE assigns a location coordinate to each element based on the way they are positioned on the work surface. This graphical information does not affect the calculation (it can be deleted from the input code), but it helps a lot in visual organization and understanding. By using this program, the time required to produce the input has been significantly reduced.

1.6 DESCRIPTION OF TH MODELS

1.6.1 RELAP5 3D

The S-Allegro model for RELAP5-3D code described in this chapter is based on design parameters [5] . The full nodalization scheme of S-Allegro RELAP5-3D model developed by VUJE including numbering of components is presented on Figure 1-13.

The system is composed of 3 separate circuits. The primary and secondary system with helium coolant, the tertiary circuit with water coolant.

The RELAP5-3D model contains all relevant components and systems as reactor vessel, primary heat exchanger and secondary heat exchanger, blowers and primary and secondary ducts. The DHR system is part of the model but for the purpose of the benchmark it was considered disconnected.

1.6.1.1 REACTOR PRESSURE VESSEL

The electrically heated core is composed of the 7 hexagonal assemblies, each consist of 18 mullite ceramic tubes with internal diameter of 20 mm and inside the tube the heating Kanthal wire is modelled.

The pressure vessel is modeled by 3channels – Core 50, Bypass 52 and Downcomer 18 (see Figure 1-7). The heat structures modelled inside the vessel are explained into details in the Table 1-7.

The model is based on the S-Allegro facility geometric data described in [5] . The detailed description of all the components is part of the Engineering handbook of S-Allegro RELAP5-3D model [6] .
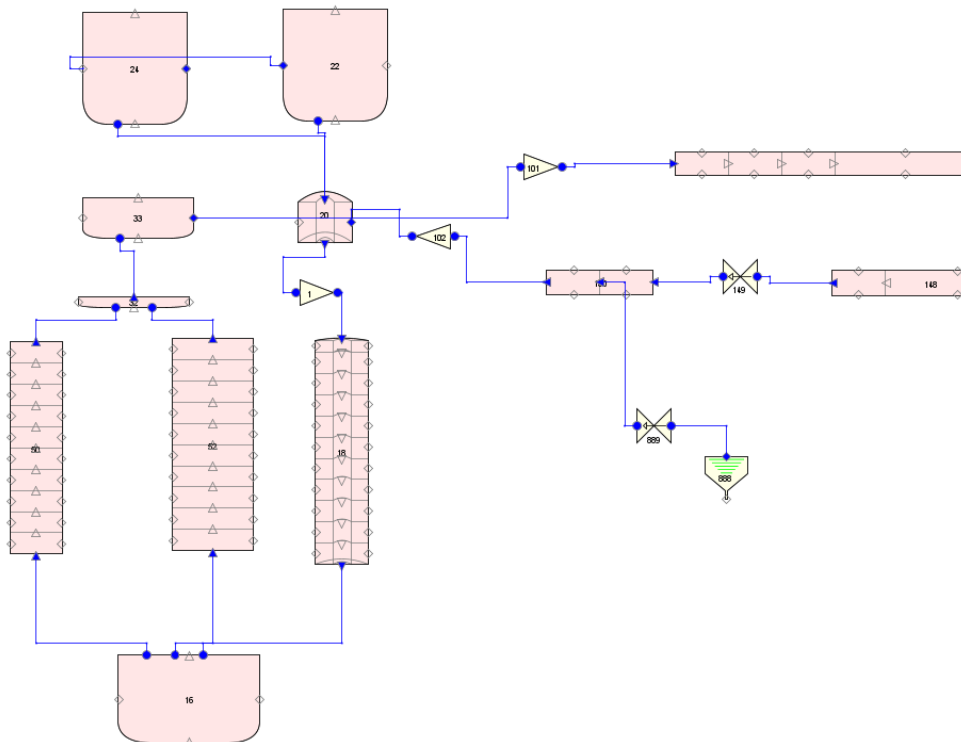
Figure 1-7: S-Allegro core nodalization (RELAP5-3D)

Table 1-7: Heat structures of S-Allegro core

Hydraulic components of S-Allegro core model			Heat structure		
Component	No.	Type			
Downcomer	18	Annulus	HS 310		HS 240 (52,32,33) -(18,20)
Downcomer inlet nozzle	20	Annulus			
CORE outlet	32	Branch			
CORE, outlet nozzle region	33	Branch			
Bypass	52	Pipe		HS 230	
CORE	50	Pipe	HS 210		
Lower plenum	16	Branch	HS 320		
RPV head	22	Branch	HS 311		
RPV head	24	Branch			

1.6.1.2 PRIMARY AND SECONDARY SYSTEM COMPRESSORS

The models of helium compressors in primary and secondary system have been elaborated based on the data published in [5]   . They are of the one-stage radial high speed design. Maximum operational flowrate is 0.5 kg/s. The design working point of primary compressor is defined in Table 1-8

The Primary blower is modelled by the *cprssr* component. The working point of the compressor is defined through rated rotation velocity (7958.7 rad/s), rated mass flow rate (0.5 kg/s), rated stagnation sonic speed (1609 m/s) and rated stagnation fluid density (4.54 kg/m3). The moment of inertia is not known and due to this the generic value of 2 kg/m2 was used. The compressor performance data were defined by the compressor maps seen in Figure 1-8. Calculation of the performance data for the working spectrum of rotation speeds have been done in VUJE based on non-dimensionless characteristics provided by the supplier (Table 1-10). The compressor maps are described in the form of 4 dimensional dependence among a) relative corrected non-dimensional mass flow, 2) pressure ratio, 3) compressor efficiency and 4) non-dimensional rotation speed.

Table 1-8: The nominal parameters of the primary blower

Primary compressor				
Inlet temperature	460	°C		
Inlet pressure	7	MPa		
Pressure rise	0.135	MPa		
Flowrate	1800	kg/h	0.5	kg/s
Rotation speed	76000	rpm	7958.7	rad/s
Adiabatic efficiency	69	%		
Torque	2	N.m		
Nominal flowrate	0.5	kg/s		

Correspondingly the secondary blower was modelled. The working point of the compressor is defined through rated rotation velocity (6911.5 rad/s), rated mass flow rate (0.5 kg/s), rated stagnation sonic speed (1503 m/s) and rated stagnation fluid density (4.84 kg/m3). The data are present in Table 1-9.

Table 1-9: The nominal parameters of the secondary blower

Secondary compressor				
Inlet temperature	364	°C		
Inlet pressure	6.5	MPa		
Pressure rise	0.135	MPa		
Flowrate	1800	kg/h	0.5	kg/s
Rotation speed	66000	rpm	6911.5	rad/s
Adiabatic efficiency	69	%		
Torque	2	N.m		
Nominal flowrate	0.5	kg/s		

Table 1-10: The nominal characteristics of primary and secondary compressor

Rotor diameter		63 mm			
Inlet pressure		**7 MPa**			
Inlet temperature		**460 °C**			
Speed		**70 000**	**Non-dimensional numbers**		
m [kg/s]	PR	P [W]	Φ	χ	Σ
0.2188	1.019	5657	0.026	0.552	0.485
0.2625	1.019	6762	0.032	0.550	0.483
0.3500	1.018	8657	0.042	0.528	0.464
0.4375	1.017	10059	0.053	0.491	0.431
0.5250	1.015	10669	0.063	0.434	0.381
0.6125	1.013	10433	0.074	0.364	0.319
0.7000	1.010	9041	0.084	0.276	0.242
0.7875	1.006	6435	0.095	0.174	0.153
0.8 For	1.002	2293	0.105	0.056	0.049

Nomenclature:

PR) Compressor pressure ratio

P) Compressor power

m) Mass flowrate
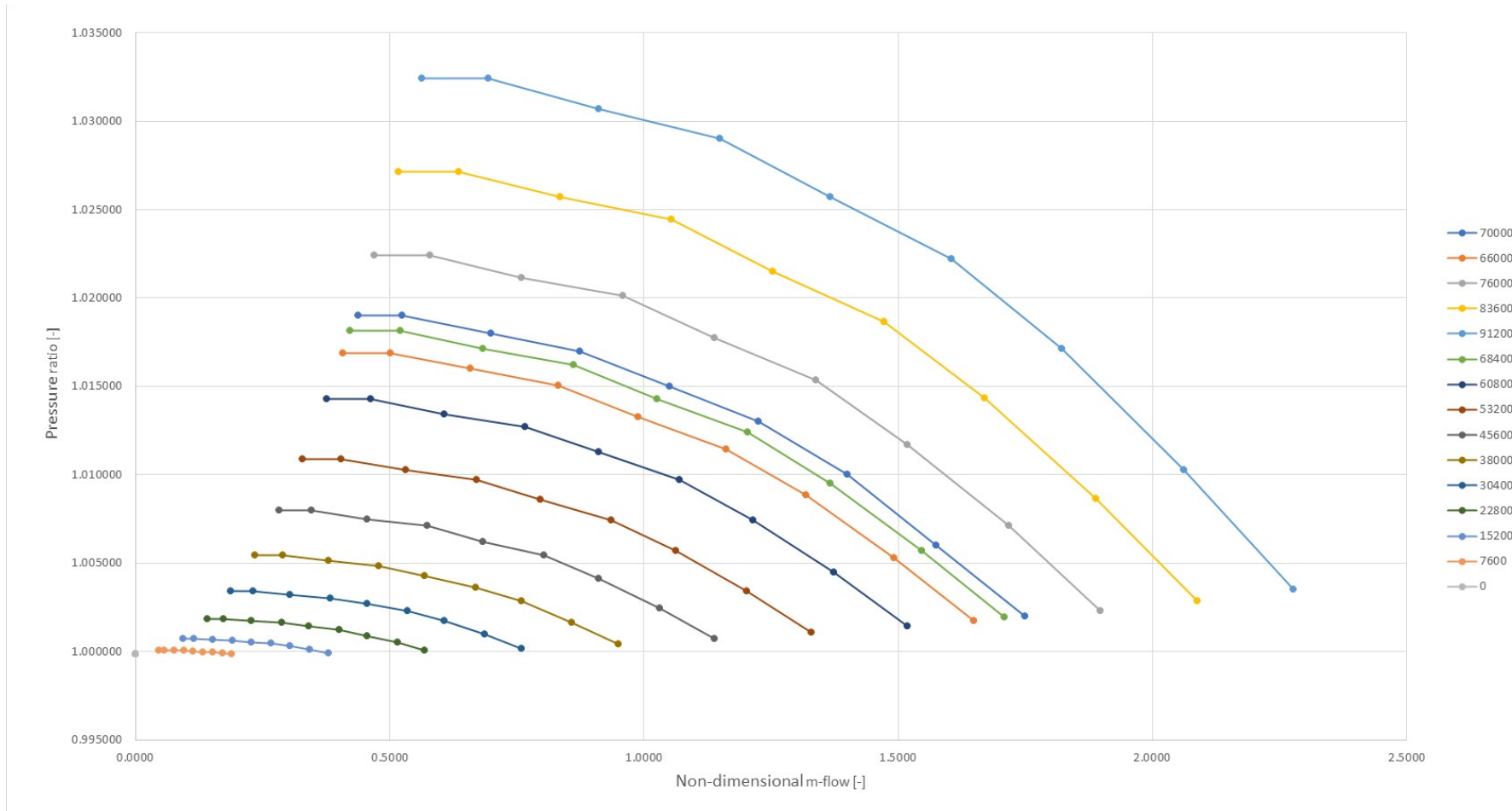
Figure 1-8: S-Allegro primary and secondary system compressor maps.

1.6.1.3 PRIMARY HEAT EXCHANGER

The primary heat exchanger (PHX) is a gas – gas (He – He) vertical U-tube HX with primary (hot) helium on the tube side and secondary He on the shell side. Main geometric parameters of the primary HX U-tubes are mentioned in following table. The nodalization scheme of the primary heat exchanger is shown on Figure 1-9.
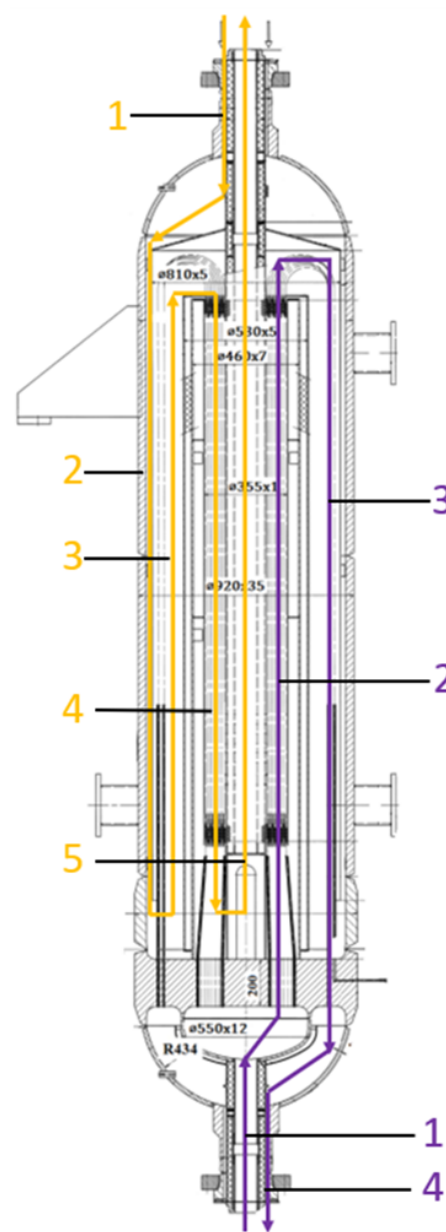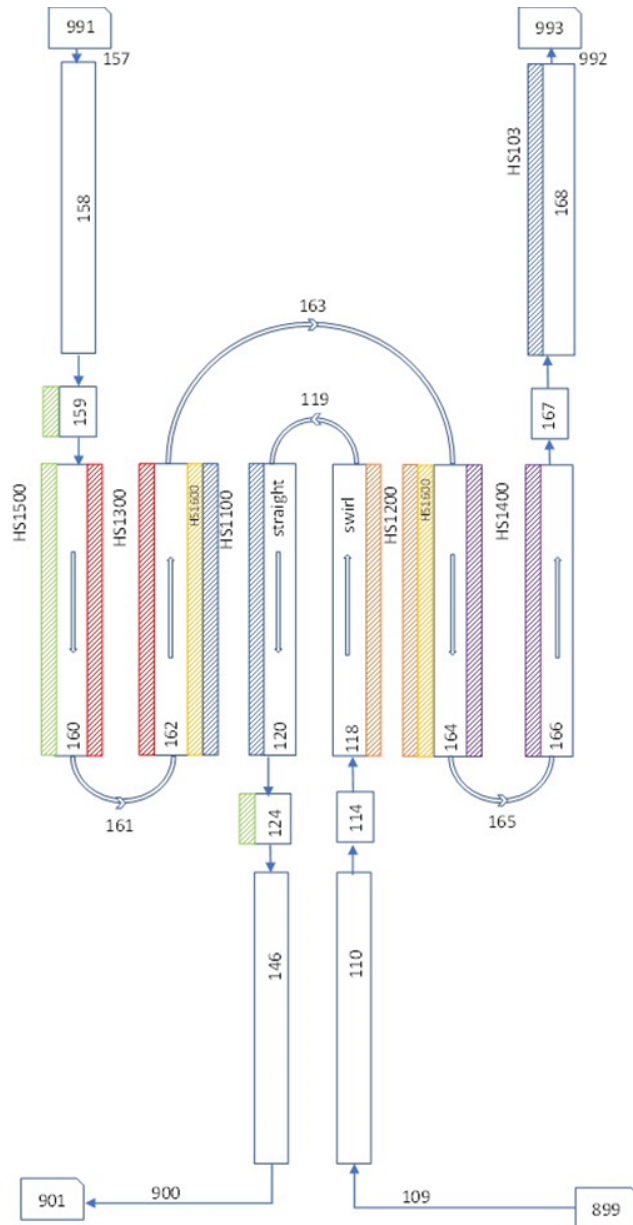
Figure 1-9: Primary Heat Exchanger nodalization (RELAP5-3D)

Figure 1-10: Primary Heat Exchanger flow paths

The detailed description of model components is part of the Engineering handbook of S-Allegro RELAP5-3D model [6]   . From the geometric point of view, the PHX is the most complex component. The large dimensions of the heat transfer area are given by relatively high convective heat transfer resistance at both sides (gas-gas HX). The primary helium flows in tube side, secondary helium flows in the shell side.

The RELAP5-3D model of PHX is presented in Figure 1-9 and the design flow paths are depicted in the Figure 1-10. The description of the primary and secondary sides of PHX are presented in more detail bellow.

PRIMARY SIDE OF PHX

The primary hot helium enters from the bottom through the inner leg of the coaxial pipe (1 - purple in Figure 1-10= component 114 – PHX inlet chamber see Figure 1-9) and flows through the swirl tube sheet on tube side (2 - purple in Figure 1-10 = pipe 118 – PHX up comer - swirl tubes see Figure 1-9). In the top part the tubes turn 180° degrees and are guided downwards through the outer annular volume (3 - purple in Figure 1-10 = pipe 120- PHX down comer – straight tubes see Figure 1-9). The heat transfer and pressure loss in this part is low as the tubes are straight and low velocity flow is reached in the shell side. Helium exits the component through the outer leg of the coaxial pipe (4 - purple in Figure 1-10 = component 124 – PHX outlet chamber see Figure 1-9).

SECONDARY SIDE OF PHX

The secondary cold helium enters the shell side through the outer leg of the secondary cold duct (1 - orange in Figure 1-10 = component 159 – PHX secondary inlet chamber see Figure 1-9). It flows downwards through the outer down comer (2 – orange in Figure 1-10 = pipe 160 - PHX secondary inlet down comer see Figure 1-9) and then turn 180°degrees and flows upwards through the up comer channel (3 – orange, thermally coupled with the primary flow path number 3 purple in Figure 1-10 = pipe 162 – PHX secondary up comer see Figure 1-9). The flow path 4 – orange corresponds to the main heat transfer volume, which is thermally coupled with primary flow path number 2 – purple (this corresponds to pipe 164 – PHX secondary down comer see Figure 1-9). Secondary helium leaves the PHX through the central up comer (5 – orange in Figure 1-10) into the inner leg of secondary duct.

The heat structures in S-Allegro PHX model were considered between straight primary tubes and secondary up comer annulus and between swirl primary tubes and secondary down comer annulus. The heat transfer between internal HX structures, HX shell and ambient was also modeled. The heat structures considered in PHX S-Allegro model are listed in the following table.

Table 1-11: Heat structures in PHX model of S-Allegro

PHX Heat structure number	Component number related to HS	Note
HS 1100	120-162	Straight U-tubes
HS 1200	118-164	Swirl U-tubes
HS 1300	162-160	Tube – down comer
HS 1400	164-166	Tube – up comer
HS 1500	160	Heat exchanger external shell

| HS 1600 | 162-164 | Promalight insulation and Static Helium (between up-comer and down-comer) |
| HS 1700 | 159-167 | Promalight insulation |

1.6.1.4 SECONDARY HEAT EXCHANGER

The secondary heat exchanger transfers heat from the secondary helium (tube side) to the tertiary water circuit (shell side). The nodalization of the SHX is described in Figure 1-11.
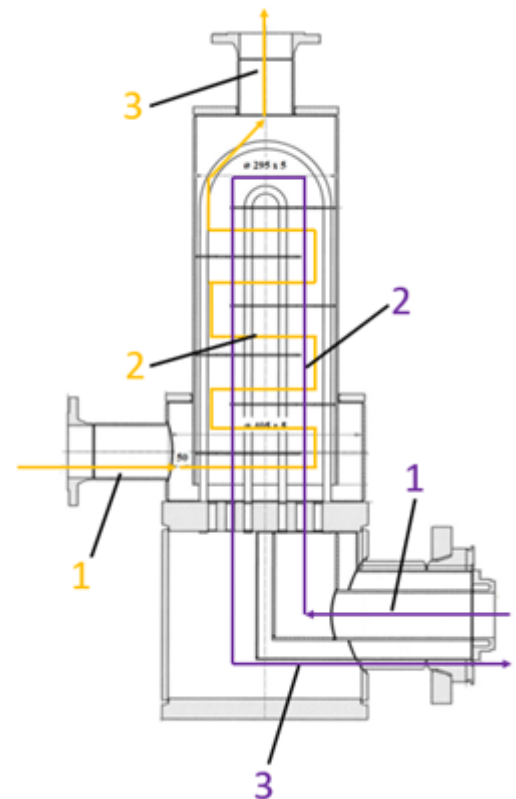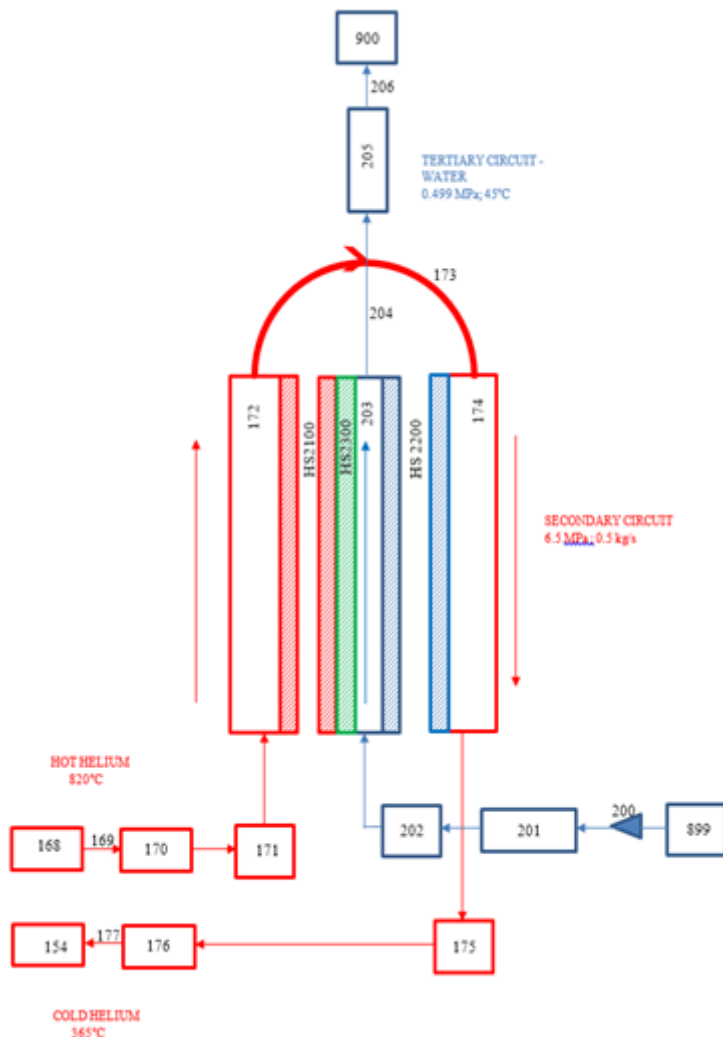
Figure 1-11: Secondary Heat Exchanger nodalization (RELAP5-3D)   **Figure 1-12: Flow route in the SHX**

The detailed description of model components is part of the Engineering handbook of S-Allegro RELAP5-3D model [6]   . The secondary heat exchanger transfers heat from the secondary helium (tube side) to the tertiary water circuit (shell side). Although both the primary and secondary HX are designed to the nominal power of 1.05MW, dimensions of the secondary HX are smaller due to better heat transfer at the water side.

The flow paths in the model are described on Figure 1-11 and correspondingly in the Figure 1-12. The helium enters SHX (tube side) through the inner leg (component 170; purple line 1). It then continues to the SHX inlet chamber (component 171; purple line 1). From the inlet SHX chamber the helium enters U-tube bundle upward (component 172; purple line 2) and downward (component 174; purple line 2). The SHX up-comer (component 171) and down comer (component 174) are connected through the heat structures (hs 2100 and hs 2200) with

the shell side water volume (component 203; yellow line 2) modeling the heat exchange between the secondary and tertiary system. The helium leaves the SHX from the down comer U-tubes via outlet chamber and outlet coaxial pipe (component 175, 176; purple line 3). The U-tubes are modeled as the simple upward and downward pipe component with equivalent flow area, hydraulic diameter and keeping volume. The pressure losses in U-tubes are calculated in order to keep desired pressure difference.

The tertiary water flows from the bottom part of SHX to the top through upward volume which is divided by 6 horizontal baffles in order to increase heat transfer. In the S-Allegro model this part is modelled by simple pipe component no. 203 (yellow line 2). The baffles are not directly modelled but the flow area is adjusted to keep proper water velocity through SHX and the hydraulic diameter is adjusted to keep proper heat transfer from the tube side to the shell side of SHX. In this case, however, the shell side water volume cannot be kept and it is under estimated contributing to lover thermal inertia of the water coolant in tertiary side.
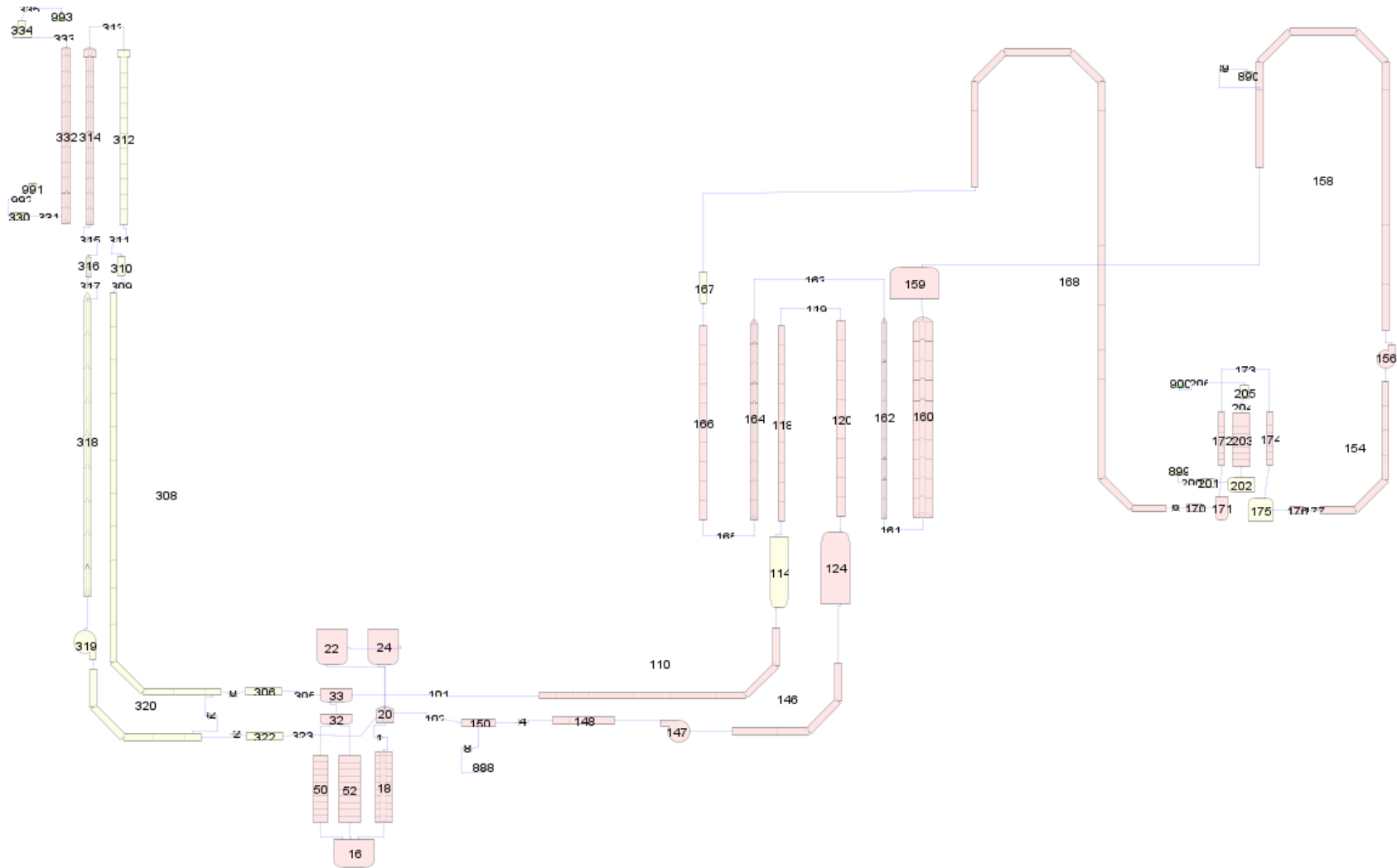
Figure 1-13: General S-Allegro RELAP5-3D model nodalization (RELAP5-3D)

1.6.2 APROS

The BME Apros model, developed for the S-Allegro benchmark exercise, contains the reactor vessel, primary and secondary heat exchangers, blowers, main valves and coaxial pipes of the facility. However, during the benchmark exercise, the DHR loops were disconnected, therefore no DHR model was built in the model so far. The model was created in version 6.12 of APROS, using the one-phase solver. In this version of the solver, Helium is defined as a perfect gas, and can be used in most hydraulic components of the software. The basic overlay of the model is shown in Figure 1-14.

Heat·losses¶

PHX¶

RV¶

Valves¶

SHX¶

Blowers¶
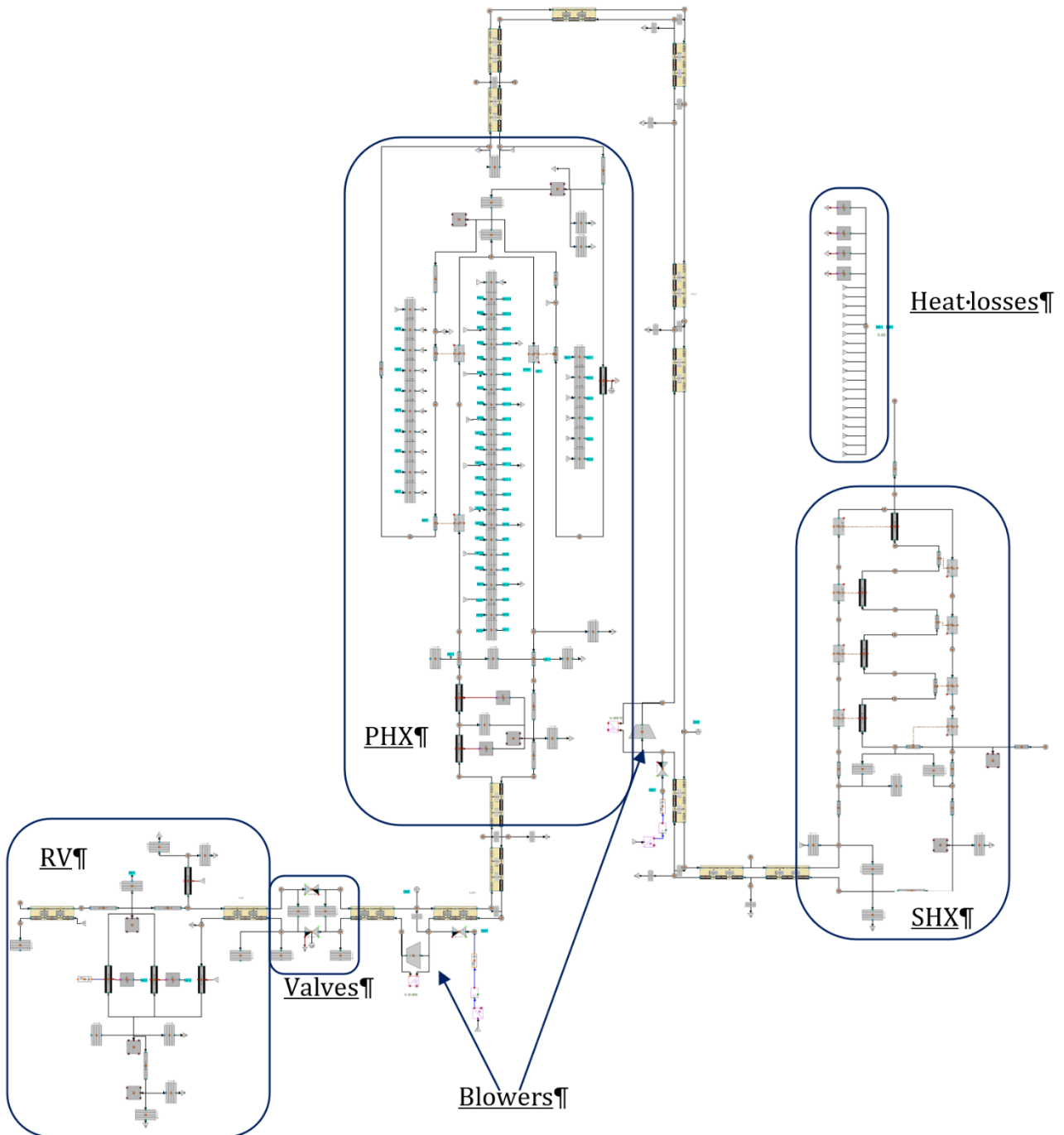
Figure 1-14: Overview of the S-Allegro (APROS)

1.6.2.1 PIPING NETWORK

The piping system of S-Allegro primary and secondary loops is of a coaxial design, where the high temperature fluid flows in the inner leg, while the colder fluid flows in the outer annular leg. There is a significant amount of insulation both between the inner and outer legs, and around the outer leg towards the environment. The piping consists of highly similar sections of this coaxial pipeline, with different lengths and hydraulic resistances. For this reason, we created a custom user component in APROS, that is capable of modelling a coaxial pipe with a wide range of geometrical parameters. The configuration of the user component contains most of the geometric data and material composition for the S-Allegro coaxial pipes, including the diameters, material properties and layer thicknesses of both legs. The only parameters that the user has to modify for each instance of the pipeline are the length, the inlet/outlet elevation, the nodalization, and the form loss coefficient.

Based on the experimental steady state data, it is very likely that the piping system of S-Allegro contains significant thermal bridges between the inner and outer legs, and to a lesser extent, between the outer leg and the environment. The most apparent consequence of this is that the heat flow between the inner and outer legs is greatly increased, leading to the fluid gradually cooling down as it flows in the inner legs, and heating up in the outer legs. To model the thermal bridges, we created extra heat structures in addition to the ones already included in the *Coax pipe* components, in which we postulated that the heat insulation layers are missing, and only the metal layers are present. This means that the heat transport through the heat bridges becomes very efficient, without adding a significant amount of excess heat capacity into the model. Regarding the heat bridges towards the environment, the effects are much less significant, therefore modelling them carries a lot more uncertainty. Nevertheless, we used the same approach, defining extra heat structures without the insulation layers. The lengths of the defined heat bridges can be seen in Table 1-12.

Table 1-12: The lengths of extra heat structures defined for heat bridge modelling

Location	Heat flow direction	Length [m]
main valves	inner leg to outer leg	0.23
primary blower	inner leg to outer leg	0.25
between primary blower and PHX	inner leg to outer leg	0.35
secondary pipe "B"	inner leg to outer leg	0.16
secondary pipe "C"	inner leg to outer leg	0.16
secondary pipe "D"	inner leg to outer leg	0.16
secondary pipe "E"	inner leg to outer leg	0.6
secondary pipe "F"	inner leg to outer leg	0.16
between primary blower and PHX	outer leg to environment	0.05
secondary pipe "C"	outer leg to environment	0.05
secondary pipe "D"	outer leg to environment	0.05
secondary pipe "E"	outer leg to environment	0.05
secondary pipe "F"	outer leg to environment	0.05

1.6.2.2 REACTOR VESSEL

The pressure vessel symbolizing the reactor is modelled in relatively simple terms. The vessel is located between two coaxial pipes, one coming from the main isolation valves, and one leading to the DHR. However, since the DHR loop was not connected during this benchmark exercise, this short pipe section is defined as a dead end. The RV downcomer is modelled with a heat pipe component, and there are two nodes representing the volume at the lower plenum. The heated section of the RV consists of two parallel channels, one for the flow inside the heated core, the other for the presumed bypass flow. We have set the hydraulic resistance of the bypass channel such that approx. 4% of the total flowrate goes through it in steady state conditions. Both channels are modelled with heat pipes, with heat transfer components connecting the outer surface of the main flow channel to the bypass flow, and likewise, the outer surface of the bypass channel is connected to the downcomer. The two parallel channels are joined together at the top of heated section, which is connected to two *Coax pipe* with branches. The free volume and heat capacity at the upper end of the RV are also accounted for using one more heat pipe.

We also modelled the Main valves next to the reactor vessel, using two basic valve components (one for inner and one for outer leg), and four heat structures in total. Two heat structures represent the heat bridge effects as presented in Table 1-12, and the other two heat structures model the remaining solid mass. The geometry of these additional structures is greatly simplified, they are defined as cylindrical rings with 72 mm inner diameter, 50 mm thickness (plus 2*50 mm of insulation), and 250 mm length each, resulting in a total mass of 240.7 kg.

1.6.2.3 PRIMARY HEAT EXCHANGER

The primary heat exchanger (PHX) is by-far the most complex part of the S-Allegro loop, and therefore it is the component we modelled in the most detailed fashion. The primary He flows twice through the tube bundles of the HX, while the secondary side He flows four times through the length of HX on the shell side. In addition to these hydraulic flow paths, we identified five distinct significant thermal phenomena that we modelled using various types of heat structures:

- Heat exchange between the primary and secondary fluids (the intended function of the HX).

- Thermal bridges at the bottom of the HX, leading to heat exchange between the primary inlet and outlet.

- Thermal bridges at the top of the HX, leading to heat exchange between the secondary inlet and outlet.

- Heat insulation layers on the secondary side, separating the increasing temperature secondary fluid from itself along the flow path.

- Outer heat insulation and losses to the environment.

The primary side inlet of the HX is a 389 mm long regular coaxial pipe, which can be modelled with the *Coax pipe* user component described above. The active part of the heat exchanger is separated to 3 parts: The first is the straight section at the bottom of the HX before the pipes are coiled, the second is the main coiled region, and the third is the straightened downcomer. All of these are modelled with *Heat exchanger tubeside* (HTS) components, which are dedicated APROS modules for providing heat transfer between a flow in thin-walled metal tube bundles and a pipe representing the shell side.

After the fluid returns from the downcomer, it goes through the thick bottom plate of the HX, and flows down on the outside in a shell around the primary inlet flow. This part of the outlet

flow is in thermal contact with the hot He coming into the HX, therefore the heat flow between the two fluids was modelled with additional heat structures.

The hydraulic flow path of the secondary side consists of four straight sections and four 180 degree turns. The straight sections are modelled with simple pipes, with the exception of the outermost downcomer part, where a *heat pipe* was used to account for the insulation and heat losses of the HX. Three *pipe* components represent the active part of the HX, each connected to the corresponding primary HTS components mentioned above. In order to stop heat from leaking between each secondary flow path, the walls between the adjacent up- and downcomer sections are insulated. To model the heat flow and heat capacity of these layers, we included heat structures between the calculation level nodes of the secondary pipes.

1.6.2.3.1   Heat transfer coefficient calculation

Heat transfer coefficient calculation in the PHX caused a significant deviation of outlet temperatures compared to all steady state measurements during our test runs. The HTC in APROS is calculated by the Dittus-Boelter formula as a default, which yielded significantly higher values on the shell side of the coiled upcomer section of the PHX than what could be deduced from experimental data. To compensate for these discrepancies, the HTC on the shell side had to be tuned quite significantly for the model to show a close match with experimental data. Reynolds numbers were found to be between 2000-10 000 in the PHX, therefore, at first we did not change the default correlation, so the HTC was calculated with the default Dittus-Boelter formula, and multiplied by constant coefficient of **0.345** in order to provide realistic results.

With this tuning factor, the model achieved a good agreement with experimental results. Nevertheless, the fact the HTC calculated by the Dittus-Boelter formula severely **overestimated** heat transfer in a HX where the geometry is specifically configured for ideal heat transfer conditions is very unusual. The expected model behaviour under these circumstances would be for the calculation to **underestimate** the HTC (for example, as presented later for the case of the SHX), therefore further investigations were necessary. There are two possible explanations for this behaviour: First, it is possible that there is a user mistake in the HX model, however after multiple rounds of review and examination of the HX components, so far we could not find any meaningful errors in model configuration.

The other possible explanation is that there might be a significant bypass flow in the PHX. This would mean that a large portion of the mass flowrate does not flow through the coiled tube bundle, it instead flows around it, near the outside and inside walls of the shell side (Figure 1-15). Clearly, the hydraulic resistance in this bypass region is much lower than that of the tube bundle, and approx. 30% of the total free volume of the coiled shell side section is found outside of the tube bundle. From this, it is reasonable to assume that relatively large mass flow rate goes through the bypass region rather than the tube bundle. However, the effect of the bypass flow on the heat transfer is highly uncertain, since even if this relatively large flowrate does not participate directly in the heat transfer at the surface of the HX tubes, there are most likely very strong mixing effects present due to the geometry of the tube bundle. This results in a 3D flow pattern that causes even the flow in the bypass region to carry some of the heat from the tube bundle.

To further examine the bypass phenomena, we created a second version of our APROS model where we introduced a parallel pipe next to the pipe representing the shell side of the PHX. This approach models a complete separation of the bypass and main flows, neglecting any mixing between them. In this version, 30-35% of the secondary flow is diverted into the bypass channel, and the HTC calculation was not tuned by constant coefficients in the coiled part of the

PHX. In fact, the HTC in the coiled region was calculated by the Zukauskas correlation [3] , as recommended by the APROS developers [4] .

For the purpose of the S-Allegro benchmark, both versions of the model were used, the one containing a single channel and HTC tuning is called **"simple"**, while the one that contains the bypass channel, and uses the Zukauskas correlation with no tuning is called **"bypass"** version. Lastly, we note that the HTC one the tube side of the coiled pipes was calculated in both versions by the Dittus-Boelter correlation, and increased by a constant coefficient of 1.1. The reason for this increase is the presence of secondary flows in coiled tubes due to centrifugal force, which provide slightly better heat transfer compared to straight tubes[4] .
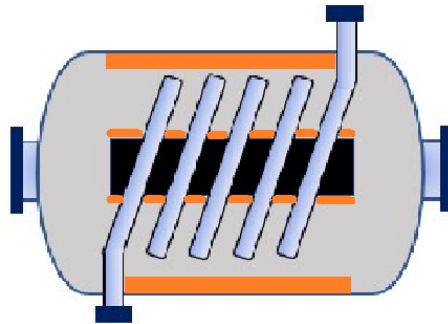
Figure 1-15: Schematic figure showing the bypass regions in a helically coiled heat exchanger
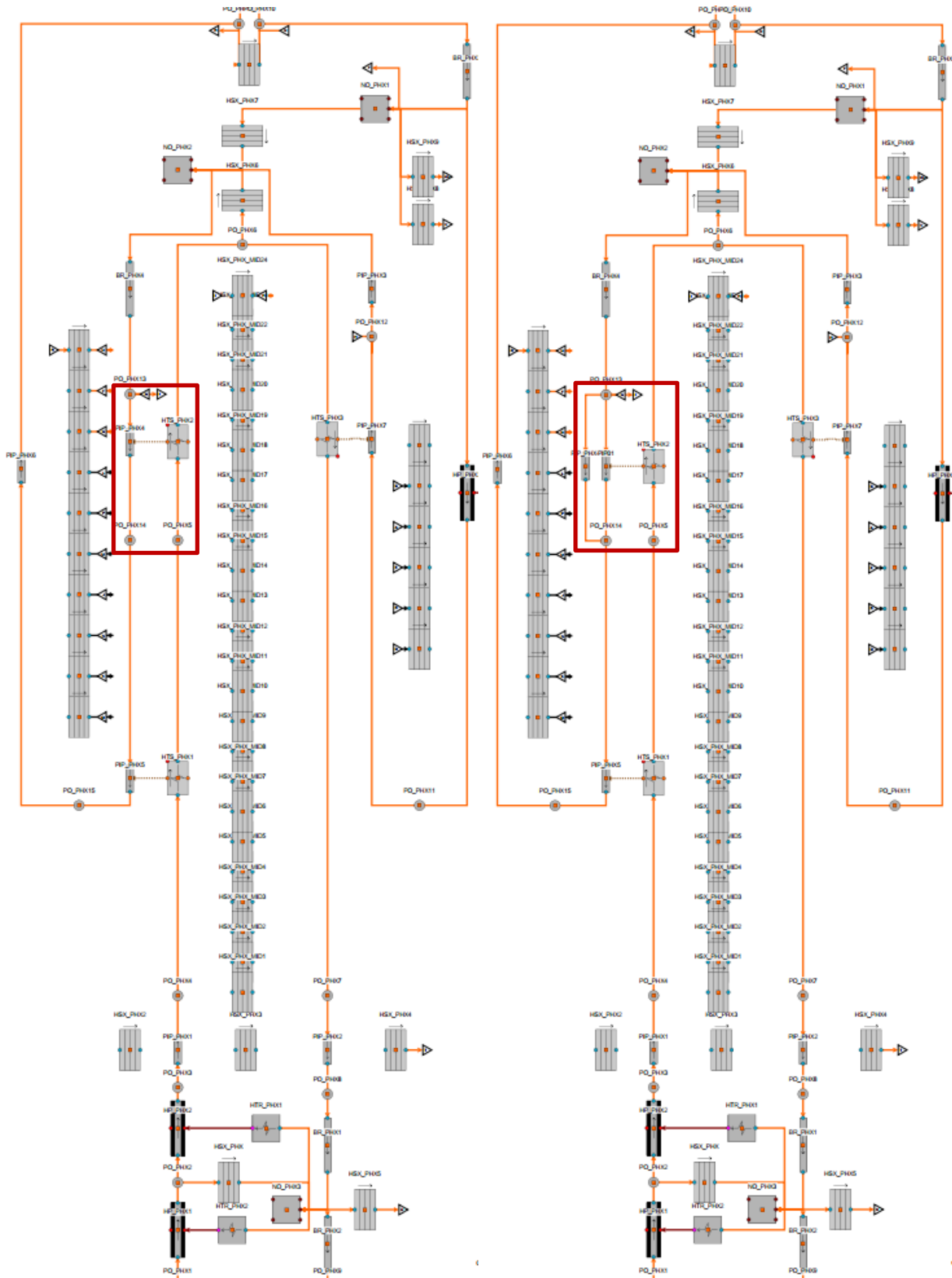
Figure 1-16: The primary heat exchanger in the two model versions, the "simple" model to the left, and the "bypass" model to the right (APROS).

1.6.2.4 SECONDARY HEAT EXCHANGER

With the secondary HX, we took a similar approach as the PHX. However, due to the simpler design, a less detailed model was sufficient. Also, since the tertiary loop is containing nearly room-temperature water, heat losses here could be neglected, and only the heat capacity of the HX wall and insulation needed to be accounted for. Moreover, heat flows are not present between the inlet and outlet fluids of the tertiary side, while on the secondary side, they can be modelled in very simple terms.

The SHX model utilizes the same structure as the PHX: the flow in the tube bundle is modelled with HS components, while the shell side is represented with pipes (or heat pipes when the HX wall is modelled). In order to improve the heat transfer in the HX, there are 6 baffles restricting the flow direction of the cooling water. This results in a flow pattern where water alternates between exchanging heat with the inlet side He and the outlet side. To try to represent the alternating heat exchange, we used 6 HTS-pipe pairs, each representing one section between two baffles, and connected every second pipe to the returning side of the tube bundles, as shown in Figure 1-17. The tertiary flow outside the HX was not modelled, we used a temperature, pressure, and mass flow boundary condition instead.

HTC in the SHX was likewise tuned to match experimental data, only in this case, it had to be significantly increased from the default values, since the baffles provide much better heat transfer conditions compared to developed straight flow. In this case, the Dittus-Boelter correlation is sufficient to model the HX behavior with some tuning factors: on the tube side, HTC was increased by 5-10%, while on the shell side, it was increased by 110%.
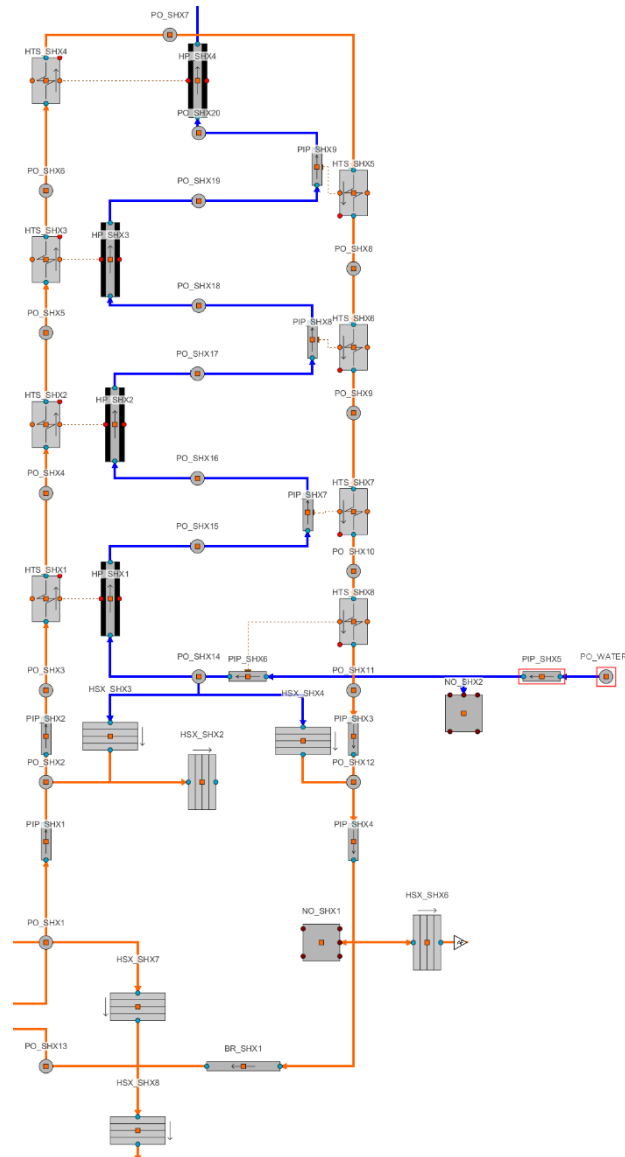
Figure 1-17: The secondary heat exchanger model (APROS)

1.6.2.5 BLOWERS

For the model of the blowers, we used APROS's default compressor module. This Apros module is currently quite simplistic, and therefore so is our model. There is no dynamic model behind this component, meaning that the relationship between torque and rotation speed is not modelled, the rotation speed is treated as a boundary condition. As an input, the module takes the basic geometric data of the compressor, the nominal operational parameters, and compressor map in terms of pressure ratio-mass flow curves for different rotation speeds. The compressor map we used can be seen in Figure 1-17.

The heat capacity of the blowers (and the pipelines and structures surrounding the blower) was estimated with two heat structures for each blower. We estimated that a 4 m long cylindrical heat structure is sufficient for each blower, with a total mass 390 kg including the 2*50 mm thick insulation layers.
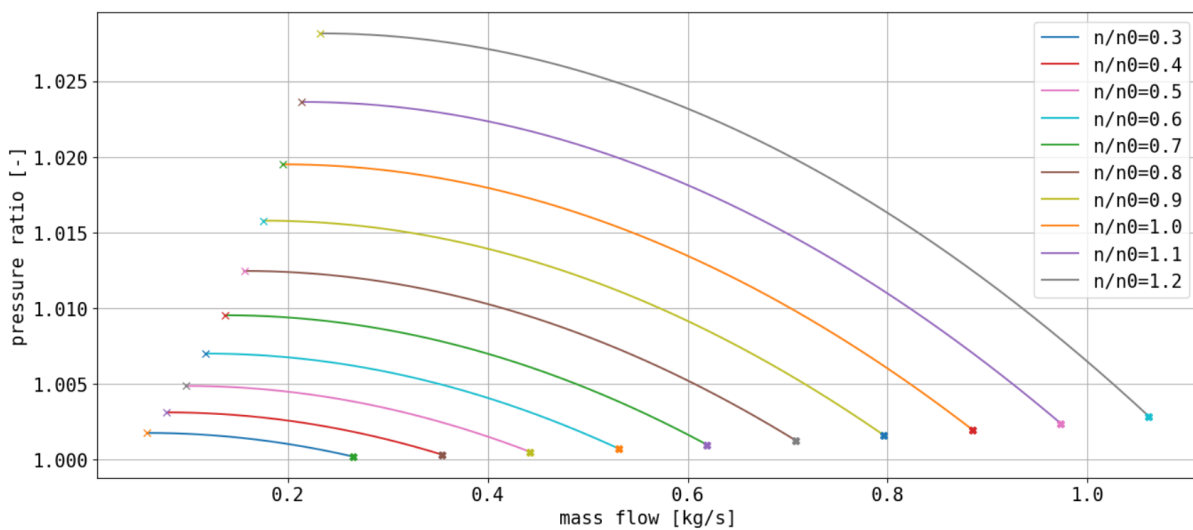

Figure 1-18: The compressor map used in the model

1.6.3 DYMOLA

The Dymola model based on design parameters [5]   should be able to represent the behavior of the circulation in both stationary and transient states. Therefore, the model contains following characteristics for reaching a good similarity with the real facility. These are:

- Piping geometry containing dimensions, length, disposition including extensions/contractions or bends and also elements needed for control and safety of the facility like valves, check valves, etc.

- Geometry of heat exchangers

- Turbomachines characteristics

- Material characteristics of piping and heat exchangers, including insulation materials.

- Heat transfer and pressure drop correlations.

For the transient simulations, it is especially important to include turbomachines characteristics that describe the dependencies between the rotational speed of the machine, its power consumption, pressure ratio and mass flow rate. Another factor that affects the behavior of the circuit during transient states is thermal inertia, which depends on the material from which the device is made, its weight, and also on heat losses, which are influenced by the material and the thickness of the insulation.

Dymola model of S-Allegro facility, shown in Figure 1-19, contains primary and secondary circuit, even the DHR circuit, which was disconnected for purposes of this benchmark. Water side is modelled only from secondary heat exchanger and eventually DHR heat exchanger point of view, with boundary conditions of water mass flow and inlet temperature / pressure.
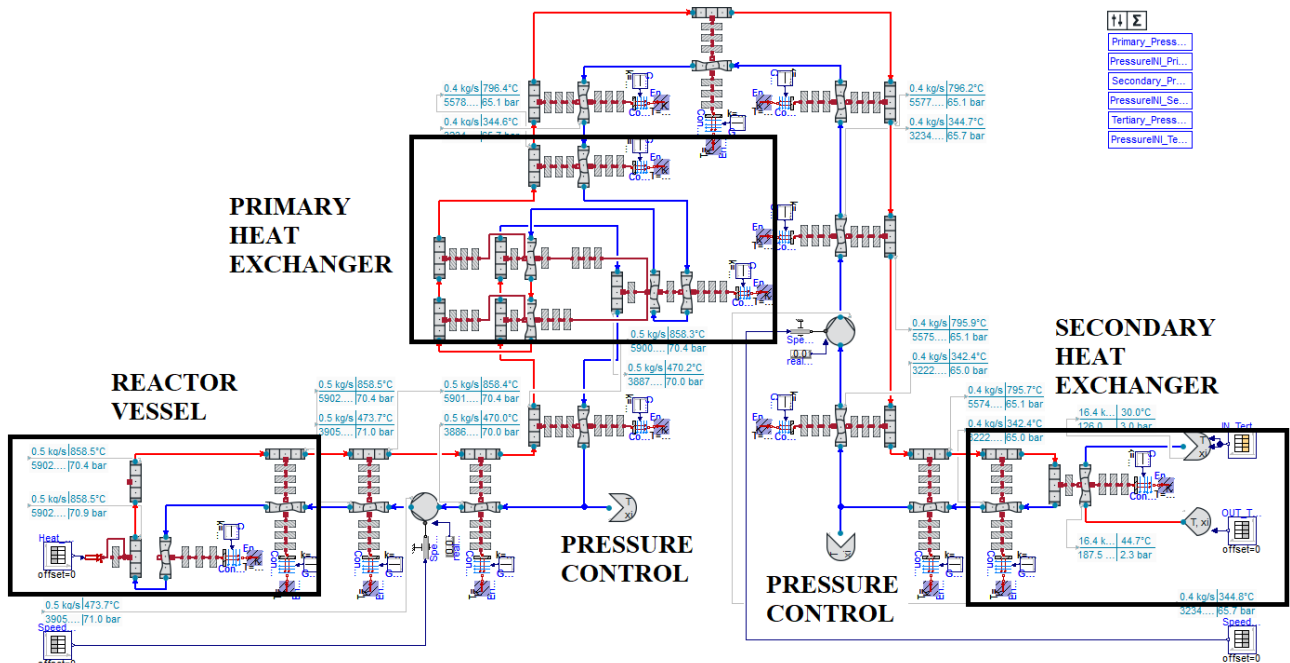

Figure 1-19: S-Allegro model (Dymola)

1.6.3.1 PIPING AND FITTINGS

The main components of cycle are connected by coaxial pipes. The piping, including valves, is modelled with respect to the conceptual topology and dimensions of the real cycle. The model allows calculations of the local and friction losses, as well as heat transfer between inner tube and outer ring tube or heat losses and heat accumulation to the piping walls.
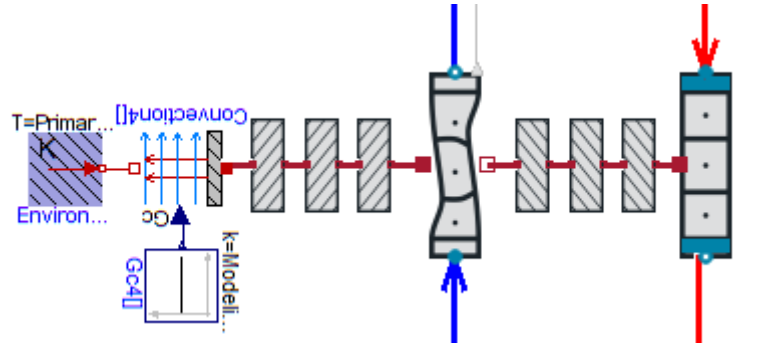
Figure 1-20: Pipe model assembly (Dymola)

The ClaRa+ library from Dymola contains all the components needed for the pipes and fittings. The whole pipe model assembly in the Dymola environment is shown in Figure 1-20. One can see several walls in Figure 1-20. The set of three walls between shell and tube represents the steel wall of inner tube, insulation, and inner steel wall of the shell. The second set of three walls represents outer steel wall of the shell, insulation, and its aluminum shielding. External heat losses are represented by a convective boundary condition. The pipeline modelling is important from the standpoint of determining the amount of Helium that will fill the facility.

Integral parts of the piping are fittings like control, closing or check valves.

1.6.3.2 PRIMARY AND SECONDARY COMPRESSORS

Compressor maps which were obtained by some CFD analyses is possible to described by three non-dimensional parameters based on similarity approach described in [8]   , which allow to perform simulations in a wide range of working conditions. These three parameters are:

Dimensionless Volume Flow Rate

$$\dot{V}^* = \Phi = \frac{\dot{V}}{2\pi N D^3} \qquad (1)$$

$\dot{V}$... volumetric flow [m^3/s]

N... revolutions of the rotor [rev/s]

D... outer diameter of the rotor [m]

Dimensionless Pressure

$$p^* = \chi = \frac{dh_{ie}}{u^2} \qquad (2)$$

dh_{ie}... isentropic enthalpy difference (discharge - intake) [J/kg]

u... peripheral speed at discharge from the impeller [m/s]

Dimensionless Power

$$P^* = \Sigma = \frac{dh}{u^2} \qquad (3)$$

dh... enthalpy difference (discharge - intake) [J/kg]

u... peripheral speed at discharge from the impeller [m/s]

The Dymola model of compressor based on this approach and compatible with ClaRa+ components was developed in CVR.

1.6.3.3 REACTOR VESSEL

The reactor vessel with electrical heated zone which represents an active zone consists of 7 hexagonal segments of 18 mullite tubes. These tubes are fixed by hexagonal spacers which hold the tubes in position and direct the flow of helium across the tube bundle. Heating wires from Kanthal material are placed in tubes.

This geometry is modelled as Shell&Tube heat exchanger in Dymola model. Wires in tubular channels are neglected and heat source boundary condition is connected directly with tube walls. The complex geometry of the real reactor vessel led to some CFD analyses. Correlation for Nusselt number and nominal pressure drop were obtained from these analyses. These results were used in thermos-hydraulic model, shown in Figure 1-21, which is described in this document.
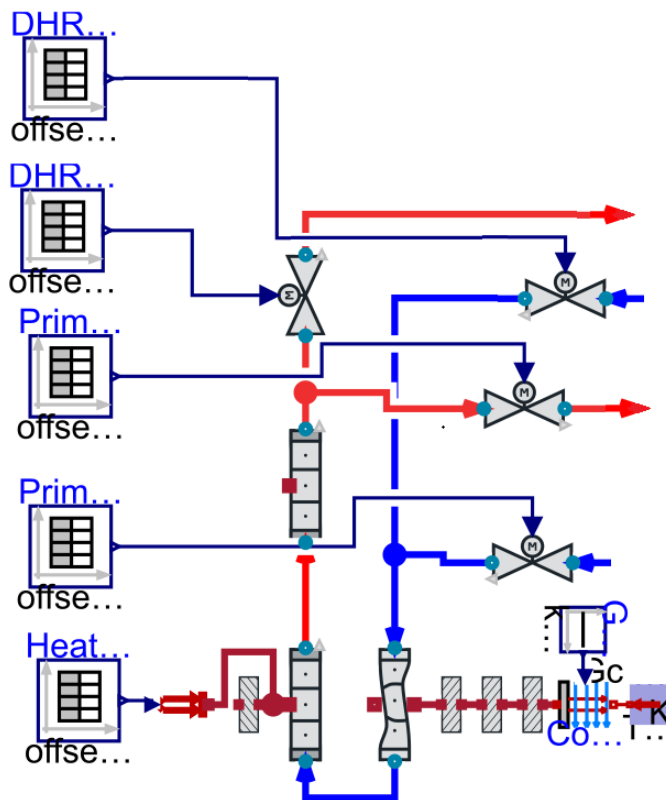
Figure 1-21: Reactor Vessel model (Dymola)

Cold helium flows around the tube bundle of active zone to the bottom of the reactor vessel, where changes the direction and flows to the tubular channel of active zone. The hot helium than flow through the pressure drop plate to the inner tube of the coaxial piping and to the primary heat exchanger.

1.6.3.4 PRIMARY HEAT EXCHANGER

In principle, the primary heat exchanger is Shell&Tube type. However, the arrangement of currents is more complicated than with a conventional tube exchanger with several changes of flow direction and cross flow area. Therefore, the primary heat exchanger is the most complex component of S-Allegro thermo-hydraulic model. Despite this complexity, standard components from native Modelica and ClaRa+ libraries were used for PHX assembly as one can see in Figure 1-22.
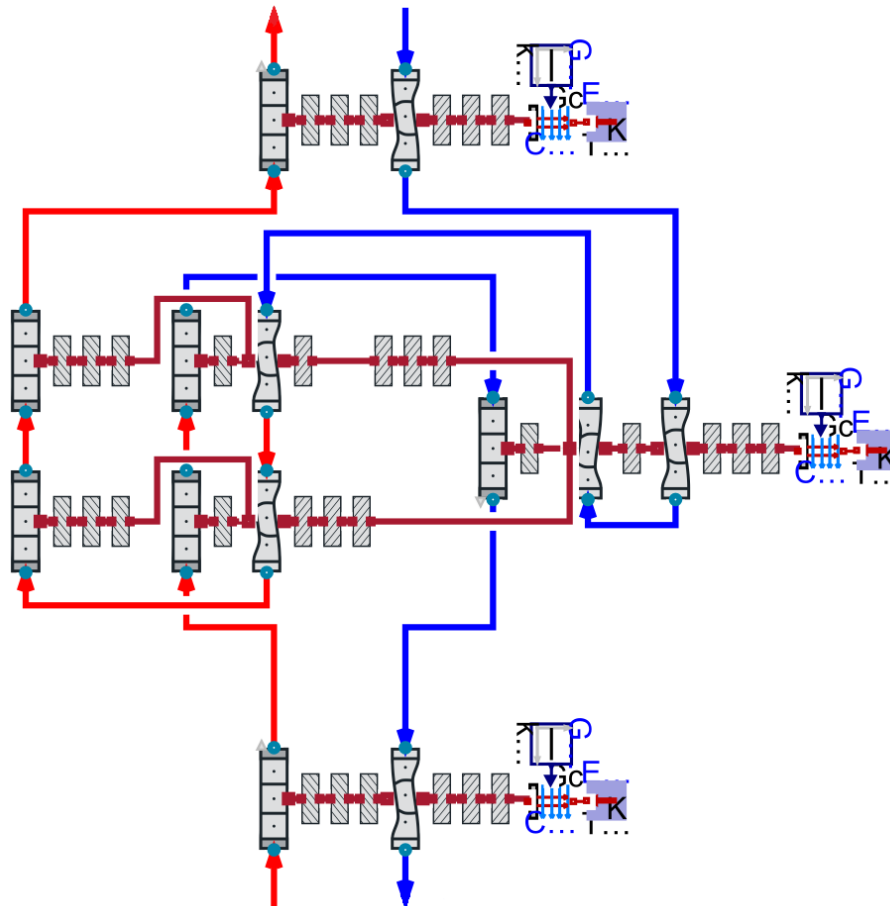

Figure 1-22: Primary Heat Exchanger (Dymola)

On primary (hot) side of the PHX, helium flows from the bottom central tube of primary loop, through the head to coiled U-tubes up, where tubes bend down and change to straight. Helium flow through this straight pipe bundle down and to the outer ring tube of primary loop.

On secondary (cold) side of PHX, helium enters at the top and is directed to flow to the bottom along the shell with the help of guiding plates. Then helium changes direction and flow lengthwise the straight tube bundle to the top where changes direction again and flows across the coiled tube bundle to the bottom. There the collector is placed, and helium is discharged through the central tube up and out of the PHX.

Due to complexity of PHX, some simplifications of cross-sectional areas were done. For example, coiled tube bundle is modelled as straight tube bundle, some transitions between different diameter are missing, etc.

For pressure drop calculation is used model QuadraticNominalPoint_L4 from ClaRa+. This model calculates pressure drop coefficient from nominal parameters and using it different states. This method is used for better numerical stability and shorter calculation times while maintaining acceptable accuracy of results.

$$\zeta = \frac{2\,\Delta p_{nom}\,D_h}{\rho_{nom}\,u_{mean}^2\,L} \tag{4}$$

For heat transfer calculations at tube side is used modified Dittus and Boelter correlation with coefficients defined by the manufacturer of the heat exchanger.

$$Nu = 0.06\,Re^{0.8}\,Pr^{1/3} \tag{5}$$

At shell side, the Gnielinski correlation was used

$$Nu = \frac{(\xi/8)\,(Re - 1000)\,Pr}{1 + 12.7\sqrt{\xi/8}\,(Pr^{2/3} - 1)}, \tag{6}$$

where

$$\xi = (1.82\,log(Re) - 1.64)^{-2}. \tag{7}$$

1.6.3.5 SECONDARY HEAT EXCHANGER

This heat exchanger helium-water is vertical Shell&Tube type. There are some baffles at shell side as one can see in Figure 1-23. These baffles direct the flow across the tube bundle, improving heat transfer and at the same time support the tube bundle. Some methods which describing 1-D calculations of these cases were used and implemented in the model.
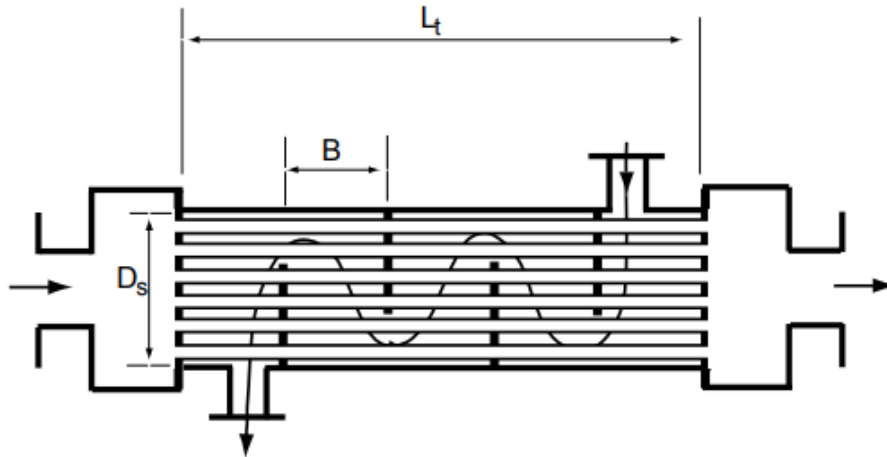

Figure 1-23: Secondary Heat Exchanger (Dymola)

For a flow type description at shell side, the crossflow area of the shell side is defined by following equation based on determination of free space between tubes in tube bundle, in the area delimited by two baffles.

$$A_C = \frac{D_S C_T B}{P_T}, \tag{8}$$

where D_s is shell inside diameter, B is baffle spacing

$$B = \frac{L_t}{N_b + 1}. \tag{9}$$

P_T and C_T are defined from cross section of tube bundle and an arrangement of tubes in it. In following Figure 1-24, two arrangements of tube bundle are described – square pitch layout and Triangular pitch layout. Each layout has different definition of hydraulic (equivalent) diameter.

$$D_{h-sq} = \frac{4(P_T^2 - \pi d_o^2/4)}{\pi d_o} \tag{10} \qquad D_{h-tr} = \frac{4\left(\frac{\sqrt{3}P_t^2}{4} - \frac{\pi d_o^2}{8}\right)}{\pi d_o/2} \tag{11}$$
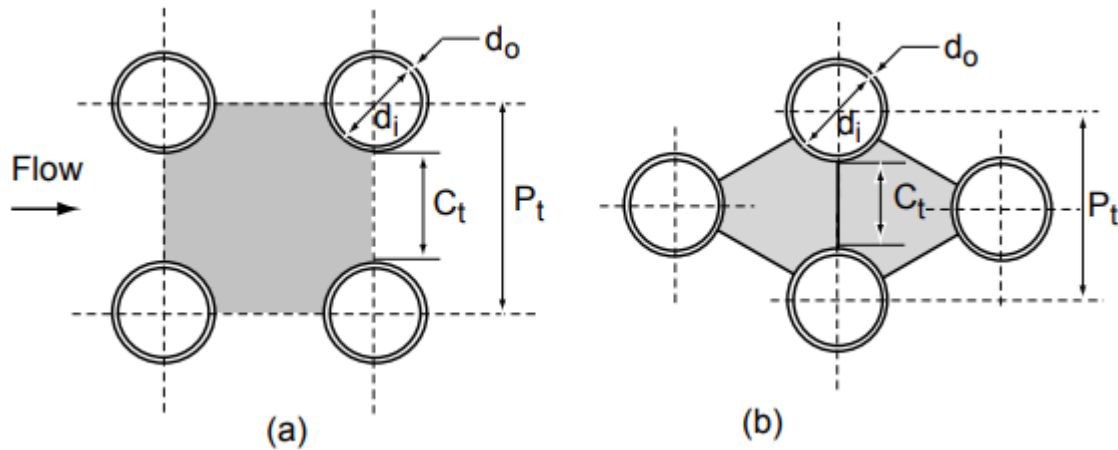
Figure 1-24: Tube arrangement types - (a) square pitch layout, (b) triangle pitch layout

For a pressure drop calculation is used model QuadraticNominalPoint_L4 from ClaRa+, same as in case of primary heat exchanger. The nominal pressure drop was obtained by external calculations based on VDI [9] and WMU [10] methods.

The ClaRa+ library implements a model for heat transfer, based on Dittus-Boelter correlation, which allows modification of coefficients C and m. Therefore, there was not necessary to create a new model. Only determination of coefficients was needed. This was done by solving an equation with two unknowns (C and m) for several Reynolds and Prandtl numbers. Then, obtained coefficient C = 0.0227 a m = 0.7905 were implemented in heat transfer model of tube bundle and C = 0.553 and m = 0.555 in model of shell side. Secondary heat exchanger model is shown in Figure 1-25.

$$Nu = C\,Re^m Pr^{1/3}$$
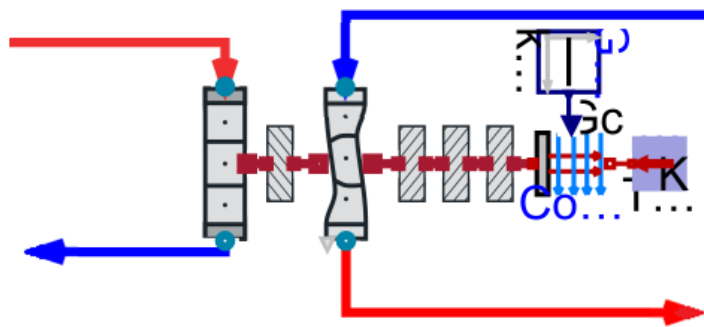
Figure 1-25: Secondary heat exchanger (Dymola)

1.6.4 CATHARE2

For nodalization, the main elements needed for modelling and their modelling method, structure had to be identified. The equipment was divided into five main parts: primary heat exchanger, secondary heat exchanger, DHR heat exchanger, pressure vessel and the pipe network connecting them. The way these units are defined will be described below. I aimed to identify the parts and define the loops based on the direction of motion of helium and water. This was done on the basis of the help material provided to users in GIUTHARE (User's Manual, User's Guideline, Dictionary of operators).

The skeleton of the model is made up of axial elements and volume elements, which had to be filled with different parameters. Since we are talking about a one-dimensional model, the most important factor is the extension of the element in the X direction, i.e. its length. This can be broken down into arbitrary sections but can only be given in meters. The "thickness" of the elements is calculated by the program according to three parameters: diameter, perimeter, intersection area. In addition, the number of divisions (from a numerical point of view), the dimensions of the joints (including the number of joints for volume elements) and the cosine of the angle of repose are important.

1.6.4.1 Pressure vessel

Following the path of the helium in the tank, the cold helium (1) enters the circular ring into an upper larger volume, five connections are built into the tank, two of which are currently in use (DHR and heat exchanger connection 1). From here it flows in a ring down to the lower mixing chamber (2). From the mixing chamber, it enters the 126 (7x18) ceramic heating duct (3), from there to the upper mixing chamber, and the already hot helium is discharged through the inner tube (5). In the figure, a protective plate is included in point (4), but this is not defined in the model.
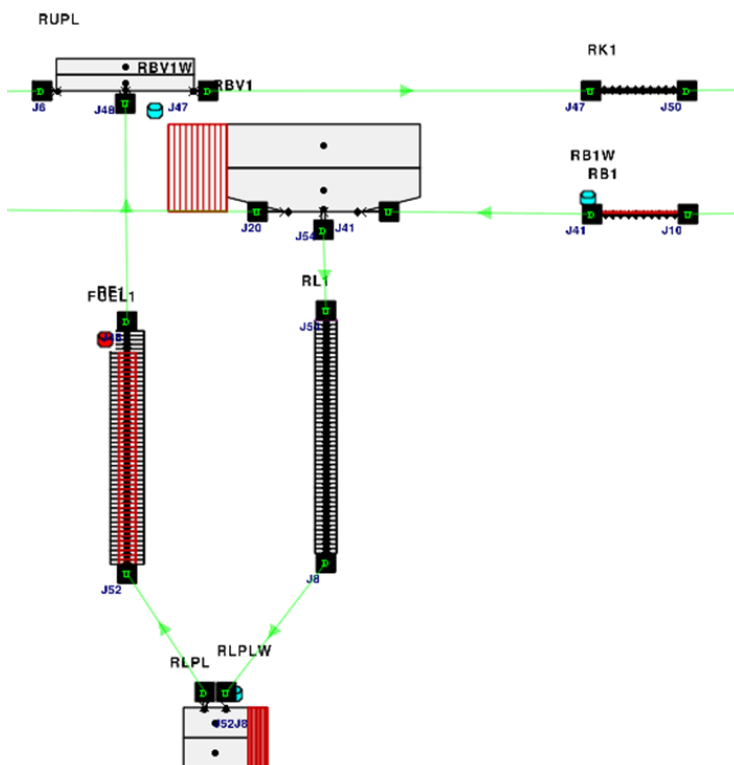

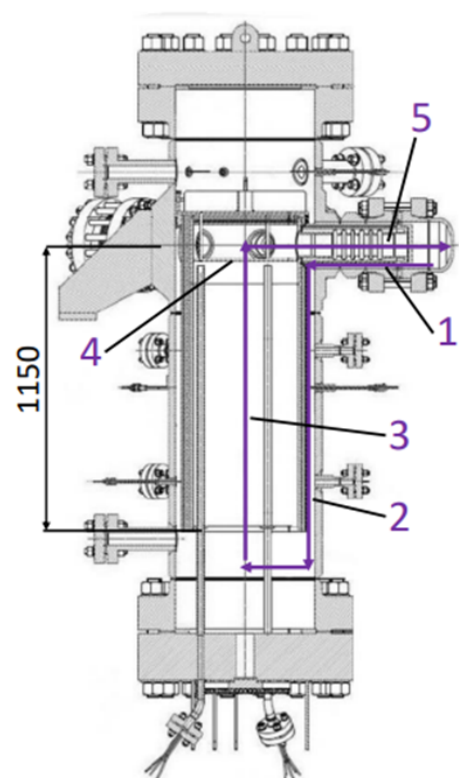**Figure 1-26: Pressure vessel (CATHARE2)**

Figure 1-27: Pressure vessel cross section with flow paths

1.6.4.2 Primary HEAT EXCHANGER

As previously shown on Figure 1-10, following the flow paths in blue color, the hot-side helium enters the bottom of the tank through the inner tube into a smaller volume element (1), from where it enters the main heat exchanger location in the form of 268 thin tubes spirally wound in eight concentric circles (2), from where they are turned out into two concentric circles and then straight down into a second volume element that surrounds the incoming volume segment (3). From this element, the medium exits the annular side of the tube towards the pressure vessel.

Shown in yellow color, the cold helium enters from the annular side of the tube on the cold side into a spherical segment-shaped volume element (1), and is then discharged through a narrow annulus at the edge of the container, where there is no heat exchange between the gases, only heat loss to the outside. Here it is turned onto an upward flowing ring, where part of the heat exchange takes place with the hot side helium flowing down the two circles (3). The next turn is made with the spiral tubes, where most of the heat exchange takes place (4). The heated helium is then turned into the outlet tube, where it is extracted in the direction of the secondary heat exchanger.
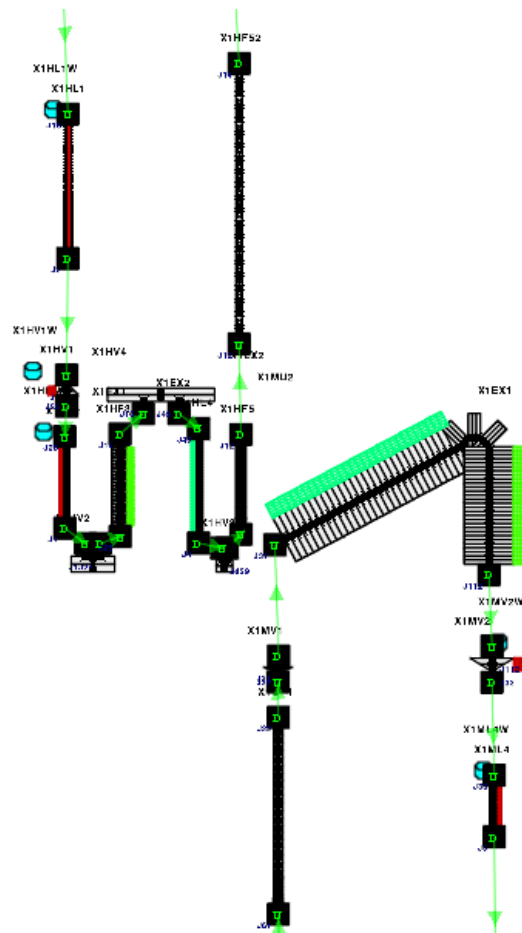

Figure 1-28: The primary heat exchanger nodalizations (CATHARE2).

1.6.4.3 SECONDARY HEAT EXCHANGER

As shown in Figure 1-12, marked in blue, the hot helium enters a relatively small volume component (1) through the inner part of the tube, from where it exchanges heat with the water side through 57 U-tubes (2) (the average length of the U-tubes is 1.588 m). The tubes run into a larger volume, from where the cooled helium flows through a circular ring to the primary heat exchanger.

Marked in yellow on the water side, the medium flows through a standard tube (1) into a volumetric element in which the upper part of the tank with the U-tubes is embedded. Six baffle plates are installed in this compartment. The water flows between the baffle plates (2) as shown in the diagram and then exits through a pipe at the top of the tank (3).
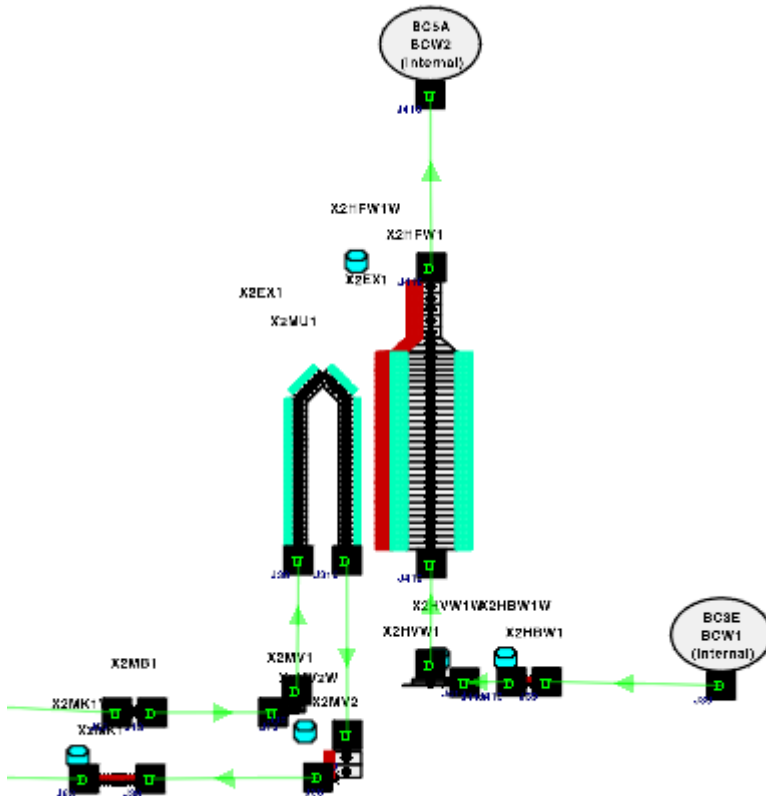

Figure 1-29: Secondary heat exchanger nodalisation (CATHARE2).

1.6.4.4 Preliminary results

For the steady state calculations, we were using the given data in the measurement results as comparison to prove the correctness of the model. This required the tuning of the controllers. The amount of intervention, the size of the time steps and the running time itself were changed several times.

Initial results of the simulations were not satisfactory in a sense that, there were dif-ferencies in the provided data and the simulated data. After further tuning, we were led to the assumption that both the primary and secondary heat exchangers are working incorrectly. This revalation warranted the need to perform component tests on them respectively.
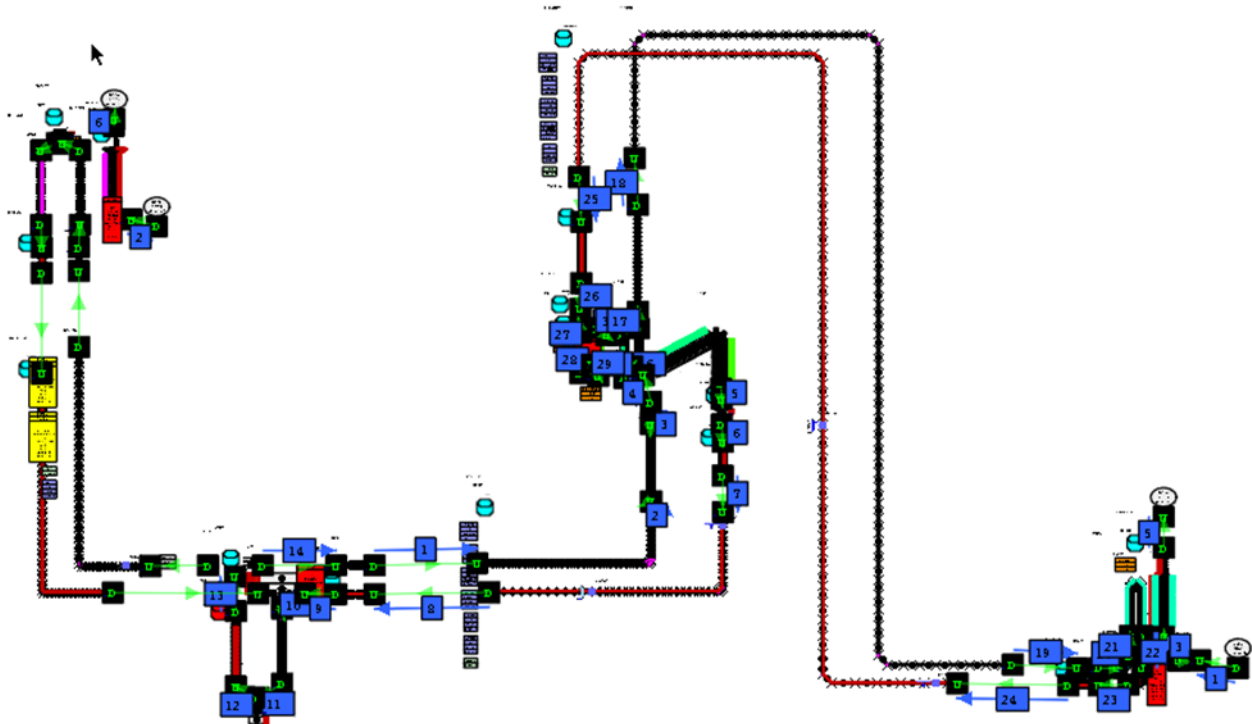
Figure 1-30: Full S-Allegro nodalization (CATHARE2).

1.6.4.4.1 Component tests

With the component tests, both the primary and secondary heat exchangers were isolated, and all inlets and outlets were replaced by boundary conditions tuned to the measured data. With some extra components added to achieve extra flexibility in tuning, the secondary heat exchanger could be made to operate within working parameters with less than 0,1 % error margin. The primary heat exchanger's error margin could be brought down to 3 % as of now, but efforts are made to reduce it further.

1.6.4.4.2 Finalizing the Steady State

The next steps of the work are to implement the corrected heat exchangers back to the main model. With that and some added components we are confident that the steady state could simulate the given measurement data set.

If we achieve that goal, we can progress to the incorporation of the transient data set. Until then we decided not to include numerical results, as to not influence the evaluation made by the other participants.

1.7 PHASE I – PHX and SHX nodalization

The TH models of the key S-Allegro components, the Primary Heat Exchanger (PHX) and the Secondary Heat Exchanger (SHX), described in the previous chapters have been validated against the measured data. For this purpose about 20 steady states have been measured in the S-Allegro loop and finally the 4 most representative were selected. The measured values are presented in the following tables.

Table 1-13: Primary heat exchanger measured data – tube side

Primary Heat Exchanger – tube side				
Steady state	Boundary conditions (inlet)			Exit temperature
	T [°C] – T102	p [MPa] – P101	m [kg/s] – F101	T [°C] – T132
#1	141.81	3.109	0.2232	72.35
#2	129.62	3.037	0.2467	57.22
#3	164.91	3.110	0.2222	63.92
#4	273.66	3.583	0.2447	141.08

Table 1-14: Primary heat exchanger measure data – shell side

Primary Heat Exchanger – shell side				
Steady state	Boundary conditions (inlet)			Exit temperature
	T [°C] – T633	p [MPa] – P604	m [kg/s] – F601	T [°C] – T601
#1	44.13	3.144	0.197	117.95
#2	48.57	2.998	0.4973	84.23
#3	53.41	3.052	0.4992	99.80
#4	69.49	3.709	0.1918	230.94

Table 1-15: Secondary heat exchanger measure data – tube side

Secondary Heat Exchanger – tube side				
Steady state	Boundary conditions (inlet)			Exit temperature
	T [°C] - T602	p [MPa] - P604	m [kg/s] - F 601	T [°C] - T631
#1	117.14	3.141	0.197	40.44
#2	82.33	2.992	0.4973	45.23
#3	101.40	3.045	0.4992	50.14
#4	223.20	3.707	0.1918	60.41

Table 1-16: Secondary heat exchanger measure data – shell side

Secondary Heat Exchanger – shell side				
Steady state	Boundary conditions (inlet)			Exit temperature
	T [°C] – T991	p [MPa] – P991	m [kg/s] – F962	T [°C] – T962
#1	20.43	0.575	2.7851	26.95
#2	22.72	0.573	2.7589	31.29
#3	21.75	0.570	2.7984	32.54
#4	21.61	0.564	3.6147	32.29

The values denominated as the "boundary conditions" in the tables above have been used to initiate the steady state conditions in PHX and SHX models. The values denominated as the "exit temperature" have been compared with the calculated values of exit temperature in PHX and SHX models.

Evaluation of the PHX models.

The comparison between measured and calculated values of T132 (tube side exit temperature) and T601 (shell side exit temperature) was performed. The figures can be seen from Figure 1-31to Figure 1-34.

In general the initial conditions at the tube side have been adjusted correctly by all participants in all steady state conditions SS#1 to SS#4. There are very small differences compared to the reference values. The same conclusion is valid for the shell side boundary conditions.

In case of DYMOLA model the T633 is slightly underestimated in SS#1, SS#2 and SS#4. Regarding the initial pressure P101 the value is overestimated in case of DYMOLA and APROS.

Generally speaking the heat transfer from primary to secondary side in the DYMOLA model seems to be underestimated for the SS#1 and SS#4 (low initial flow rate in shell side). For the case SS#2 and SS#3 (high initial flow rate in shell side) underestimation of the tube side exit temperature T132 is observed.

The APROS model predicts the T132 and T601 very well and there are very little differences with the measurement. The same is valid for the RELAP5-3D model except slight overestimation of the shell side exit temperature T601 in case of SS#4.

Evaluation of the SHX models.

The comparison between measured and calculated values of T631 (tube side exit temperature) and T962 (shell side exit temperature) was performed. The figures can be seen from Figure 1-35 to Figure 1-38.

The initial conditions at the tube side have been adjusted correctly by all participants in all steady state conditions SS#1 to SS#4. There are very small differences compared to the reference values. The same conclusion is valid for the shell side boundary conditions.

For the calculation of the exit temperature T631 (tube side) and the T962 (shell side) all codes predictions are in very good agreement with measurement. There were no major discrepancies observed. There is only very small overestimation of the T631 value in DYMOLA calculation.
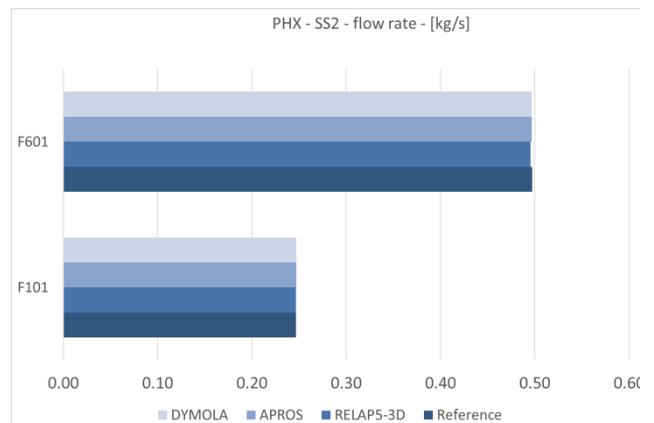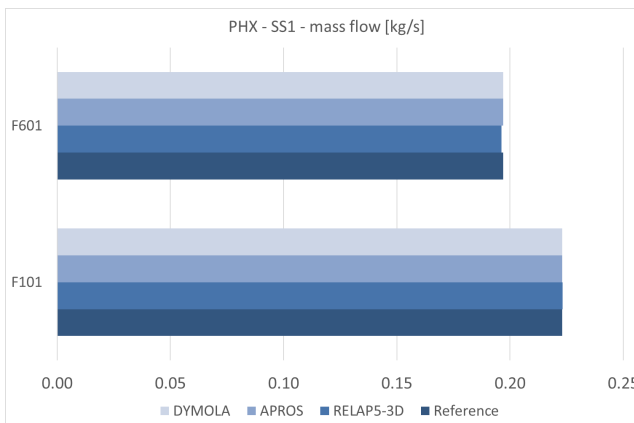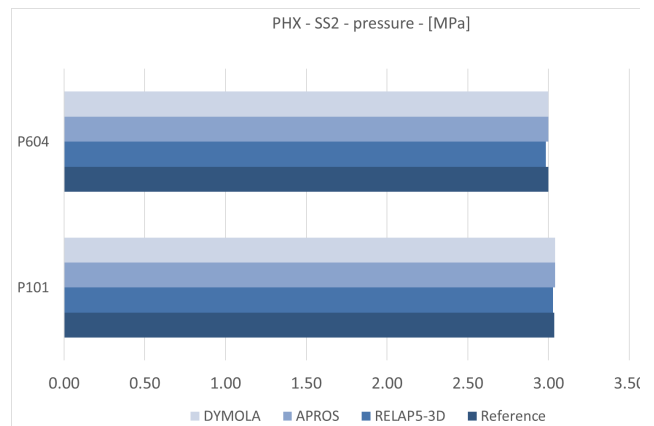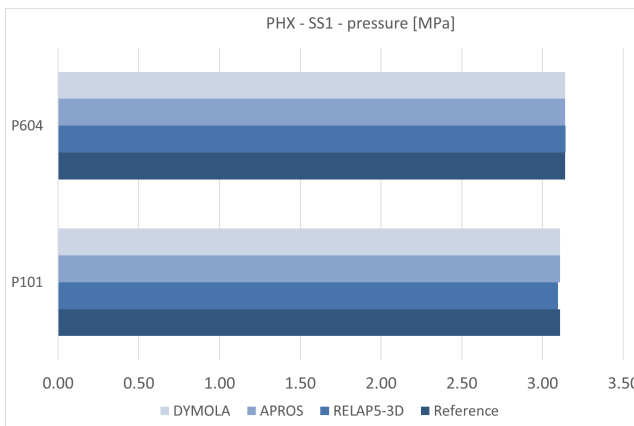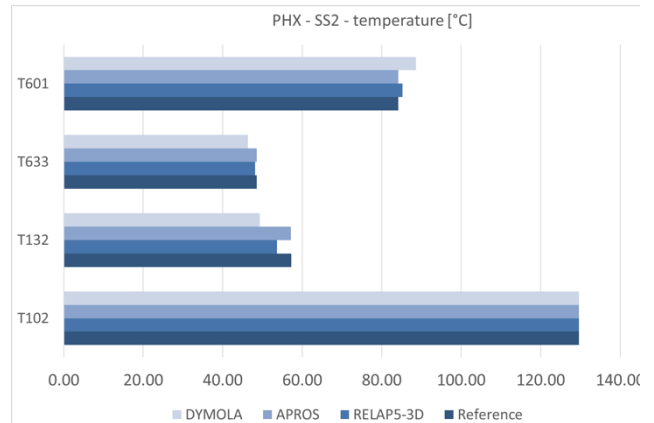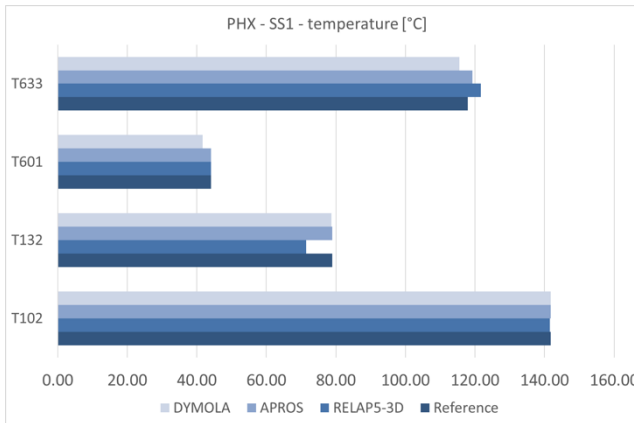
Figure 1-31: PHX - Steady state 1 results

Figure 1-32: PHX - Steady state 2 results
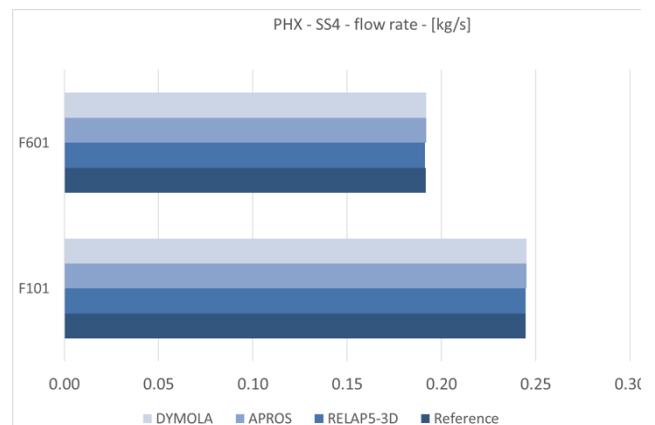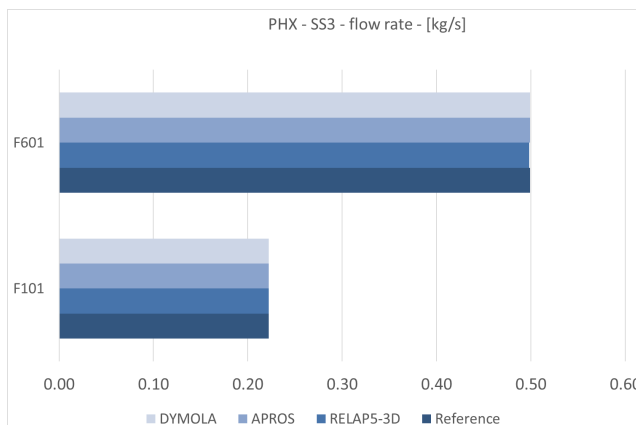
Figure 1-33: PHX - Steady state 3 results
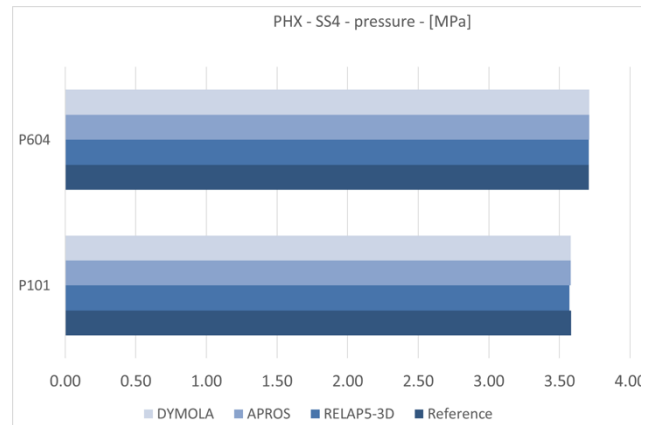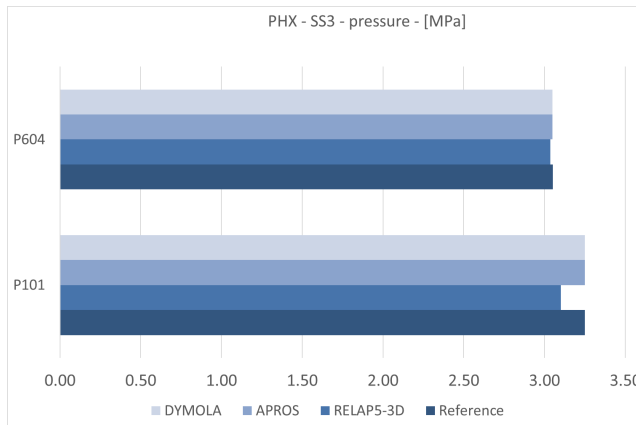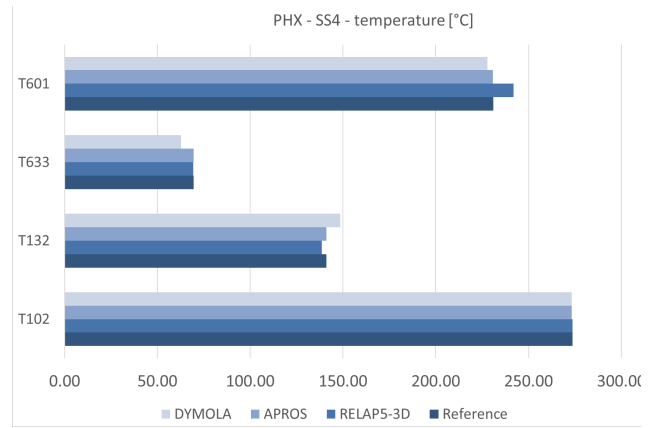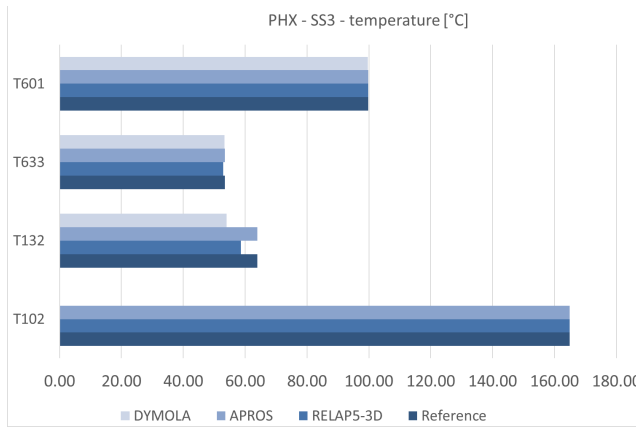

Figure 1-34: PHX - Steady state 4 results
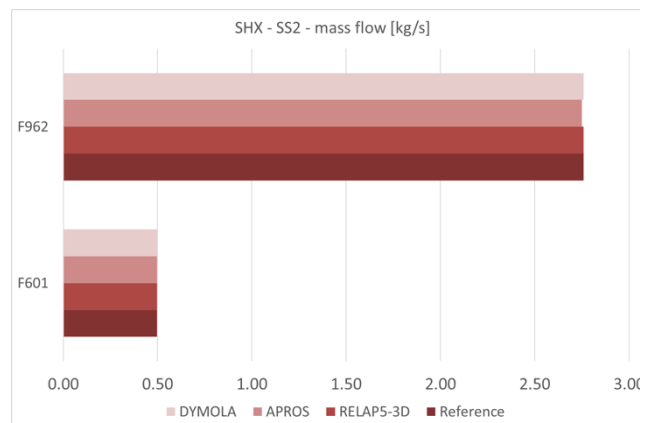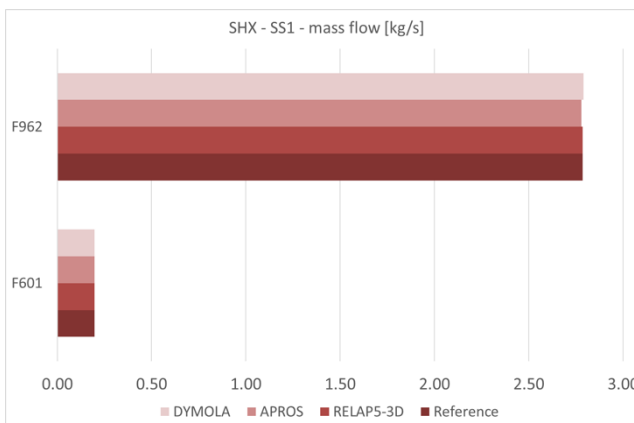
Figure 1-35: SHX - Steady state 1 results

Figure 1-36: SHX - Steady state 2 results
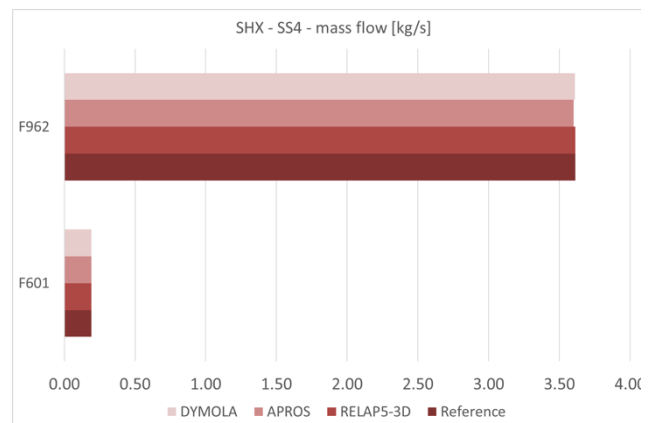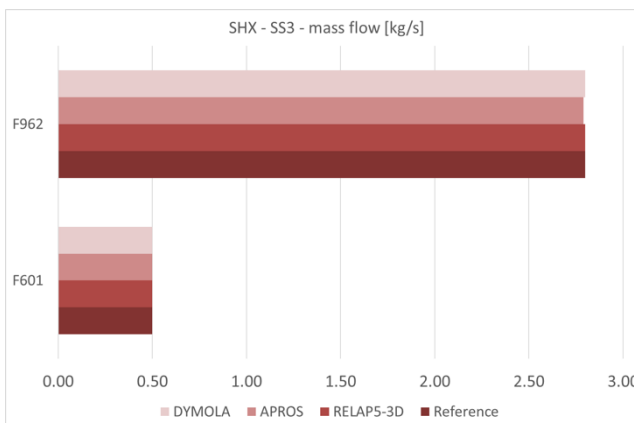
Figure 1-37: SHX - Steady state 3 results　　**Figure 1-38: SHX - Steady state 4 results**

Table 1-17: Primary heat exchanger – steady state no.1

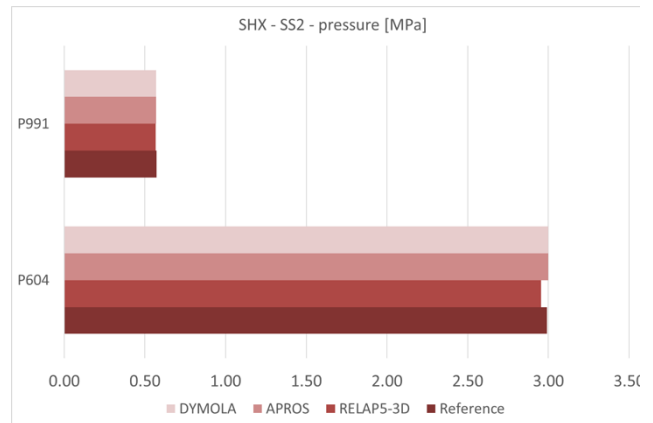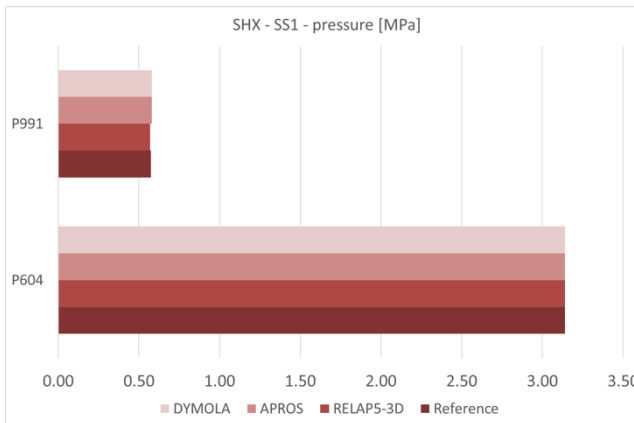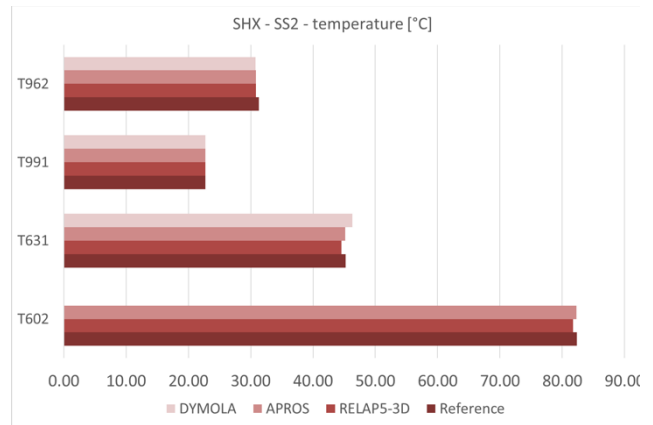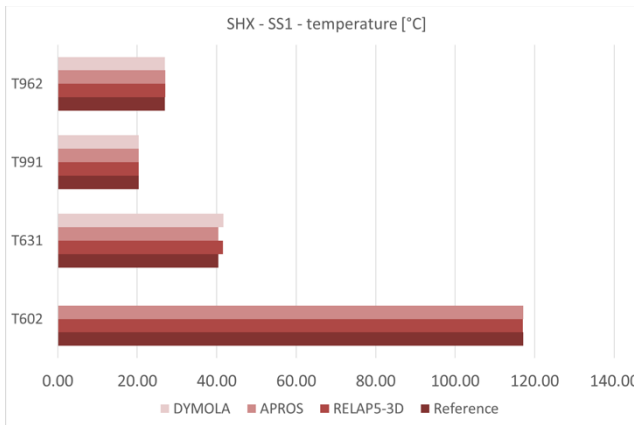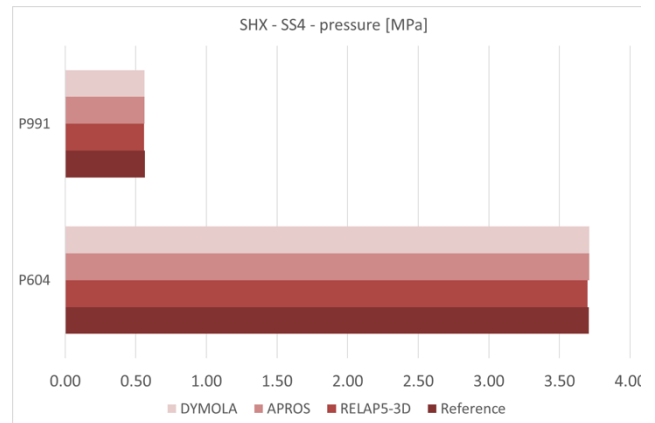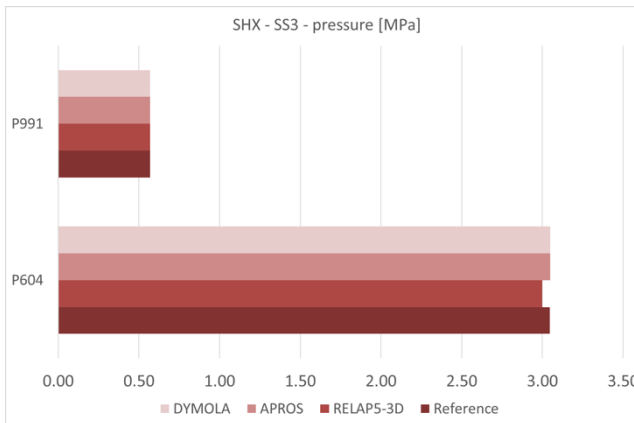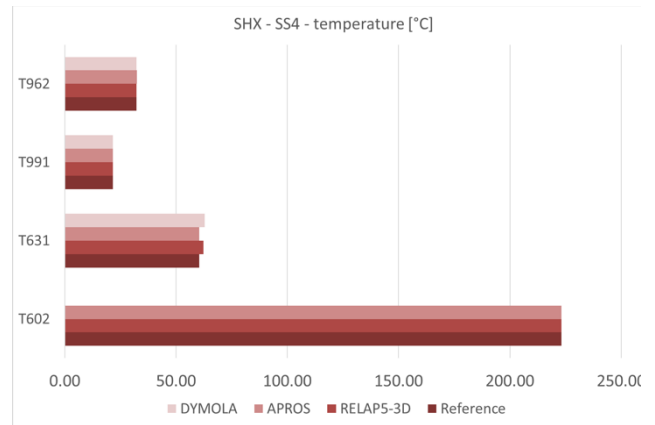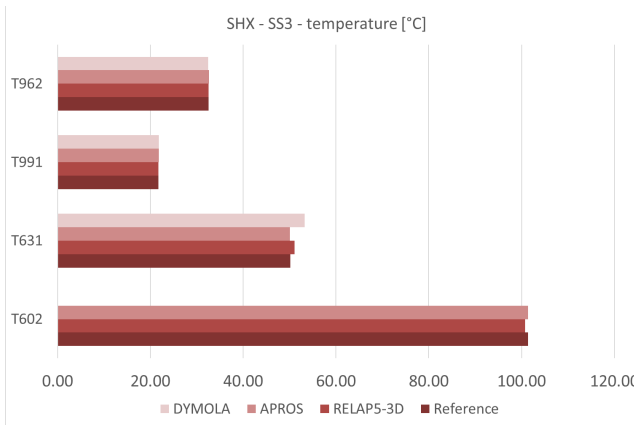| No.	Parameter	Sensor	Unit	Ref. value	Accuracy [%]	Acceptable error [%]	VUJE RELAP5-3D ver. 4.3.4	Calculated error [%]	Judgment	BME APROS ver. 6.12	Calculated error [%]	Judgment	CVR Řež DYMOLA	Calculated error [%]	Judgment
1	He temperature - inner leg I.C - PHX inlet	T102	°C	141.80	0.40	0.50	141.58	0.00	E	141.80	0.00	E	141.80	0.00	E
2	He pressure - inner leg I.C (Cerabar S PMP71)	P101	Mpa	3.11	0.25	0.10	3.10	0.23	M	3.11	0.00	E	3.11	0.00	E
3	He mass-flow rate - inner leg I.C (differential pressure Torbar)	F101	kg/s	0.22	2.50	0.50	0.22	0.00	E	0.22	0.00	E	0.22	0.00	E
4	He temperature - outer leg I.C - PHX outlet	T132	°C	79.00	0.40	0.50	71.45	9.19	M	79.00	0.00	E	78.70	0.00	E
5	He temperature - outer leg II.C - PHX inlet	T601	°C	44.10	0.40	0.50	44.05	0.00	E	44.10	0.00	E	41.70	5.06	M
6	He pressure in the PHX - II.C (Cerabar S PMP71)	P604	MPa	3.14	0.25	0.10	3.14	0.00	E	3.14	0.00	E	3.14	0.00	E
7	He mass-flow rate - inner leg II.C (differential pressure Torbar)	F601	kg/s	0.20	2.50	2.00	0.20	0.00	E	0.20	0.00	E	0.20	0.00	E
8	He temperature - inner leg II.C - PHX outlet (differential pressure Torbar)	T633	°C	117.90	0.40	0.50	121.73	2.84	M	119.31	0.79	M	115.50	1.64	M

Table 1-18: Primary heat exchanger – steady state no.2

No.	Parameter	Sensor	Unit	Ref. value	Accuracy [%]	Acceptable error [%]	VUJE RELAP5-3D ver. 4.3.4	Calculated error [%]	Judgment	BME APROS ver. 6.12	Calculated error [%]	Judgment	CVR Řež DYMOLA	Calculated error [%]	Judgment
1	He temperature - inner leg I.C - PHX inlet	T102	°C	129.62	0.40	0.50	129.62	0.00	E	129.60	0.00	E	129.60	0.00	E
2	He pressure - inner leg I.C (Cerabar S PMP71)	P101	Mpa	3.04	0.25	0.10	3.03	0.08	E	3.04	0.00	E	3.04	0.00	E
3	He mass-flow rate - inner leg I.C (differential pressure Torbar)	F101	kg/s	0.25	2.50	0.50	0.25	0.00	E	0.25	0.00	E	0.25	0.00	E
4	He temperature - outer leg I.C - PHX outlet	T132	°C	57.22	0.40	0.50	53.69	5.79	M	57.20	0.00	E	49.30	13.50	M
5	He temperature - outer leg II.C - PHX inlet	T601	°C	48.57	0.40	0.50	48.10	0.57	M	48.60	0.00	E	46.30	4.29	M
6	He pressure in the PHX - II.C (Cerabar S PMP71)	P604	MPa	3.00	0.25	0.10	2.98	0.24	M	3.00	0.00	E	3.00	0.00	E
7	He mass-flow rate - inner leg II.C (differential pressure Torbar)	F601	kg/s	0.50	2.50	2.00	0.50	0.00	E	0.50	0.00	E	0.50	0.00	E
8	He temperature - inner leg II.C - PHX outlet (differential pressure Torbar)	T633	°C	84.23	0.40	0.50	85.19	0.74	M	84.20	0.00	E	88.60	4.77	M

Note)

M – Minimal

E – Excellent

Table 1-19: Primary heat exchanger – steady state no.3

No.	Parameter	Sensor	Unit	Ref. value	Accuracy [%]	Acceptable error [%]	VUJE RELAP5-3D ver. 4.3.4	Calculated error [%]	Judgment	BME APROS ver. 6.12	Calculated error [%]	Judgment	CVR Řež DYMOLA	Calculated error [%]	Judgment
1	He temperature - inner leg I.C - PHX inlet	T102	°C	164.91	0.40	0.50	164.90	0.00	E	164.90	0.00	E		100.00	M
2	He pressure - inner leg I.C (Cerabar S PMP71)	P101	Mpa	3.25	0.25	0.10	3.10	4.34	M	3.25	0.00	E	3.25	0.00	E
3	He mass-flow rate - inner leg I.C (differential pressure Torbar)	F101	kg/s	0.22	2.50	0.50	0.22	0.00	E	0.22	0.00	E	0.22	0.00	E
4	He temperature - outer leg I.C - PHX outlet	T132	°C	63.92	0.40	0.50	58.58	7.99	M	63.90	0.00	E	54.00	15.18	M
5	He temperature - outer leg II.C - PHX inlet	T601	°C	53.41	0.40	0.50	52.94	0.48	E	53.40	0.00	E	53.30	0.00	E
6	He pressure in the PHX - II.C (Cerabar S PMP71)	P604	MPa	3.05	0.25	0.10	3.04	0.24	M	3.05	0.00	E	3.05	0.00	E
7	He mass-flow rate - inner leg II.C (differential pressure Torbar)	F601	kg/s	0.50	2.50	2.00	0.50	0.00	E	0.50	0.00	E	0.50	0.00	E
8	He temperature - inner leg II.C - PHX outlet (differential pressure Torbar)	T633	°C	99.80	0.40	0.50	99.72	0.00	E	99.80	0.00	E	99.70	0.00	E

Table 1-20: Primary heat exchanger – steady state no.4

No.	Parameter	Sensor	Unit	Ref. value	Accuracy [%]	Acceptable error [%]	VUJE RELAP5-3D ver. 4.3.4	Calculated error [%]	Judgment	BME APROS ver. 6.12	Calculated error [%]	Judgment	CVR Řež DYMOLA	Calculated error [%]	Judgment
1	He temperature - inner leg I.C - PHX inlet	T102	°C	273.30	0.40	0.50	273.64	0.00	E	273.30	0.00	E	273.30	0.00	E
2	He pressure - inner leg I.C (Cerabar S PMP71)	P101	Mpa	3.58	0.25	0.10	3.57	0.11	M	3.58	0.00	E	3.58	0.00	E
3	He mass-flow rate - inner leg I.C (differential pressure Torbar)	F101	kg/s	0.24	2.50	0.50	0.24	0.00	E	0.25	0.00	E	0.25	0.00	E
4	He temperature - outer leg I.C - PHX outlet	T132	°C	141.08	0.40	0.50	138.50	1.43	M	141.10	0.00	E	148.60	4.91	M
5	He temperature - outer leg II.C - PHX inlet	T601	°C	69.49	0.40	0.50	69.43	0.00	E	69.50	0.00	E	62.80	9.26	M
6	He pressure in the PHX - II.C (Cerabar S PMP71)	P604	MPa	3.71	0.25	0.10	3.71	0.00	E	3.71	0.00	E	3.71	0.00	E
7	He mass-flow rate - inner leg II.C (differential pressure Torbar)	F601	kg/s	0.19	2.50	2.00	0.19	0.00	E	0.19	0.00	E	0.19	0.00	E
8	He temperature - inner leg II.C - PHX outlet (differential pressure Torbar)	T633	°C	230.94	0.40	0.50	241.98	4.36	M	230.90	0.00	E	227.80	0.96	M

Note)

M – Minimal

E – Excellent

Table 1-21: Secondary heat exchanger – steady state no.1

No.	Parameter	Sensor	Unit	Ref. value	Accuracy [%]	Acceptable error [%]	VUJE RELAP5-3D ver. 4.3.4	Calculated error [%]	Judgment	BME APROS ver. 6.12	Calculated error [%]	Judgment	CVR Řež DYMOLA	Calculated error [%]	Judgment
1	He temperature - inner leg II.C	T602	°C	117.14	0.40	0.50	117.00	0.00	E	117.10	0.00	E		100.00	M
2	He pressure in the PHX - II.C (Cerabar S PMP71)	P604	MPa	3.14	0.25	0.10	3.14	0.00	E	3.14	0.00	E	3.14	0.00	E
3	He mass-flow rate - inner leg II.C (differential pressure Torbar)	F601	kg/s	0.20	2.50	2.00	0.20	0.00	E	0.20	0.00	E	0.20	0.00	E
4	He temperature - outer leg II.C - SHX outlet	T631	°C	40.44	0.40	0.50	41.56	2.36	M	40.40	0.00	E	41.70	2.70	M
5	Water inlet temperature (Pt100)	T991	°C	20.43	0.62	0.50	20.43	0.00	E	20.40	0.00	E	20.40	0.00	E
6	Water inlet pressure (Cerabar PMP11)	P991	MPa	0.58	0.25	0.10	0.57	0.80	M	0.58	0.62	M	0.58	0.62	M
7	Water flow rate in SHX (Promag 10L80)	F962	kg/s	2.79	0.00	2.00	2.79	0.00	E	2.78	0.18	E	2.79	0.18	E
8	Water temperature - SHX outlet	T962	°C	26.95	0.40	0.50	27.05	0.00	E	27.05	0.00	E	27.00	0.00	E

Table 1-22: Secondary heat exchanger – steady state no.2

No.	Parameter	Sensor	Unit	Ref. value	Accuracy [%]	Acceptable error [%]	VUJE RELAP5-3D ver. 4.3.4	Calculated error [%]	Judgment	BME APROS ver. 6.12	Calculated error [%]	Judgment	CVR Řež DYMOLA	Calculated error [%]	Judgment
1	He temperature - inner leg II.C	T602	°C	82.33	0.40	0.50	81.74	0.32	E	82.30	0.00	E		100.00	M
2	He pressure in the PHX - II.C (Cerabar S PMP71)	P604	MPa	2.99	0.25	0.10	2.96	0.99	M	3.00	0.02	E	3.00	0.02	E
3	He mass-flow rate - inner leg II.C (differential pressure Torbar)	F601	kg/s	0.50	2.50	2.00	0.50	0.00	E	0.50	0.00	E	0.50	0.00	E
4	He temperature - outer leg II.C - SHX outlet	T631	°C	45.23	0.40	0.50	44.58	1.04	M	45.20	0.00	E	46.30	1.96	M
5	Water inlet temperature (Pt100)	T991	°C	22.72	0.62	0.50	22.72	0.00	E	22.70	0.00	E	22.70	0.00	E
6	Water inlet pressure (Cerabar PMP11)	P991	MPa	0.57	0.25	0.10	0.57	0.62	M	0.57	0.27	M	0.57	0.27	M
7	Water flow rate in SHX (Promag 10L80)	F962	kg/s	2.76	0.00	2.00	2.76	0.00	E	2.75	0.32	E	2.76	0.04	E
8	Water temperature - SHX outlet	T962	°C	31.29	0.40	0.50	30.86	0.98	M	30.83	1.07	M	30.80	1.17	M

Note)

M – Minimal

E – Excellent

Table 1-23: Secondary heat exchanger – steady state no.3

No.	Parameter	Sensor	Unit	Ref. value	Accuracy [%]	Acceptable error [%]	VUJE RELAP5-3D ver. 4.3.4	Calculated error [%]	Judgment	BME APROS ver. 6.12	Calculated error [%]	Judgment	CVR Řež DYMOLA	Calculated error [%]	Judgment
1	He temperature - inner leg II.C	T602	°C	101.40	0.40	0.50	100.80	0.19	E	101.40	0.00	E		100.00	M
2	He pressure in the PHX - II.C (Cerabar S PMP71)	P604	MPa	3.05	0.25	0.10	3.00	1.23	M	3.05	0.00	E	3.05	0.00	E
3	He mass-flow rate - inner leg II.C (differential pressure Torbar)	F601	kg/s	0.50	2.50	2.00	0.50	0.00	E	0.50	0.00	E	0.50	0.00	E
4	He temperature - outer leg II.C - SHX outlet	T631	°C	50.14	0.40	0.50	51.06	1.43	M	50.10	0.00	E	53.30	5.88	M
5	Water inlet temperature (Pt100)	T991	°C	21.75	0.62	0.50	21.75	0.00	E	21.80	0.00	E	21.80	0.00	E
6	Water inlet pressure (Cerabar PMP11)	P991	MPa	0.57	0.25	0.10	0.57	0.00	E	0.57	0.00	E	0.57	0.00	E
7	Water flow rate in SHX (Promag 10L80)	F962	kg/s	2.80	0.00	2.00	2.80	0.00	E	2.79	0.30	E	2.80	0.06	E
8	Water temperature - SHX outlet	T962	°C	32.54	0.40	0.50	32.57	0.00	E	32.61	0.00	E	32.50	0.00	E

Table 1-24: Secondary heat exchanger – steady state no.4

No.	Parameter	Sensor	Unit	Ref. value	Accuracy [%]	Acceptable error [%]	VUJE RELAP5-3D ver. 4.3.4	Calculated error [%]	Judgment	BME APROS ver. 6.12	Calculated error [%]	Judgment	CVR Řež DYMOLA	Calculated error [%]	Judgment
1	He temperature - inner leg II.C	T602	°C	223.20	0.40	0.50	223.10	0.00	E	223.20	0.00	E		100.00	M
2	He pressure in the PHX - II.C (Cerabar S PMP71)	P604	MPa	3.71	0.25	0.10	3.70	0.00	E	3.71	0.00	E	3.71	0.00	E
3	He mass-flow rate - inner leg II.C (differential pressure Torbar)	F601	kg/s	0.19	2.50	2.00	0.19	0.00	E	0.19	0.00	E	0.19	0.00	E
4	He temperature - outer leg II.C - SHX outlet	T631	°C	60.41	0.40	0.50	62.36	2.82	M	60.40	0.00	E	62.80	3.54	M
5	Water inlet temperature (Pt100)	T991	°C	21.61	0.62	0.50	21.60	0.00	E	21.60	0.00	E	21.60	0.00	E
6	Water inlet pressure (Cerabar PMP11)	P991	MPa	0.56	0.25	0.10	0.56	0.82	M	0.56	0.46	M	0.56	0.46	M
7	Water flow rate in SHX (Promag 10L80)	F962	kg/s	3.61	0.00	2.00	3.61	0.00	E	3.60	0.41	E	3.61	0.13	E
8	Water temperature - SHX outlet	T962	°C	32.29	0.40	0.50	32.20	0.00	E	32.35	0.00	E	32.30	0.00	E

Note)

M – Minimal

E – Excellent

1.8 STEADY STATE evaluation

The PHX and SHX TH models, validated in the previous step have been merged into the complex S-Allegro TH models. The details are described in the chapters 6.1, 6.2 and 6.3.

The calculation of the steady state no. S-S_2306-01 and S-S_2306-02 was performed by the RELAP5-3D, APROS and DYMOLA codes. The results of both steady state runs are summarized in the Table 1-25 and Table 1-26. Here bellow the evaluation of the most important steady state results is presented.

Generally speaking, APROS (BME) model prediction is the one being most coherent with the measurement. The reason is mostly due to the fact the BME incorporated the thermal bridges into the primary and secondary system allowing to reach exact initial conditions. The RELAP5-3D and DYMOLA models does not use these bridges involved. Therefore the resulting steady states are less coherent with the measurement.

Without the thermal bridges involved it would not be possible to reach the measured steady state. Based on this observation it is clear that a thermal bridges are present or there is internal helium leakage between the inner and outer ducts. However their precise identification based on the measurements have not been performed yet. Separate tests are needed to identify and quantify the thermal bridges in S-Allegro loop. Another important factor are the total heat losses that needs to be quantified as well. Here below a short evaluation of the open benchmark and semi-blind benchmark steady state is presented.

S-S_2306-01 – The open benchmark

The initial conditions for the S-S_2306-01 have been defined in Table 1-4. The results of all steady state runs are presented in Table 1-25.

The primary system initial mass flow (F101) is clearly underestimated in the APROS model. Considering the constant core power and constant heat removal in PHX and SHX it contributes to higher core heat up (dT). Concerning other models, the RELAP5-3D and DYMOLA, the primary system mass flow predictions are coherent with measurement. However the RELAP5-3D model overestimates the F101 value. This contributes to lower temperatures in the primary and secondary circuits.

The exit temperature from the core (T900) is well predicted by APROS and RELAP5-3D. The DYMOLA prediction of T900 is overestimated, which is clearly result of the overestimation of inlet core temperature (T131). The influence of "artificial" thermal bridge considered in APROS model is well visible in prediction of the PHX inlet temperature (T102). While in RELAP5-3D and DYMOLA model the T900 and T102 are of the same value the APROS T102 value (still coherent with the measurement), dropped by 18 °C compared to T900 value. This clearly indicates some real thermal bridge between hot to the cold primary duct or inside the PHX inlet dome.

Another problem is linked to the RELAP5-3D code ver. 4.3.4. The SHX outlet temperature T631 is largely overestimated while the other codes predictions are consistent with the measurement. In RELAP5-3D run the T631 should have been artificially elevated by the user in order to complete the transient calculation. The error was identified in the RELAP5-3D ver. 4.3.4 leading to wrong prediction of the sound speed value in the compressor component inlet volume. The code developer was contacted to fix this issue. Forced overestimation of the T631 in RELAP5-3D run led to the overestimation of the initial PHX exit temperature (T132) on primary side.

SS-_2306-02 – Semi blind benchmark

The initial conditions for the S-S_2306-02 have been defined in Table 1-5. The results of all steady state runs are presented in Table 1-26. Only a limited number of input values have been made available for participants. Those are marked in bold letters and by *). The results have been evaluated quantitatively and all values outside the criteria of acceptability defined in Chapter 1.4 were marked as M-minimal. The values marked as E-excellent have been within the range of acceptability.

The RELAP5-3D initial temperatures (T900, T102, T131, T132, T601, T602, T633) are clearly overestimated. The reason is the same as described in evaluation of SS_2306-01 steady state. The T631 (SHX outlet temperature) is artificially controlled far above the desired values of 60 °C by the user in order to complete TR_2306-02 RELAP5-3D code run. The error was identified in the RELAP5-3D ver. 4.3.4 leading to wrong prediction of the sound speed value in the compressor component inlet volume. The angular velocity and mass flow rate are entered as relative values, corrected to rated stagnation sound speed and density. It was observed that as the compressor inlet temperature decrease to less than ~ 80 °C the calculation stops followed by the error message *'Negative square root in sound speed computation for compressor upstream volume'* which is clearly not true. The result of T631 overestimation leads to overestimation of all temperature values in the S-Allegro system in RELAP5-3D run.

In DYMOLA (CVR) run the helium mass flow rate (F101) was underestimated. This leads to overestimation of core dT, core exit temperature and consequently all other temperature values in primary system. The primary system pressure (P101) is underestimated in DYMOLA run.

For the APROS (BME) model it can be concluded that most of the steady state values are in very good agreement with the measurement. It is, among other things, the result of the application of thermal bridges in the model that clearly exists in real S-Allegro ITF.

Table 1-25: Steady state S-S_2306-01 results

No.	Parameter	Sensor	Unit	Ref. value	Accuracy [%]	Acceptable error [%]	VUJE RELAP5-3D ver. 4.3.4	Calculated error [%]	Judgment	BME APROS ver. 6.12	Calculated error [%]	Judgment	CVR Řež DYMOLA	Calculated error [%]	Judgment
1	He temperature - inner leg I.C	T101	°C	361.30	0.40	0.50	367.28	1.25	M	358.69	0.32	E	378.16	4.25	M
2	He pressure - inner leg I.C (Cerabar S PMP71)	P101	MPa	5.26	0.25	0.10	5.25	0.00	E	5.26	0.00	E	5.22	0.57	M
3	He mass-flow rate - inner leg I.C (differential pressure Torbar)	F101	kg/s	0.25	2.50	0.50	0.25	0.00	E	0.24	0.58	M	0.25	0.00	E
4	He temperature - outer leg I.C	T131	°C	166.50	0.40	0.50	175.38	4.91	M	166.14	0.00	E	183.99	10.06	M
5	He temperature - outer leg I.C - PHX outlet	T132	°C	159.20	0.40	0.50	174.55	9.21	M	159.93	0.06	E	183.45	14.77	M
6	He temperature - inner leg I.C - PHX inlet	T102	°C	352.10	0.40	0.50	367.30	3.90	M	352.68	0.00	E			
7	Primary circulator speed	TC01	rpm	25288.00	0.00	1.00	25287.97	0.00	E	25290.00	0.01	E	25288.00	0.00	E
8	Primary circulator PR (Deltabar S PMD 75)	dP01	kPa	18.10	0.05	10.00	15.98	11.67	M	16.90	6.58	E	19.63	8.40	E
9	He temperature - inner leg I.C - RV outlet	T900	°C	370.10	0.40	0.50	367.47	0.31	E	369.08	0.00	E	378.31	1.81	M
10	He temperature - inner leg I.C - RV outlet	T905	°C	367.30	0.40	0.50	363.50	0.64	M	366.21	0.00	E			
11	He temperature - RV downcomer (circumferentially)	T853	°C	169.50	0.40	0.50	176.40	3.66	M	171.13	0.56	M			
12	He temperature - above the hydraulic resistor	T908	°C	361.30	0.40	0.50	363.60	0.24	E	369.08	1.75	M			
13	Heating power	POW	kW	0.25	0.50	2.00	0.25	0.00	E	0.25	0.00	E	0.25	0.00	E
14	He temperature - outer leg II.C - PHX inlet	T633	°C	96.30	0.40	0.50	100.00	3.43	M	96.06	0.00	E	86.40	9.92	M
15	He temperature - inner leg II.C - PHX outlet (differential pressure Torbar)	T601	°C	281.40	0.40	0.50	291.54	3.19	M	281.59	0.00	E	279.70	0.20	E
16	He temperature - inner leg II.C	T602	°C	274.30	0.40	0.50	291.39	5.81	M	274.44	0.00	E	279.52	1.50	M
17	He pressure - inner leg II.C (Cerabar S PMP71)	P603	MPa	4.00	0.25	0.10	3.99	0.00	E	4.00	0.00	E	3.99	0.00	E
18	He mass-flow rate - inner leg II.C (differential pressure Torbar)	F601	kg/s	0.25	2.50	2.00	0.25	0.00	E	0.25	0.00	E			
19	Secondary circulator speed	TC02	rpm	23215.62	0.00	1.00	23215.62	0.00	E	23216.00	0.00	E			
20	Secondary circulator PR (Deltabar S PMD 75)	dP02	kPa	9.83	0.05	10.00	9.35	4.84	E	9.80	0.26	E			
21	He temperature - outer leg II.C - SHX outlet	T631	°C	80.90	0.40	0.50	99.12	22.04	M	80.78	0.00	E	85.51	5.28	M
22	Water temperature - SHX outlet	T962	°C	42.20	0.40	0.50	41.28	1.79	M	42.09	0.00	E			
23	Water flow rate in SHX (Promag 10L80)	F962	kg/s	2.78	0.00	2.00	2.88	3.68	M	2.77	0.20	E			
24	Water inlet temperature (Pt100)	T991	°C	20.70	0.62	0.50	20.70	0.00	E	20.70	0.00	E			
25	Water inlet pressure (Cerabar PMP11)	P991	MPa	0.49	0.25	0.10	0.49	0.00	E	0.49	0.00	E			

Table 1-26: Steady state S-S_2306-02 results

No.	Parameter	Sensor	Unit	Ref. value	Accuracy [%]	Acceptable error [%]	VUJE RELAP5-3D ver. 4.3.4	Calculated error [%]	Judgment	BME APROS ver. 6.12	Calculated error [%]	Judgment	CVR Řež DYMOLA	Calculated error [%]	Judgment
1	He temperature - inner leg I.C	T101	°C	226.10	0.40	0.50	263.50	16.08	M	229.31	1.02	M	227.40	0.17	E
2	*) He pressure - inner leg I.C (Cerabar S PMP71)	P101	Mpa	4.48	0.25	0.10	4.47	0.00	E	4.48	0.00	E	4.43	0.87	M
3	*) He mass-flow rate - inner leg I.C (differential pressure Torbar)	F101	kg/s	0.25	2.50	0.50	0.25	0.00	E	0.25	0.00	E	0.24	1.54	M
4	He temperature - outer leg I.C	T131	°C	107.30	0.40	0.50	146.80	36.27	M	115.79	7.48	M	114.79	6.55	M
5	He temperature - outer leg I.C - PHX outlet	T132	°C	102.20	0.40	0.50	146.00	42.29	M	111.78	8.94	M	114.25	11.35	M
6	He temperature - inner leg I.C - PHX inlet	T102	°C	220.70	0.40	0.50	262.10	18.29	M	225.93	1.96	M	227.30	2.58	M
7	*) Primary circulator speed	TC01	rpm	26759.00	0.00	1.00	26759.00	0.00	E	26759.00	0.00	E	26759.00	0.00	E
8	*) Primary circulator PR (Deltabar S PMD 75)	dP01	kPa	21.50	0.05	10.00	15.42	28.23	M	17.70	17.63	M	18.09	15.82	M
9	He temperature - inner leg I.C - RV outlet	T900	°C	230.60	0.40	0.50	263.50	13.81	M	235.13	1.56	M	227.40	0.99	M
10	He temperature - inner leg I.C - RV outlet	T905	°C	229.20	0.40	0.50	263.50	14.51	M	233.52	1.48	M	227.40	0.39	E
11	He temperature - RV downcomer (circumferentially)	T853	°C	106.70	0.40	0.50	150.00	40.02	M	118.57	10.68	M	110.60	3.24	M
12	He temperature - above the hydraulic resistor	T908	°C	222.00	0.40	0.50	263.60	18.27	M	235.13	5.49	M	227.40	2.02	M
13	*) Heating power	POW	kW	151.60	0.50	2.00	151.64	0.00	E	151.60	0.00	E	151.60	0.00	E
14	He temperature - outer leg II.C - PHX inlet	T633	°C	66.90	0.40	0.50	100.00	48.88	M	68.71	2.30	M	62.28	6.53	M
15	He temperature - inner leg II.C - PHX outlet (differential pressure Torbar)	T601	°C	177.80	0.40	0.50	216.20	21.11	M	184.21	3.20	M	180.50	1.11	M
16	He temperature - inner leg II.C	T602	°C	178.20	0.40	0.50	216.10	20.79	M	179.85	0.52	M	180.40	0.83	M
17	*) He pressure - inner leg II.C (Cerabar S PMP71)	P603	MPa	3.50	0.25	0.10	3.50	0.00	E	3.50	0.00	E	3.49	0.01	E
18	*) He mass-flow rate - inner leg II.C (differential pressure Torbar)	F601	kg/s	0.25	2.50	2.00	0.25	0.00	E	0.25	0.00	E	0.25	0.00	E
19	*) Secondary circulator speed	TC02	rpm	24027.00	0.00	1.00	24027.00	0.00	E	24027.00	0.00	E	30206.00	25.72	M
20	*) Secondary circulator PR (Deltabar S PMD 75)	dP02	kPa	10.50	0.05	10.00	6.30	39.97	M	9.43	10.15	M	21.00	99.90	M
21	He temperature - outer leg II.C - SHX outlet	T631	°C	58.10	0.40	0.50	99.32	70.27	M	59.11	1.33	M	61.43	5.31	M
22	Water temperature - SHX outlet	T962	°C	33.80	0.40	0.50	84.72	149.65	M	33.81	0.00	E	33.80	0.00	E
23	*) Water flow rate in SHX (Promag 10L80)	F962	kg/s	2.78	0.00	2.00	0.57	79.48	M	2.77	0.20	E	2.78	0.00	E
24	*) Water inlet temperature (Pt100)	T991	°C	20.70	0.62	0.50	20.70	0.00	E	20.70	0.00	E	20.70	0.00	E
25	*) Water inlet pressure (Cerabar PMP11)	P991	MPa	0.49	0.25	0.10	0.50	1.79	M	0.49	0.00	E	0.49	0.00	E

1.9 ON TRANSIENT evaluation

TR_2306-01 – open benchmark

The transient TR_2306-01 lasts 6000 s and it was initiated from the SS_2306-01 steady state. The primary system loop compressor speed (TC01) was reduced at ~490 s. The speed dropped from ~25276 rpm (490 s) to about ~ 21076 rpm (690s) and then gradually decreased to ~20600 rpm (1530s). Mass flow rate in primary system (F101) dropped from 0.25 kg/s to 0.2 kg/s in ~310 s. The heating core power (POW) decreased at ~600 s from 250 kW to ~200 kW. The second event occurred in 3740 s when the heating power suddenly dropped from 210 kW to 99 kW in 50 s and then recovered.

The heating power (POW) and primary system compressor speed (TC01) dependence over time were used as a boundary condition for the simulation of TR_2306-01.

The primary system mass flow (F101) decrease leads to heating core exit temperature (T900) increase from initial 371 °C to ~396 °C (820 s). Later, since ~1200 s T900 stabilizes at 374 °C due to heating power (POW) decrease from 250 kW to ~200 kW. Consequence of heating core power (POW) swing at 3740 s the T900 decrease and recovers. The primary and secondary system pressure (P101, P603) are gradually decreasing due to heating core power (T900) decrease and as a consequence of system heat losses to ambient.

The visual comparison among RELAP5-3D, APROS, and DYMOLA runs and S-Allegro data are shown in Figure 1-39 to Figure 1-52.

From the quantitative point of view the accuracy of predictions is mostly influenced by the inconsistency in steady state initial conditions which were discussed in the previous chapter.

For RELAP5-3D simulation the largest inconsistency is a result of identified error in the code which was documented and reported to the code developer. After obtaining the fixed RELAP5-3D code the scenario will be re-run for the purpose of the further publication. As a consequence of this core error the SHX exit temperature (T631) had to be artificially elevated in order to complete the calculation. Without this user measure the calculation would trip on the 'Negative square root in sound speed computation for compressor upstream volume'. This is clearly non-physical as the values of all parameters necessary for sound speed computation are positive. The direct consequence of this measure, all related temperatures (T131, T102, T601, T602, T633) are overestimated. The helium initial mass flowrate (F101) is correct but later the value is overestimated which contributes to lower heating core dT and underestimation of heating core exit temperature (T900).

The APROS simulation is quantitatively and qualitatively most consistent with the S-ALLEGRO measurement. The reason is that APROS model has incorporated supposed thermal bridges of S-Allegro technology which have not been clearly identified yet. The definition of the thermal bridges as assumed in the APROS calculation are closely described in APROS model description.

In DYMOLA simulation the major distortions are a result of the inconsistency in initial conditions. The initial temperatures along the primary system loop are largely overestimated, RV outlet (T900), PHX inlet (T102), heating core inlet (T131), PHX outlet (132). Later during the transient the difference among the calculation and measurement is less visible. The primary system pressure (P101) is largely underestimated and decreasing gradient is higher than in measurement. This can be result of overestimation of total heat losses in primary system with effect on primary system temperatures. On the other hand the secondary system temperatures are mostly underestimated, except T631. The secondary system pressure (P603) is overestimated. Lower primary pressure P101 and higher secondary pressure P603 contributes

to lower total heat transfer through the PHX. There is an evident distortion among calculation and measurement of T633. In S-Allegro measurement the secondary compressor temperature rise is ~ 15 °C while in RELAP5-3D and DYMOLA runs it is much lower. It could indicate a thermal bridge in S-Allegro at PHX secondary inlet/outlet.

TR_2306-02 – blind benchmark

The transient TR_2306-02 lasts 10 000 s and was initiated from SS_2306-02 steady state initial conditions. The heating power (POW) change over time, depicted in Figure 1-6, was used as a boundary condition of the simulation. The heating power of 151 kW (370 s) was increased to 171 kW (2880 s) by the automatic control system. At that point the heating power dropped to zero, recovered back to ~140 kW and was further controlled by automatic system.

The quality and accuracy of the simulations were similar to what was described in evaluation of TR_2306-01 above.

The APROS and DYMOLA simulations were both very close to the measured values. In the APROS simulation the supposed thermal bridges implemented helped to improve the consistency with the measurement and therefore the APROS run is one most credible. The DYMOLA primary pressure (P101) is still largely underestimated and the same is true for the He mass flow rate (F101). These parameters are rather important and influences prediction of primary and secondary system temperatures.

The major difference was observed in RELAP5-3D result. The problem with the error in the code persists also in TR_2306-02 run. The T631 initial temperature had to be elevated up to 100 °C (60 °C is required) to complete the calculation. Obviously this measure elevates all the other temperatures in the secondary and primary system. Therefore from the quantitative point of view the RELAP5-3D run cannot be accepted. However from the qualitative point of view the RELAP5-3D run is still valid.

Based on the observation of the blind transient all participant predictions are qualitatively well. Quantitatively the biggest difference was observed in RELAP5-3D run and some distortions have been found also in DYMOLA simulation.
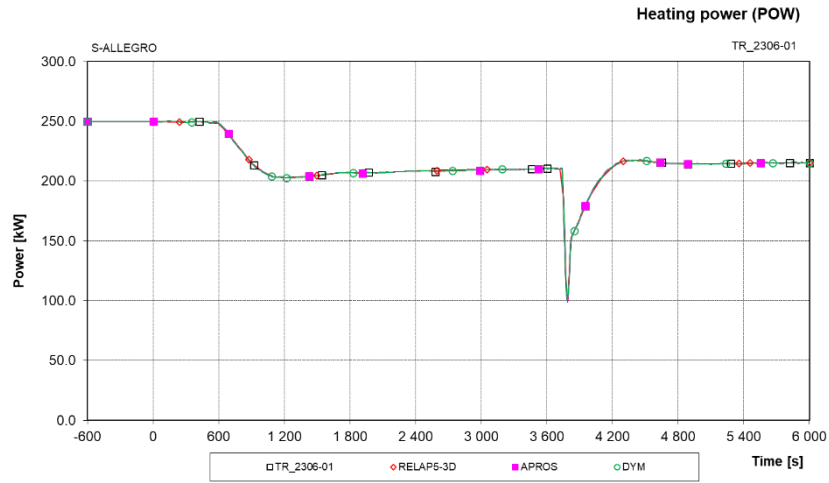
Figure 1-39: TR_2306-01 - Heating power (POW)
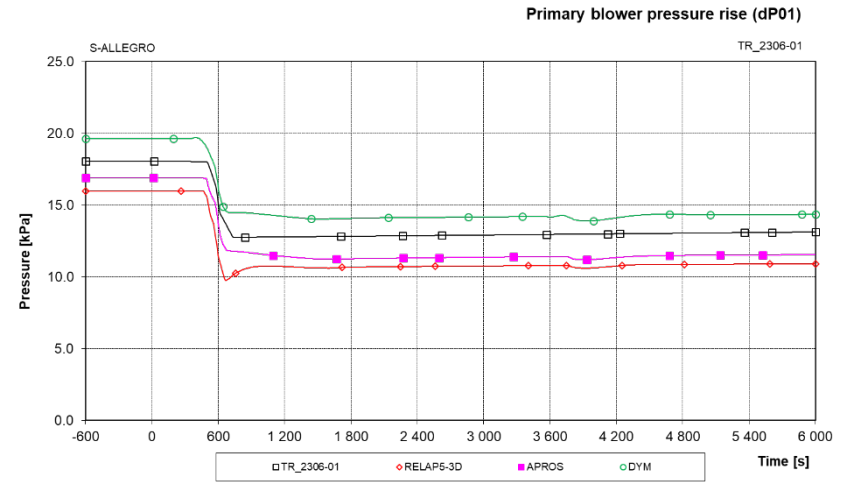
Figure 1-40: TR_2306-01 - Primary blower pressure rise (dP01)
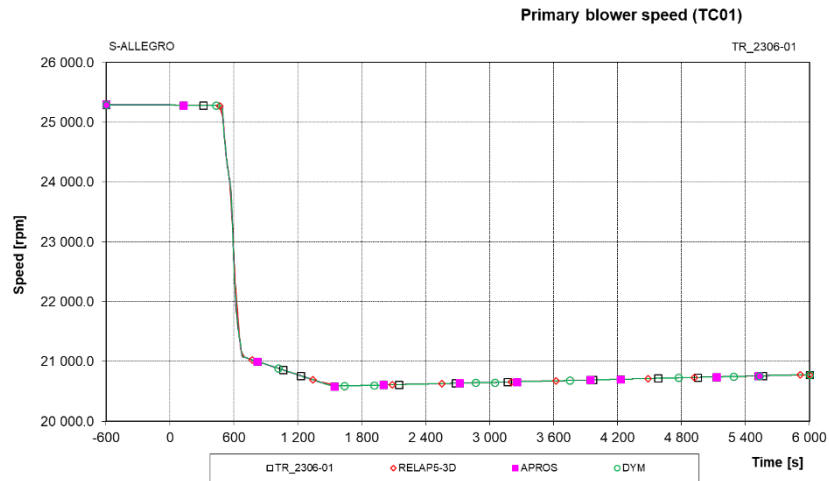
**Figure 1-41: TR_2306-01- Primary blower speed (TC01)**
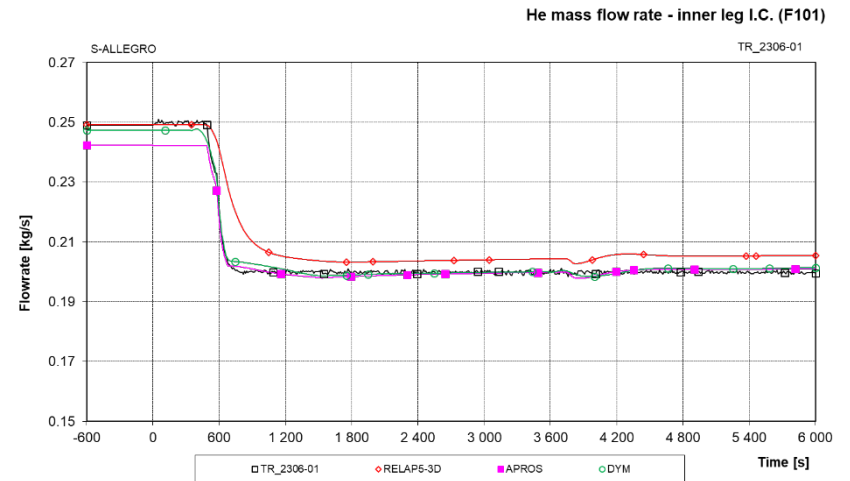
Figure 1-42: TR_2306-01 - He mass flowrate – inner leg I.C. (F101)
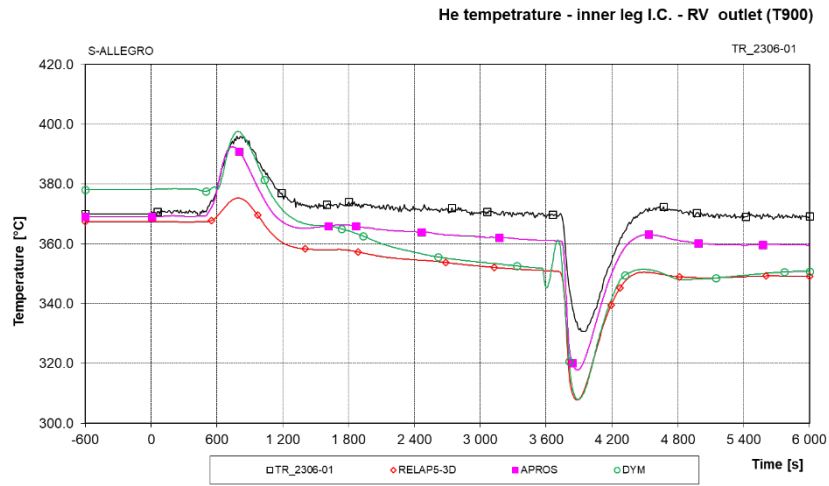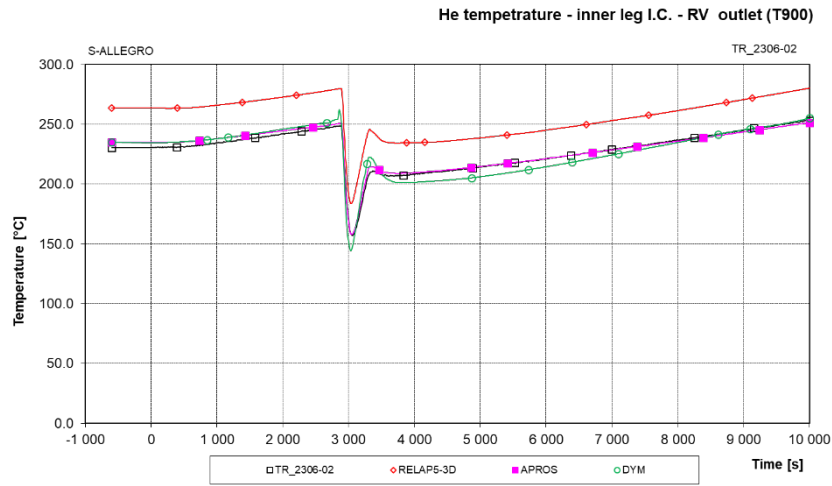
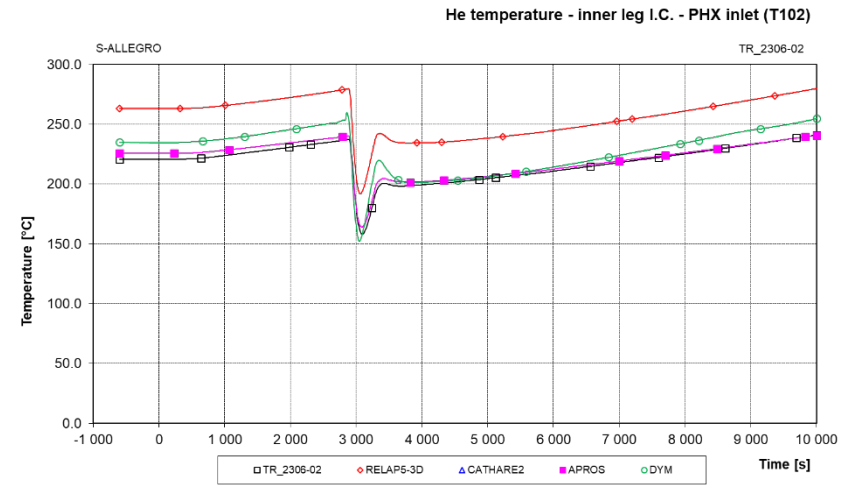**Figure 1-43: TR_2306-01 - He temperature – inner leg I.C. – RV outlet (T900)**
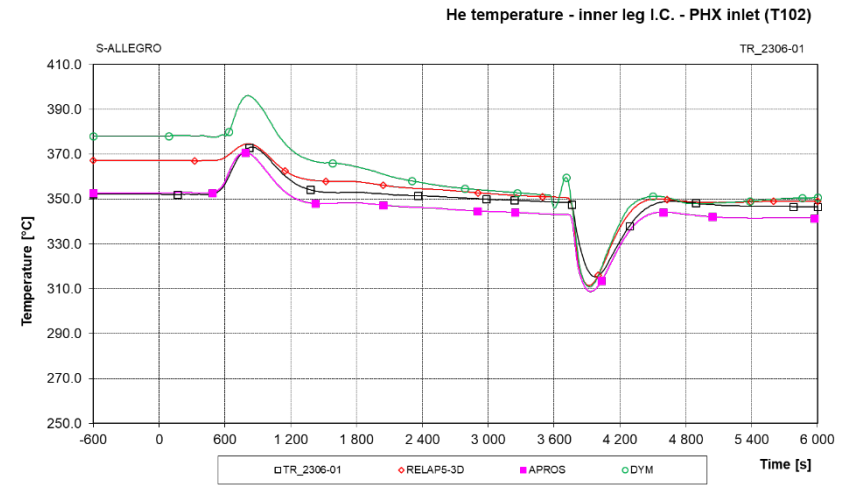
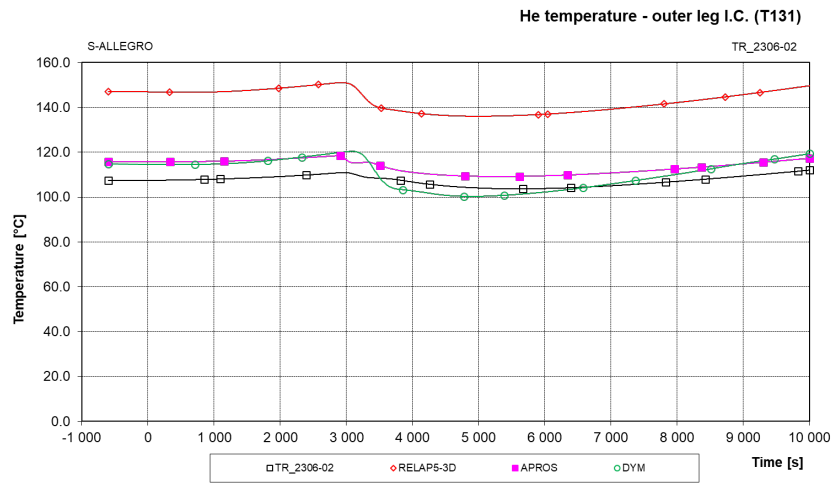**Figure 1-44: TR_2306-01 - He temperature inner leg I.C. – PHX inlet (T102)**
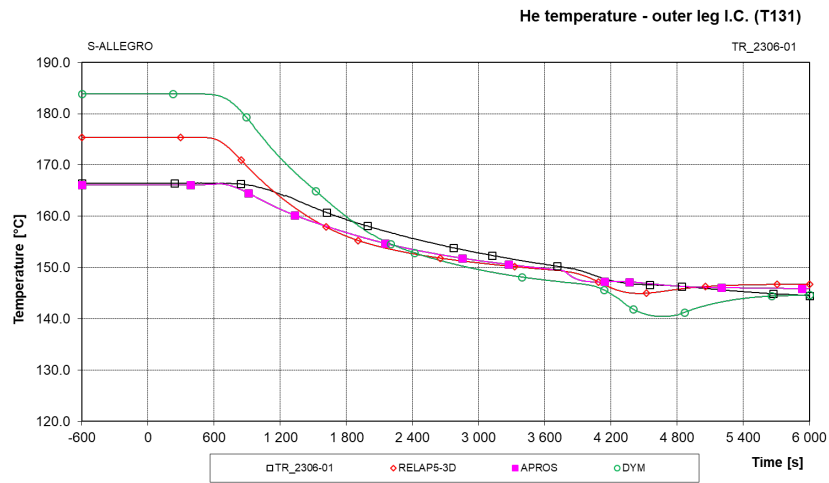
Figure 1-45: TR_2306-01 - He temperature outer leg I.C. (T131)
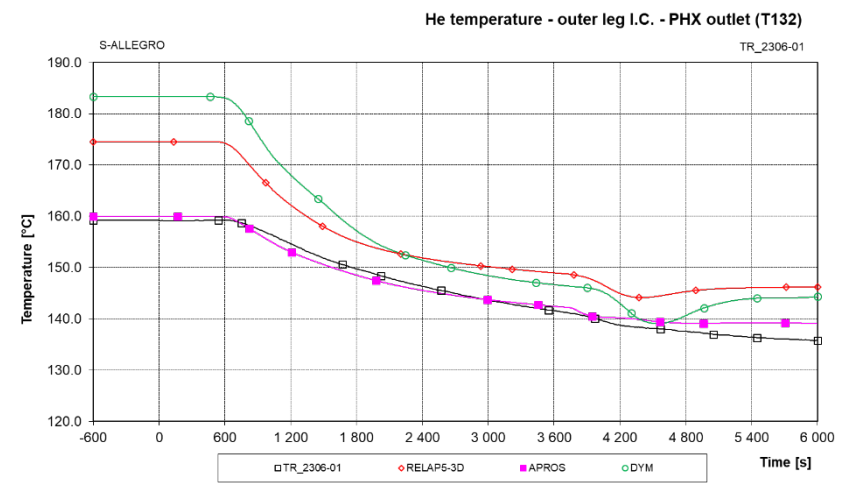
Figure 1-46: TR_2306-01 - He temperature outer leg I.C. - PHX outlet (T132)
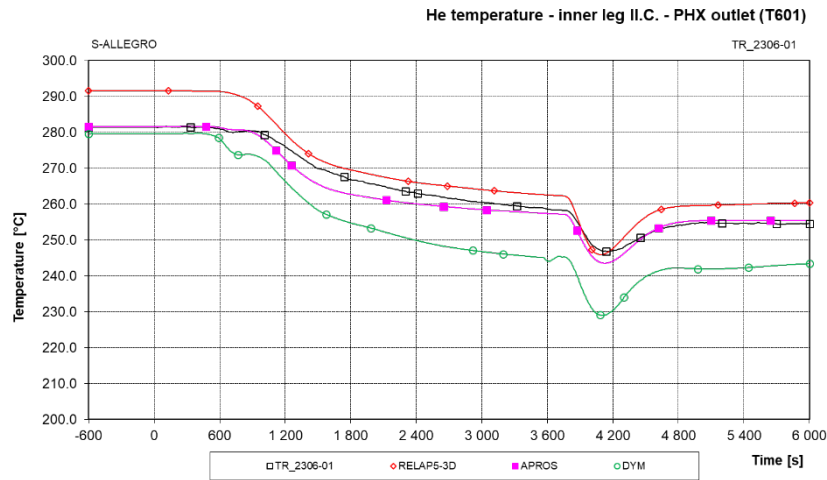
Figure 1-47: TR_2306-01 - He temperature inner leg II.C – PHX outlet (T601)
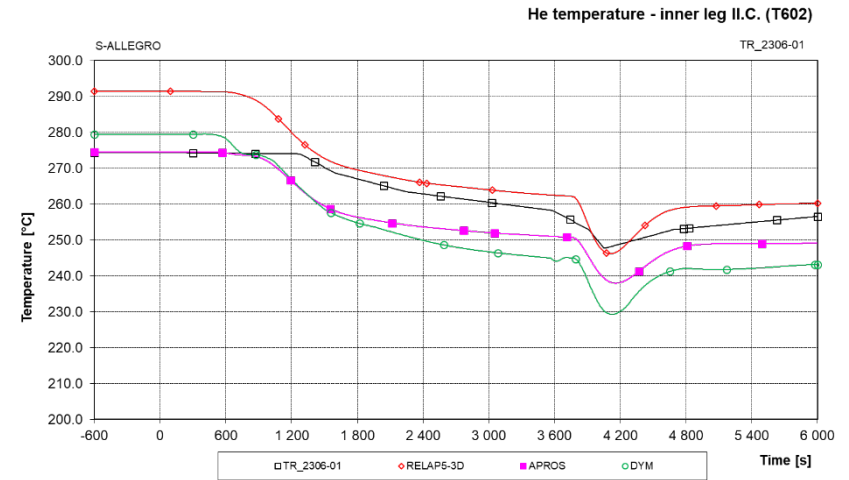
Figure 1-48: TR_2306-01 - He temperature inner leg II.C. (T602)
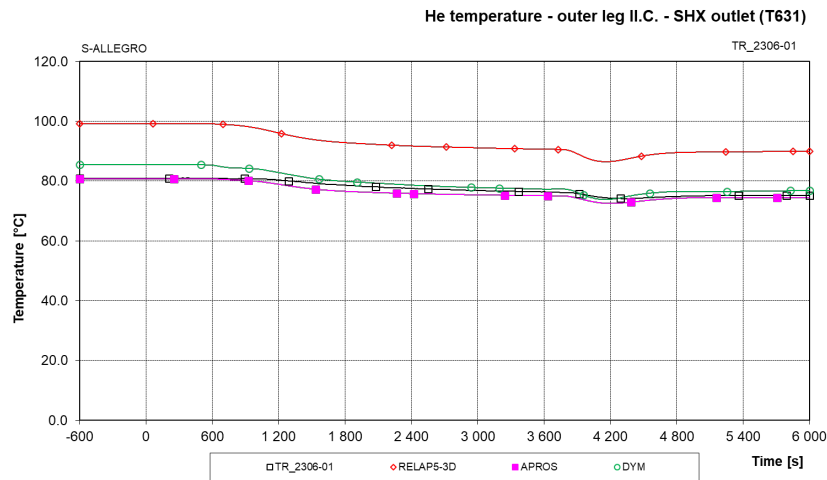
Figure 1-49: TR_2306-01 - He temperature outer II.C. – SHX outlet (T631)
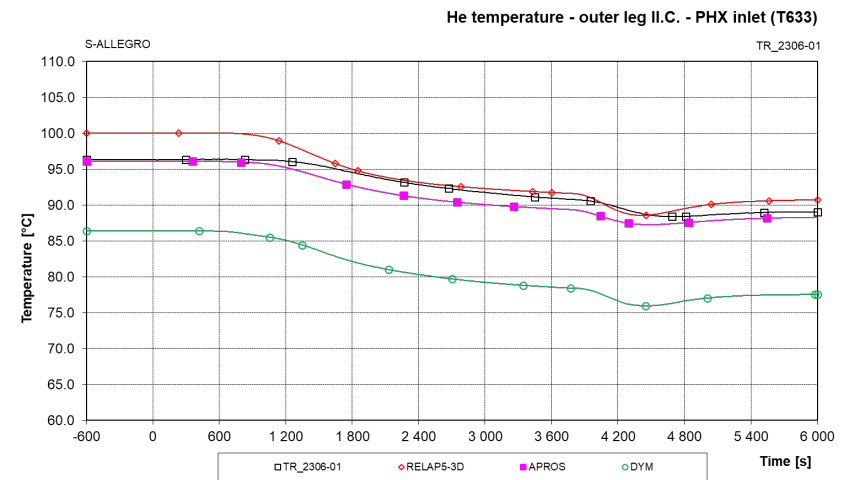
Figure 1-50: TR_2306-01 - He temperature outer leg II.C. – PHX inlet (T633)
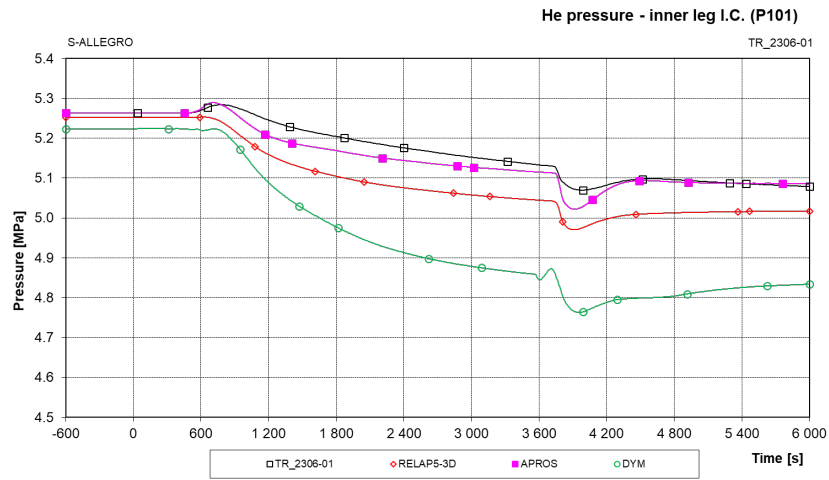
Figure 1-51: TR_2306-01 - He pressure inner leg I.C. (P101)
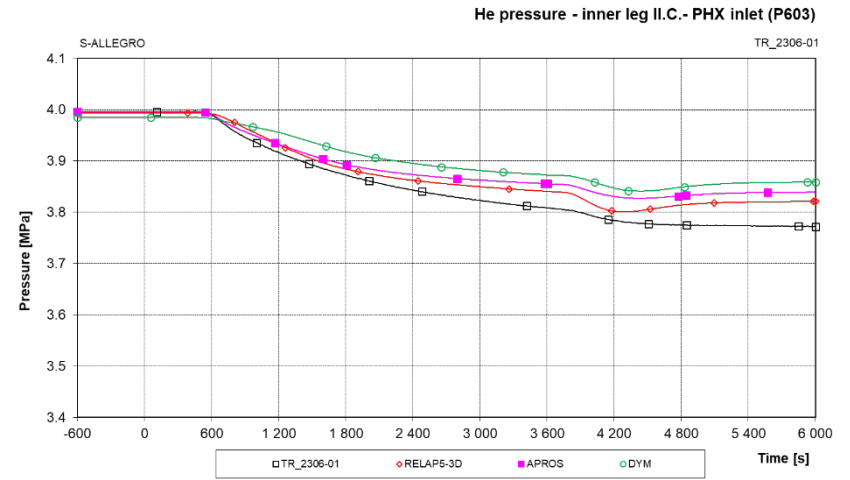
Figure 1-52: TR_2306-01 - He pressure inner leg II.C.- PHX inlet (P603)
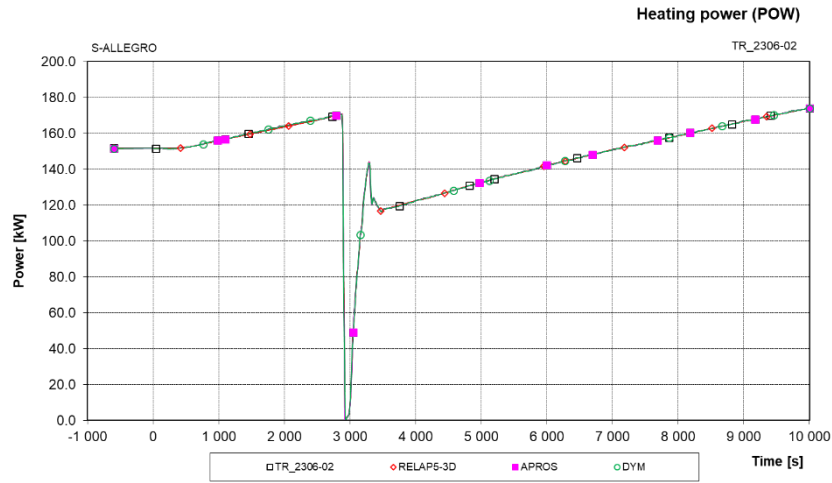
Figure 1-53: TR_2306-02 - Heating power (POW)
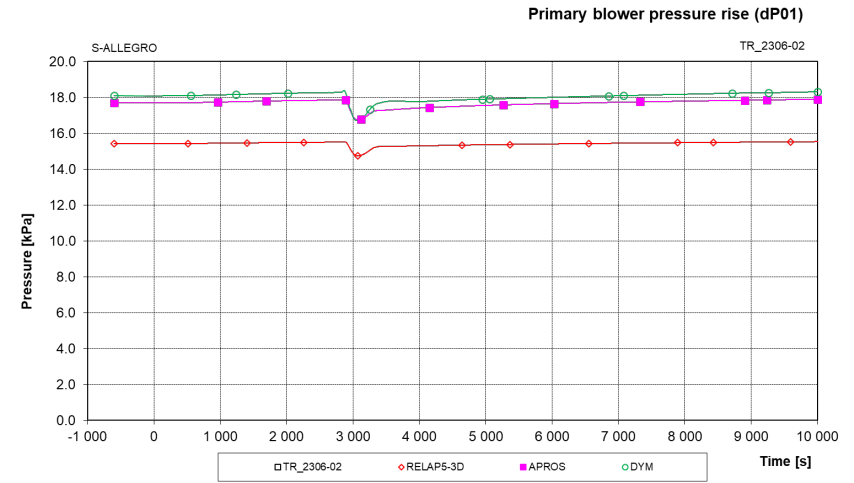
Figure 1-54: TR_2306-02 - Primary blower pressure rise (dP01)
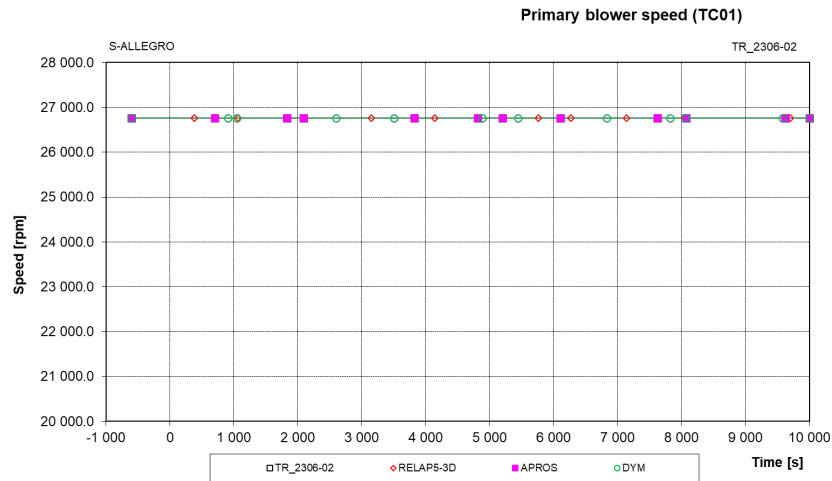
Figure 1-55: TR_2306-02- Primary blower speed (TC01)
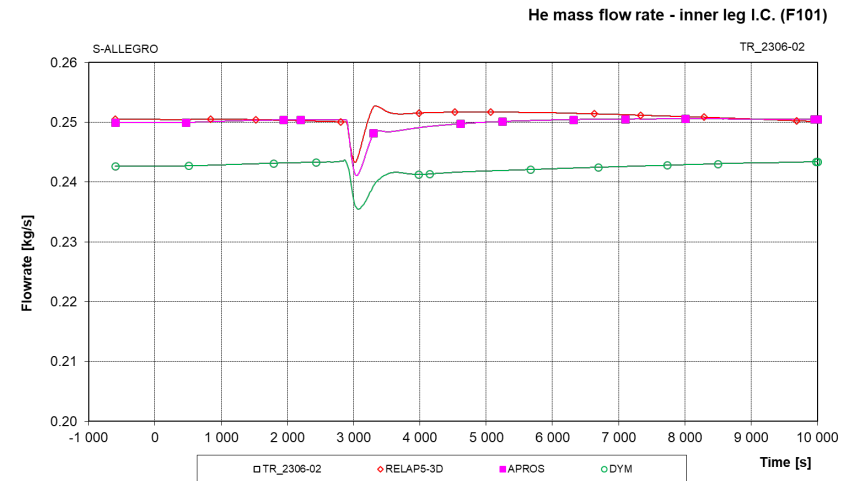
Figure 1-56: TR_2306-02 - He mass flowrate – inner leg I.C. (F101)

Figure 1-57: TR_2306-02 - He temperature – inner leg I.C. – RV outlet (T900)

Figure 1-58: TR_2306-02 - He temperature inner leg I.C. – PHX inlet (T102)

Figure 1-59: TR_2306-02 - He temperature outer leg I.C. (T131)
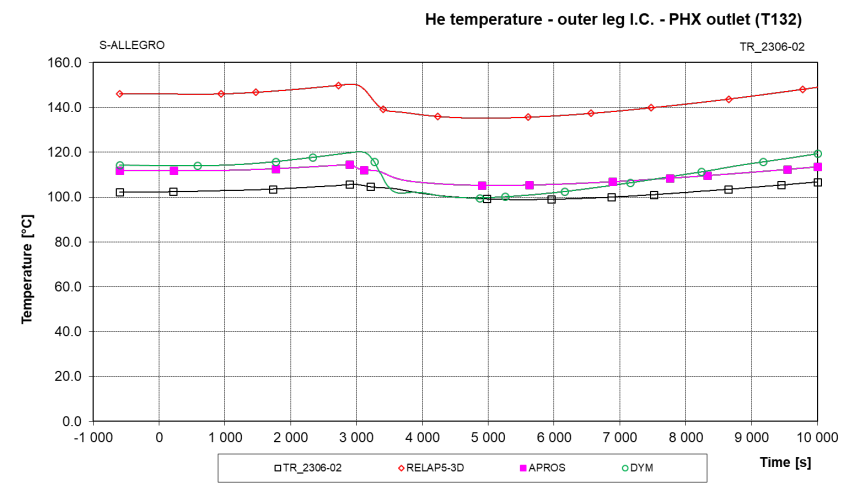
Figure 1-60: TR_2306-02 - He temperature outer leg I.C. - PHX outlet (T132)
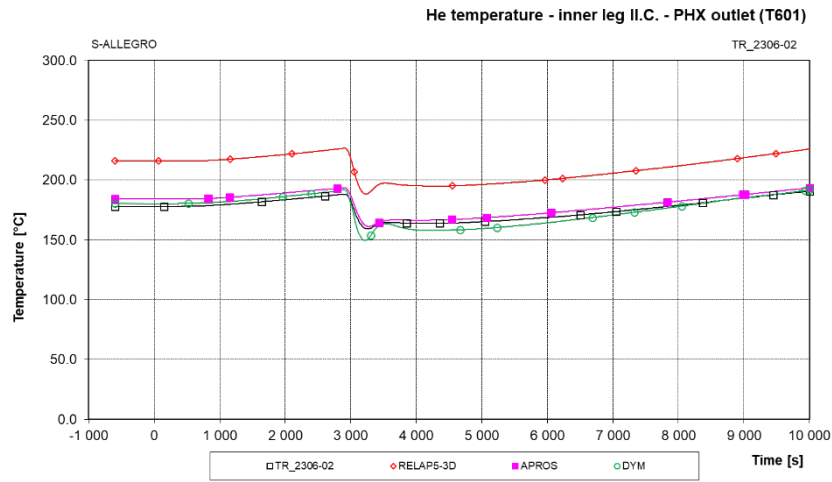
Figure 1-61: TR_2306-02 - He temperature inner leg II.C – PHX outlet (T601)
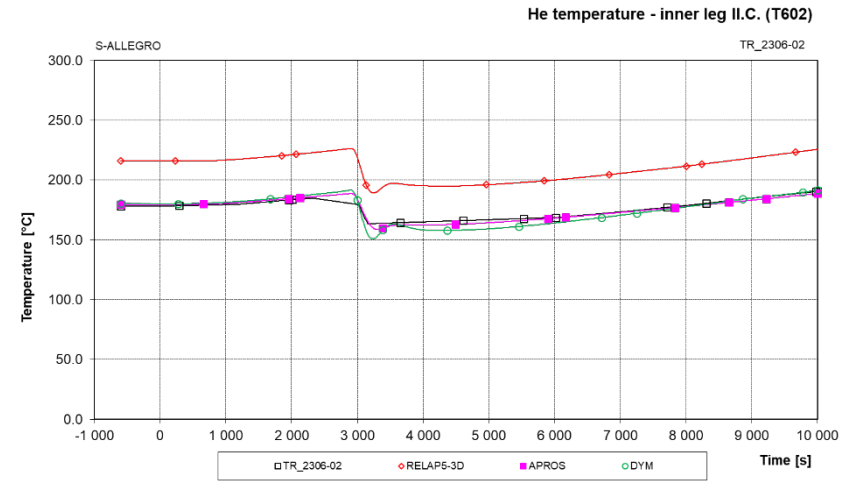
Figure 1-62: TR_2306-02 - He temperature inner leg II.C. (T602)
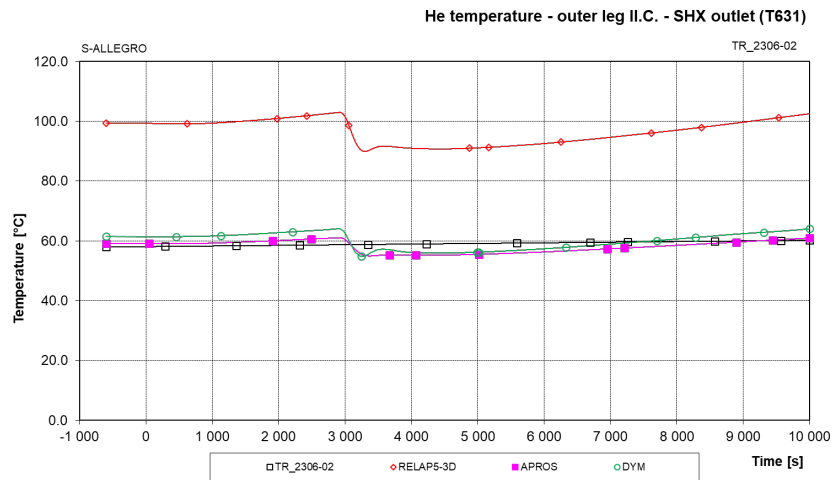
Figure 1-63: TR_2306-02 - He temperature outer II.C. – SHX outlet (T631)
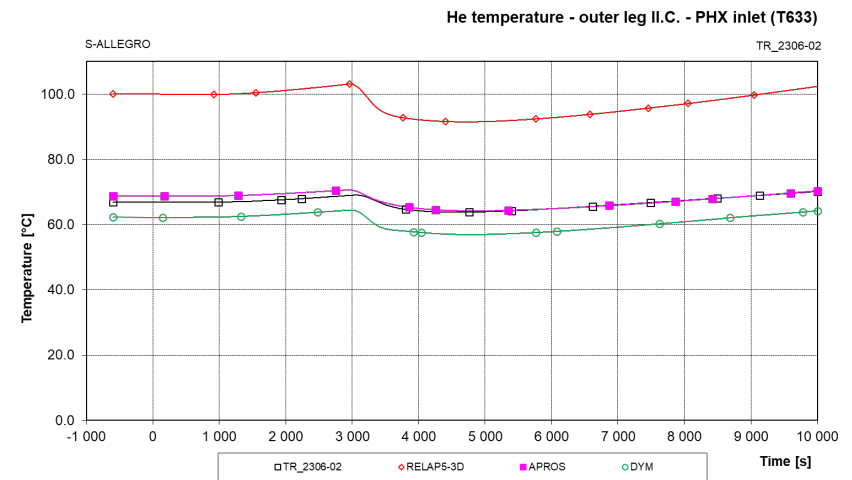
Figure 1-64: TR_2306-02 - He temperature outer leg II.C. – PHX inlet (T633)
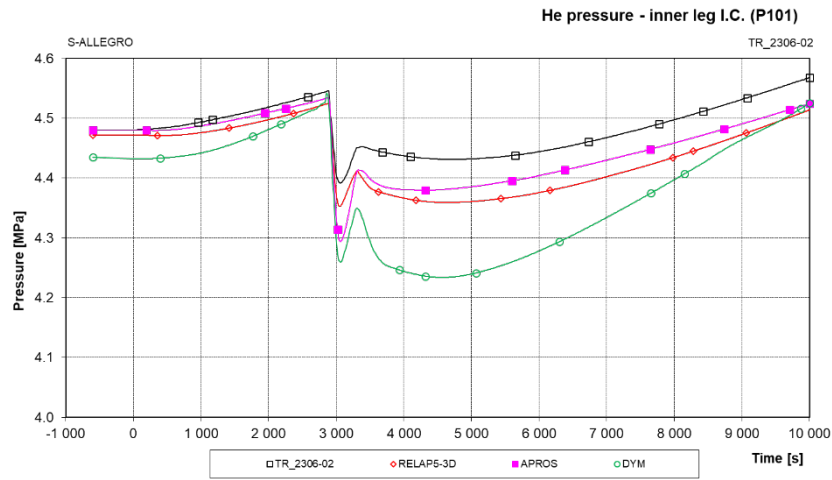
Figure 1-65: TR_2306-02 - He pressure inner leg I.C. (P101)
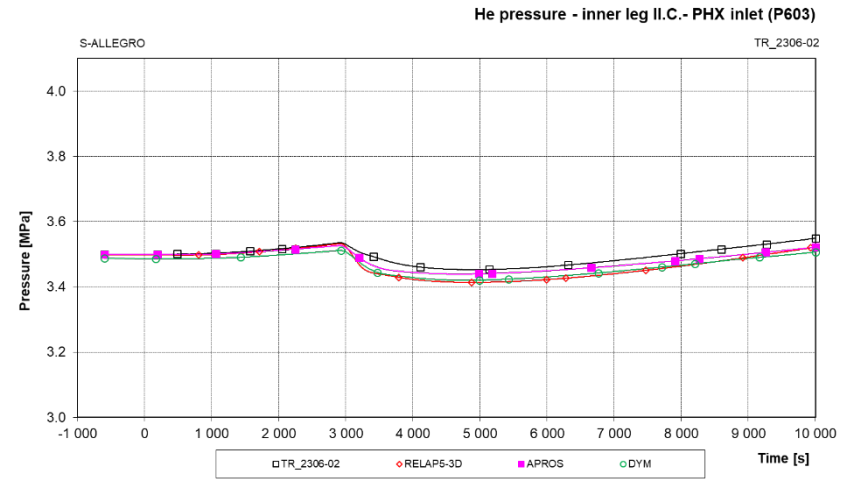
Figure 1-66: He pressure inner leg II.C.- PHX inlet (P603)

1.10 Conclusions

The SafeG project WP5 - Education and Training was focused on direct involvement of students and young professionals. Part of the activity was devoted to the TH benchmark on S-Allegro ITF which is described in this document. The main data for the TH benchmark have been gathered on the S-Allegro integral test facility. Various computational tools have been used including APROS, RELAP5-3D, DYMOLA and CATHARE2 in BME, VUJE, CVR and EK respectively. The goal was to support development of new GFR related computational models or methods and to build/increase computational skills of students and/or young professionals.

The activity have been done in several steps including:

a) Definition of the TH benchmark scenarios,
b) Creation of S-Allegro ITF specific database,
c) Collection of the relevant S-Allegro experimental data
d) Development of the TH models from the scratch
e) Validation and verification of PHX and SHX models
f) Evaluation of accuracy of the steady state runs
g) Evaluation of accuracy of the transient runs

There have been four kinds of data gathered and measured at the S-Allegro ITF utilized for the activity.

a) The description and specification of the S-Allegro design data based on which the corresponding TH models have been created by all involved partners.
b) Steady state data used for the validation of the main S-Allegro components, particularly PHX and SHX.
c) Steady state data for the SS_2306-01 (open) and SS_2306-02 (semi blind) cases.
d) Transient data for the TR_2306-01 (open) and TR_2306-02 (blind) cases.

All these information and data have been collected in [5] .

Finally the computations have been performed by the codes APROS (BME), RELAP5-3D (VUJE) and DYMOLA (CVR). CATHARE2 code was used in EK, the nodalization has been build and used for the validation of PHX and SHX however the steady state and transient runs have not been concluded at the time of D5.4 release. It is expected EK contribution will be part of the dedicated paper to be published.

All the participants prepared a complex models of the S-Allegro facility with detailed and well build nodalization capable to reproduce selected events measured from qualitative point of view. From quantitative point of view discrepancies, some of them substantial, have been identified during the evaluation process and the most relevant are listen bellow.

a) From the visual observation of the S-Allegro measurement and later by the comparison between measured and calculated values it turned out that some inevitable thermal bridges are present in S-Allegro ITF. Those have not been properly identified yet. Namely in the inlet and outlet of the heating core, PHX and SHX components. These thermal bridges have to be addressed and used to improve existing nodalizations during future activities. Thermal bridges have been partially addresses in APROS simulation which substantially increased accuracy of the calculation.

b) In DYMOLA code implementation of some GFR related components is not possible e.g. main blowers and its performance maps. This contributes to some uncertainty in mass flow calculation which has effect on the temperature behavior over time.

c) In RELAP5-3D code a bug was identified producing an error in sound speed computation in adjoin volume of the primary and secondary compressors. The result is that compressor inlet temperature could not decrease to less than ~80 °C without tripping the calculation. In order to avoid it we had to increase temperature by artificial controller to complete the simulation. This however led to substantial increase of all temperatures in primary and secondary system and increased inaccuracy of the run.

Generally the activity of the TH benchmark of S-Allegro ITF met all the expectations and tasks which have been planned at SafeG GA. The new S-Allegro models have been built from scratch, the steady and transient runs were successfully performed and properly evaluated. The students and young professionals from universities and technological institutes have been involved in the activities and increased they knowledge, experience in GFR related technology.

2 CFD BENCHMARK

2.1 Introduction

The thermal-hydraulic benchmarks are organized in SafeG project WP5 – Education and Training. The CFD benchmark was performed on the BME experimental facility PIRUETTE. Three CFD codes were employed on the CFD benchmark (ANSYS Fluent, ANSYS CFX, StarCCM+ and OpenFOAM) by six participants from five institutions (BME, CVR, CTU, UJV and VUJE). The numerical results were compared with the PIV measurement from BME.

The STH benchmark was carried out on S-Allegro facility. TBD

In this report, the numerical results are compared with the experimental data and the comparison is discussed. It should be said that as the activity is performed within the Education and Training WP and budget for this activity is limited, the main purpose is rather educational than scientific and no deep assessment is presented. However, the results of the benchmark might be utilized within the further R&D work in the field of GFR. The CFD benchmark was solved within two consecutive parts ("flow straightener" and "rod bundle") part.

2.2 CFD Benchmark Part 1

The CFD benchmark is evaluated in this section. Three CFD codes were employed on the CFD benchmark (ANSYS Fluent, ANSYS CFX, StarCCM+ and OpenFOAM) by six participants from five institutions (BME, CVR, CTU, UJV and VUJE). The numerical results were compared with the PIV measurement from the PIROUETTE facility of BME. The benchmark description including the domain, experimental facility, parameters and measuring positions is described in details in deliverable D5.3 – Definition of the thermal-hydraulic benchmark. The benchmark is split in two parts, (1) flow straightener located at the beginning of the test section and (2) the rod bundle section.

2.2.1 Models description – flow straightener

The main characteristics of the individual models of the flow straightener part is given in this section. As various information was provided by the benchmark participants, models descriptions are not fully consistent. The geometry of the flow straightener and position of the PIV measurement of shown in Figure 2-1.
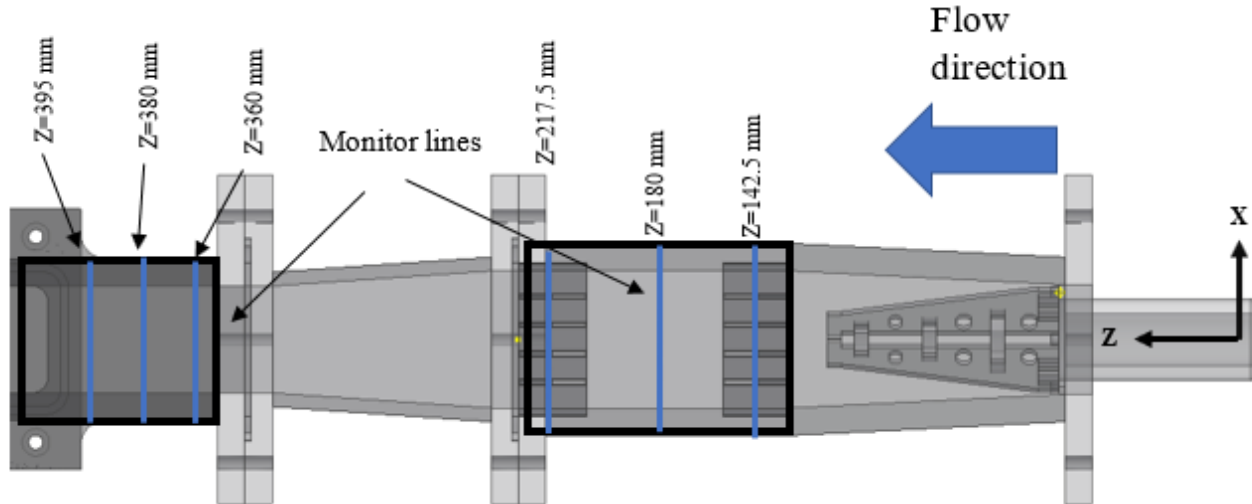
Figure 2-1: Flow straightener geometry

2.2.1.1 Model 1 - OpenFOAM and ANSYS Fluent model of CVR

The first model described in this report was prepared by CVR using combination of ANSYS and OpenFOAM software. The computational geometry and mesh was prepared using ANSYS tools. As a numerical solver, ANSYS Fluent and OpenFOAM were used. Two polyhedral meshed were created with approx. 0.38 M and 5 M mesh elements. The computational grids are shown in Figure 2-2. The mesh parameters are shown in Table 2-1.

Table 2-1: Mesh parameters (Model 1)

	Coarse mesh	**Fine mesh**
Mesh elements no. / nodes no.	0.38 M / 14 M	5 M / 20 M
Cell size	1 – 2 mm	0.7 – 1 mm
Max. aspect ratio	108	229
Min. orthogonal quality	0.058	0.070
Max / Avg. y+	24 / 12	66 / 8.5

COARSE MESH

FINE MESH
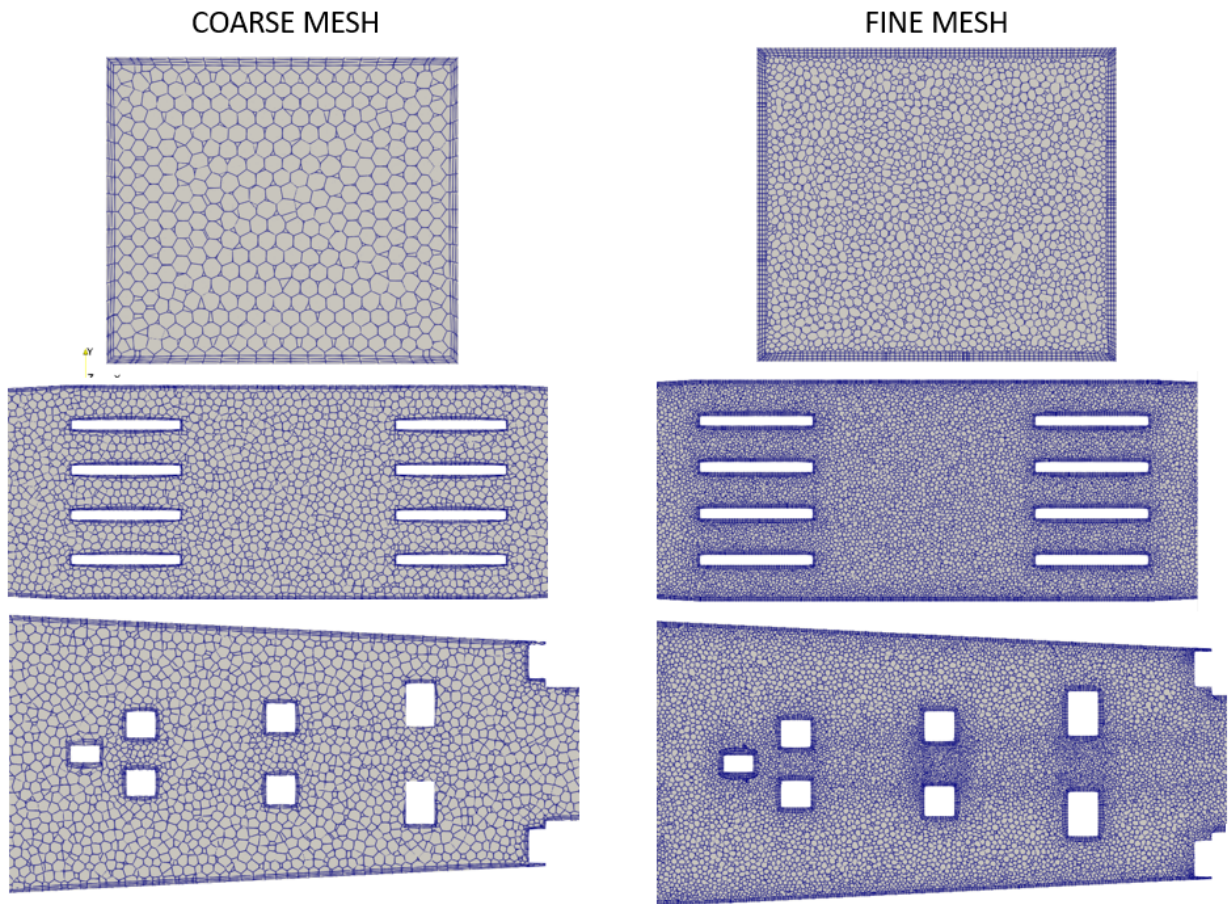
Figure 2-2: Computational mesh (Model 1)

K-epsilon Realisable and RSM with scalable wall functions models of turbulence were used for the Fluent simulation. Pseudo-transient option was enabled. For OpenFOAM, k-epsilon Realisable model with wall functions was used with SIMPLE algorithm. All simulations were run until all residuals reached level below 0.001. Fluent simulation was run on both meshes, the OpenFOAM simulation was only run with the coarse mesh. Contours of velocity distribution are depicted in Figure 2-3.

FLUENT (FINE MESH)   FLUENT (COARSE MESH)   OpenFOAM (COARSE MESH)
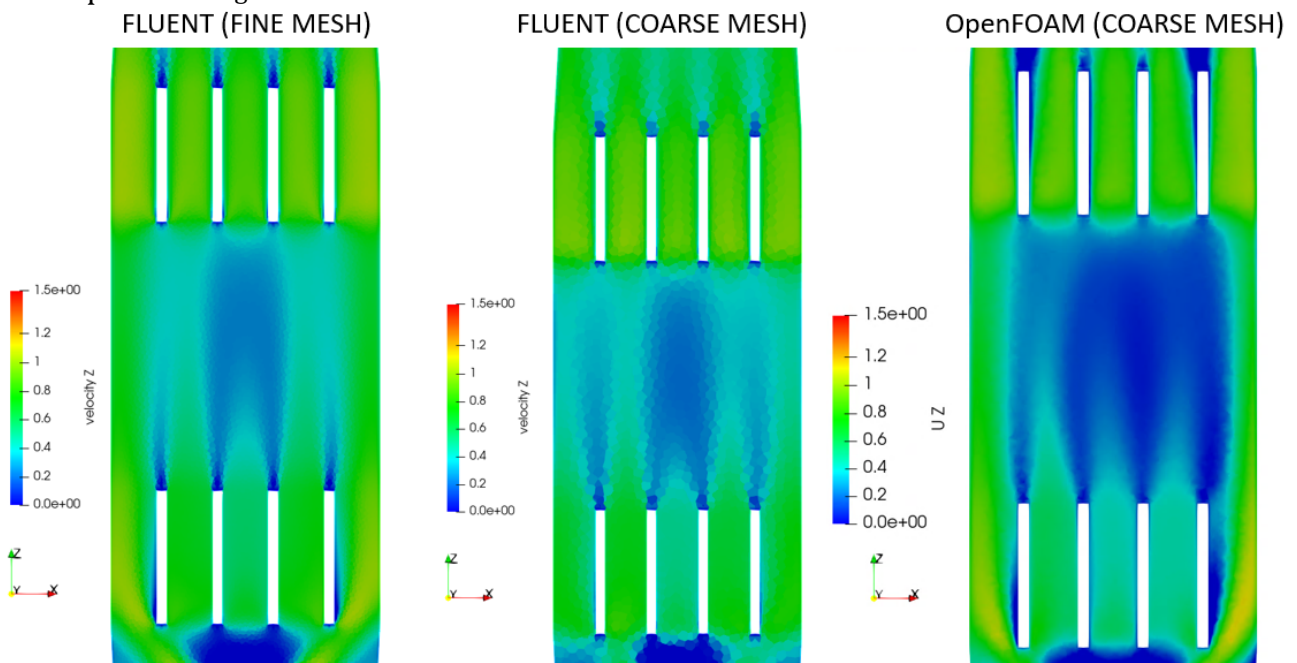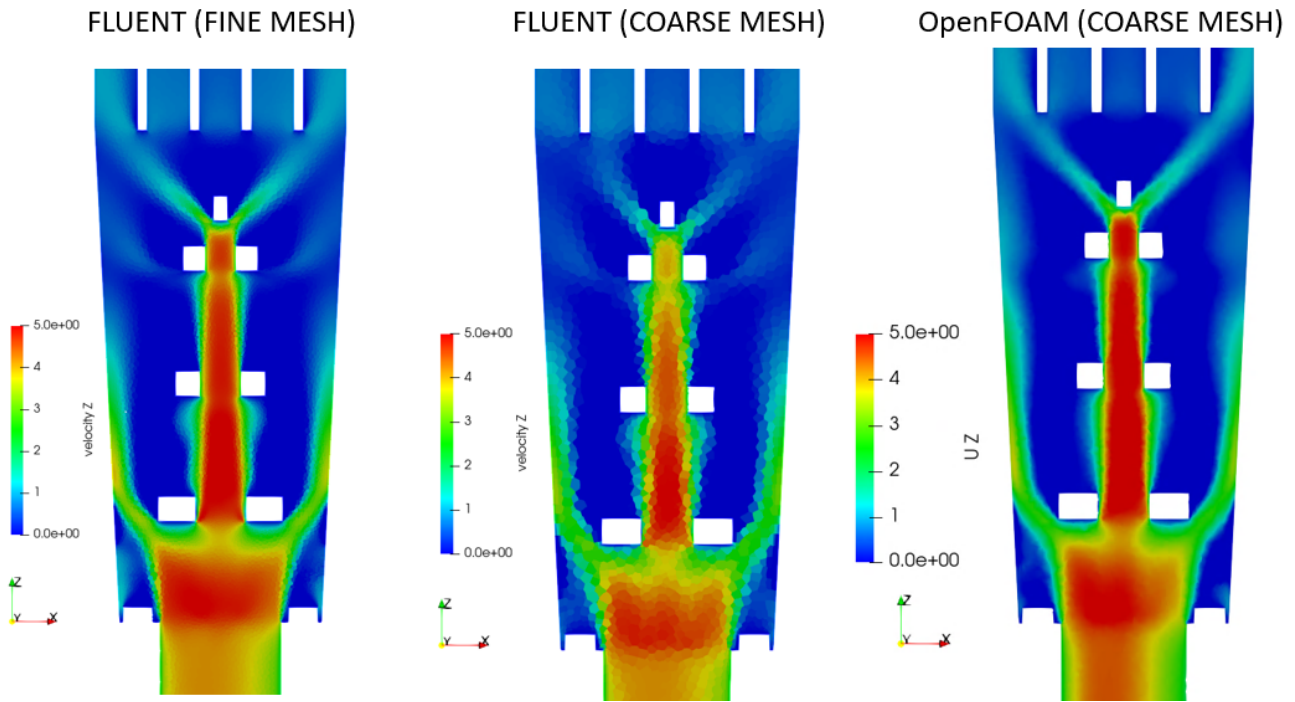
Figure 2-3: Contours of velocity (Model 1)

Numerical results on the predefined lines are compared in Figure 2-4.
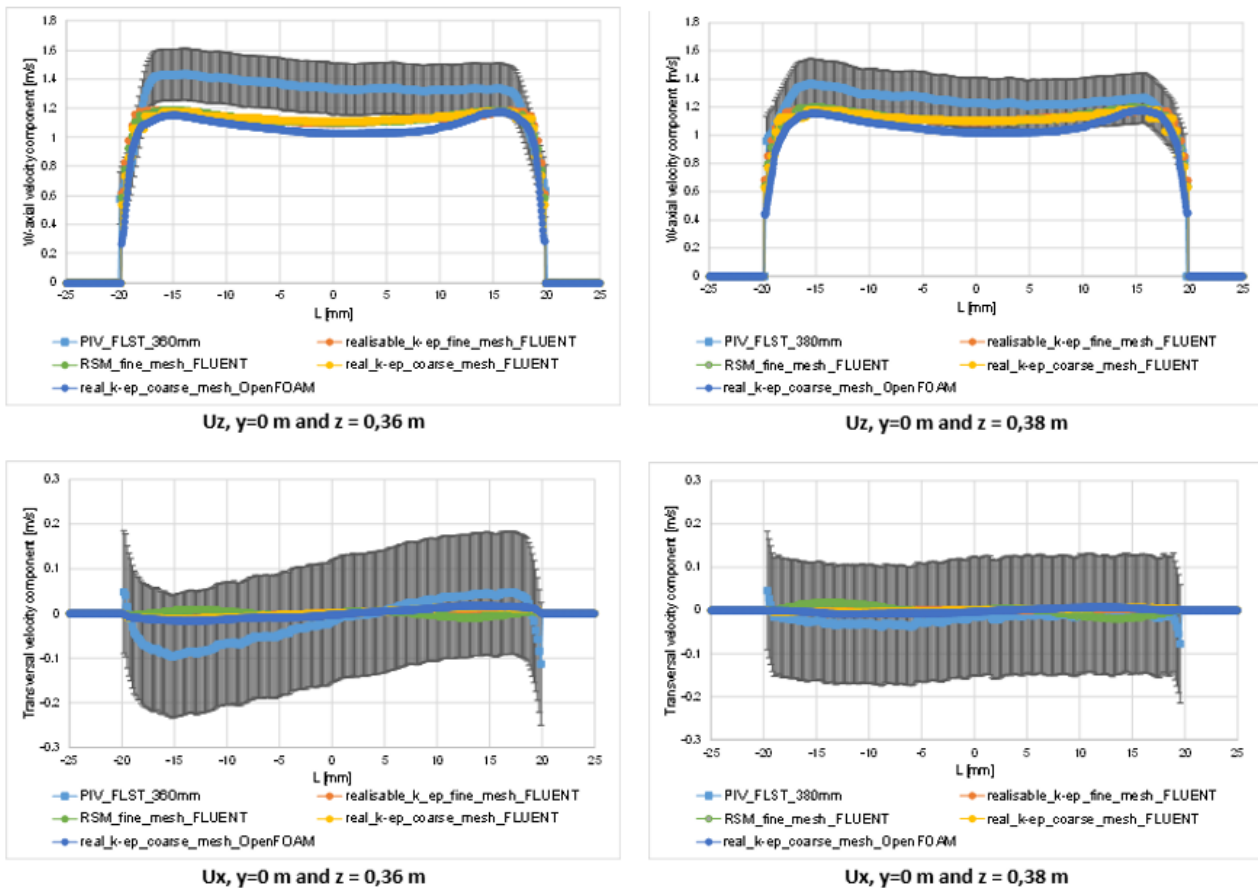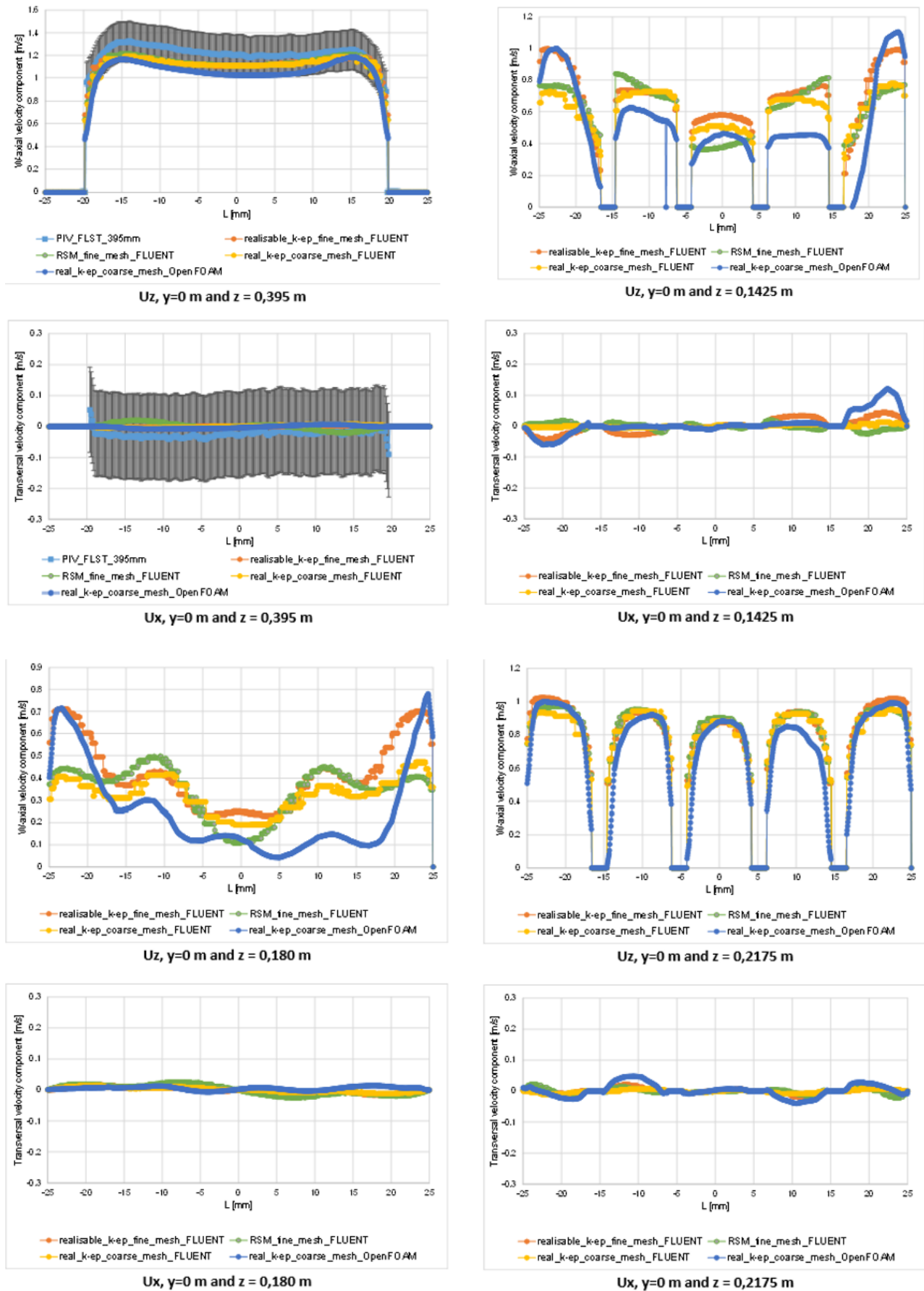
Figure 2-4: Results comparison (Model 1)

2.2.1.2 Model 2 – StarCCM+ model of CTU

StarCCM+ 2022.1 version was used as a numerical solver for model of CTU. A polyhedral mesh with approx. 3.35 M of mesh elements was selected. Max. y+ value is 81 while average value is 19.4. Standard k-epsilon low Re model of turbulence with all y+ wall treatment was used. The final mesh is shown in Figure 2-5.
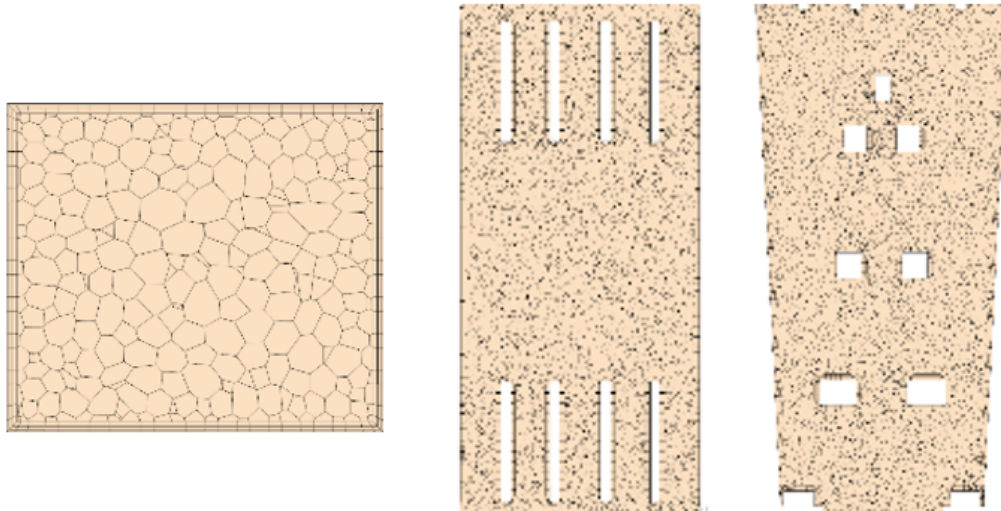
Figure 2-5: Computational mesh (Model 2)

A mesh sensitivity study was carried out with seven different meshes. Comparison if tested meshed compared with the experimental data is shown in Figure 2-6. Mesh 1 and 2 have different mesh sizing (0.5 and 3 mm), other meshes have different setting of the gap mesh / surface mesh.
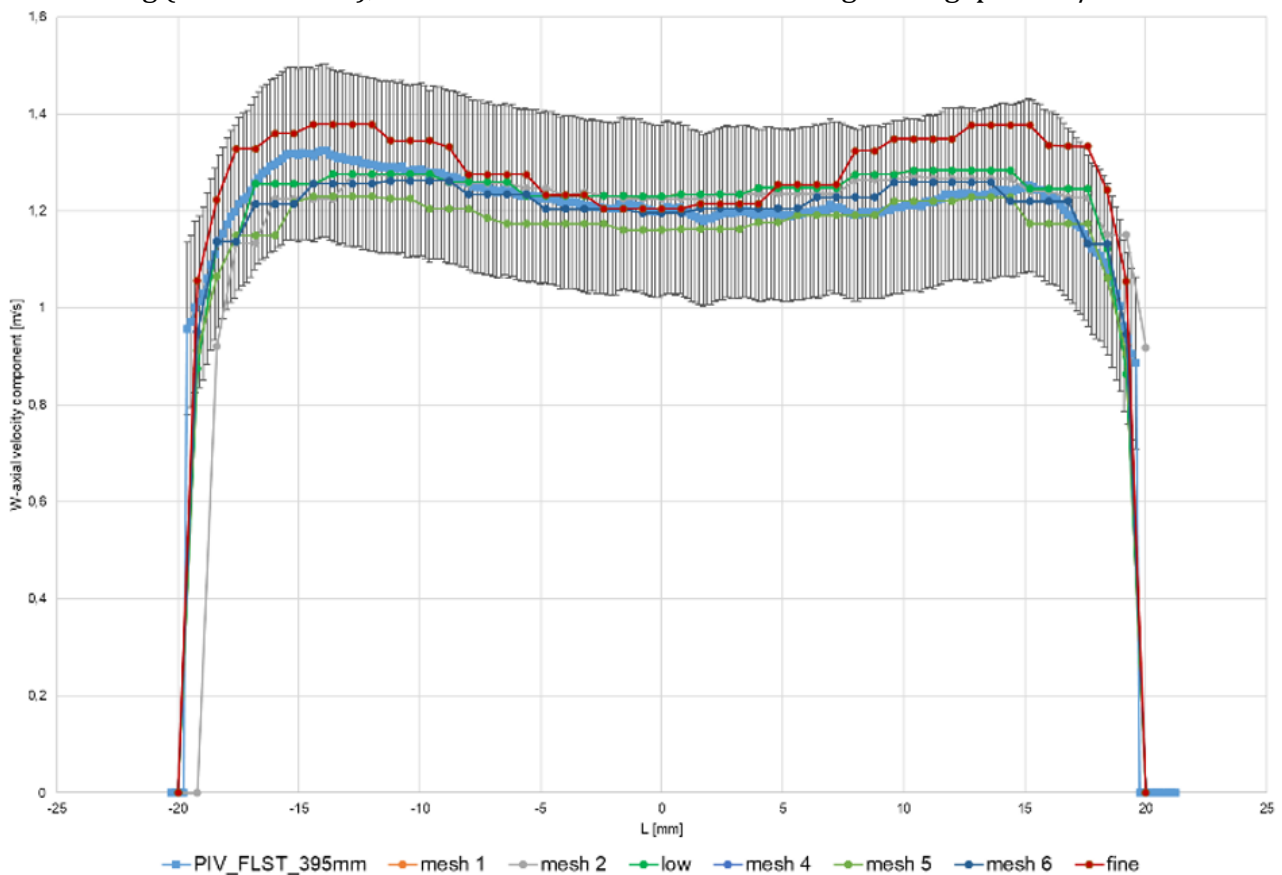
Figure 2-6: Mesh sensitivity study (Model 2)

Simulation was run until 1e-6 residuals level was reached (1000 iterations). Contours of velocity are shown in Figure 2-7.
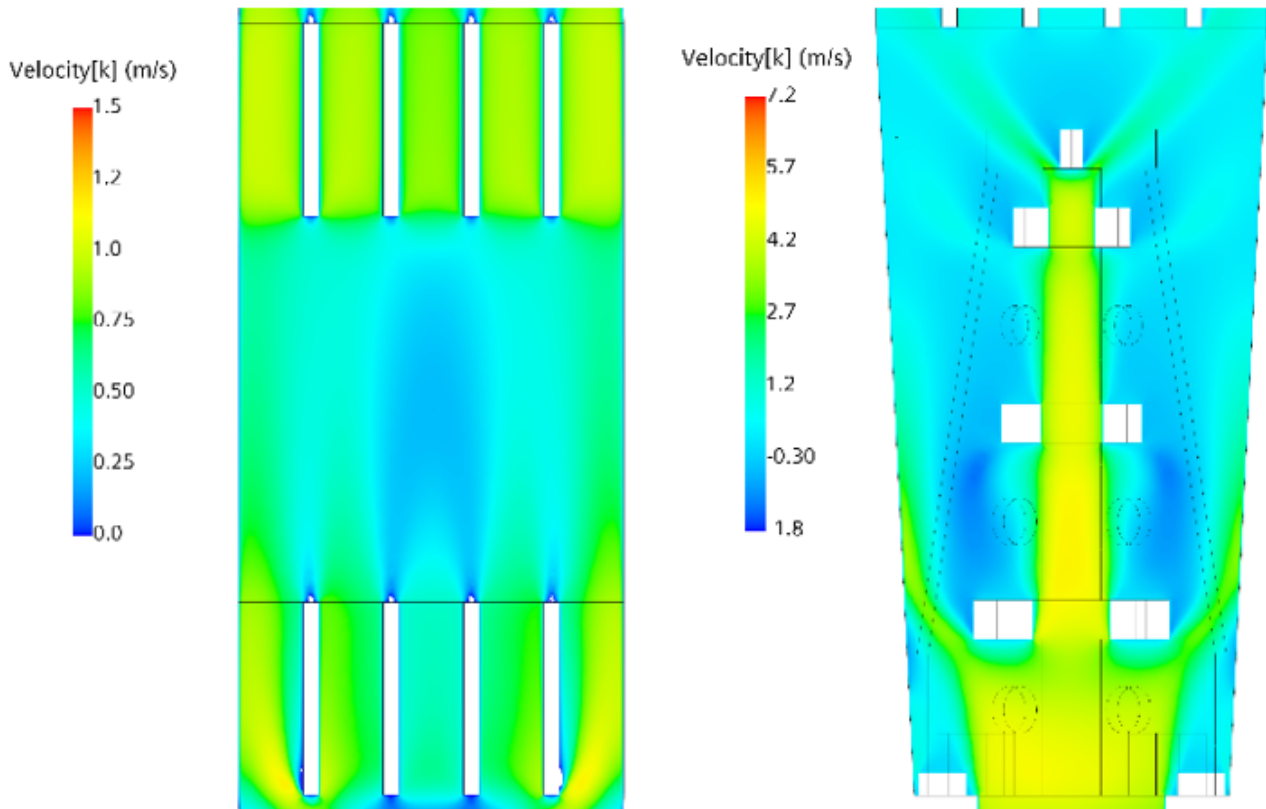
Figure 2-7: Contours of velocity (Model 2)

2.2.1.3   Model 3 – Fluent model of CTU

Another model of CTU used ANSYS Fluent 2021 R2 as numerical solver. Seven polyhedral meshes with size between 0.116 and 0.28 M elements were tested and a mesh with 0.28 M elements was selected. However, relatively low difference was observed between the individual meshes. Max. aspect ratio of the final mesh is 110, min. orthogonal quality is 0.25. Max. / avg. Y+ is 177 and 3.7 respectively. K-omega SST model of turbulence was used. 700 iterations were run with final level of the continuity residual was 0.00226 (other residuals below 1e-4).
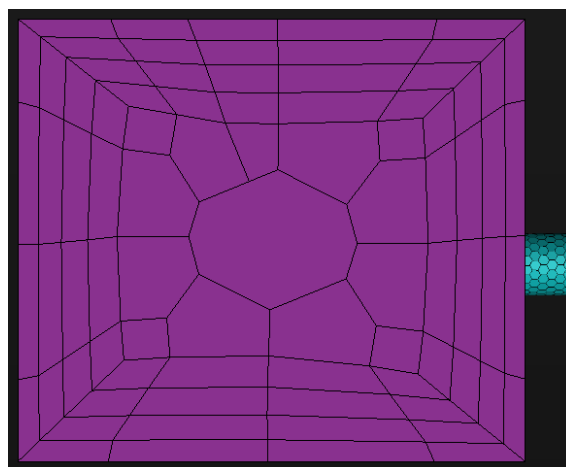
Figure 2-8: Computational mesh (Model 4)
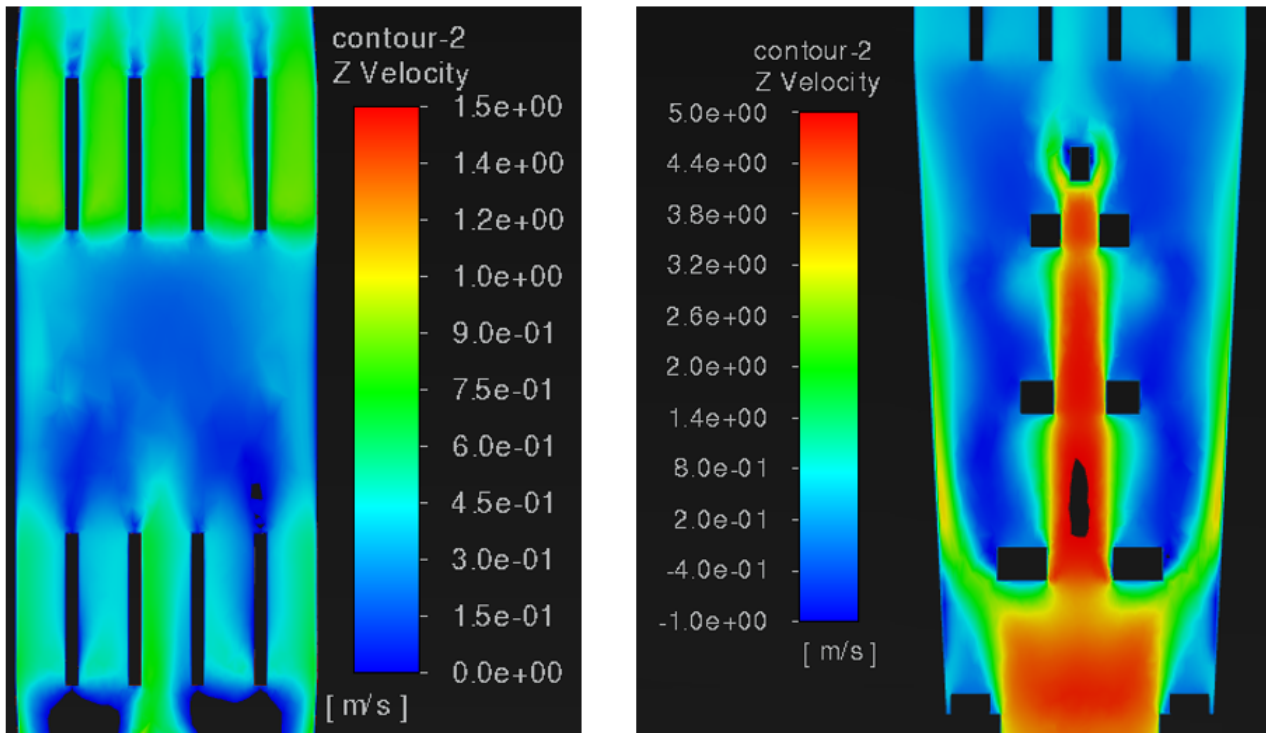
Figure 2-9: Contours of velocity (Model 3)

2.2.1.4 Model 4 – Fluent model of UJV

A model with the use of ANSYS software was prepared by UJV. ANSYS Fluent was used as a numerical solver. Polyhedral mesh was prepared with 7.1 M mesh elements. Max. aspect ratio of the final mesh is 262, min. orthogonal quality os 0.14. Max. Y+ is 48, avg. Y+ is 0.94. The final computational mesh is shown in Figure 2-10.
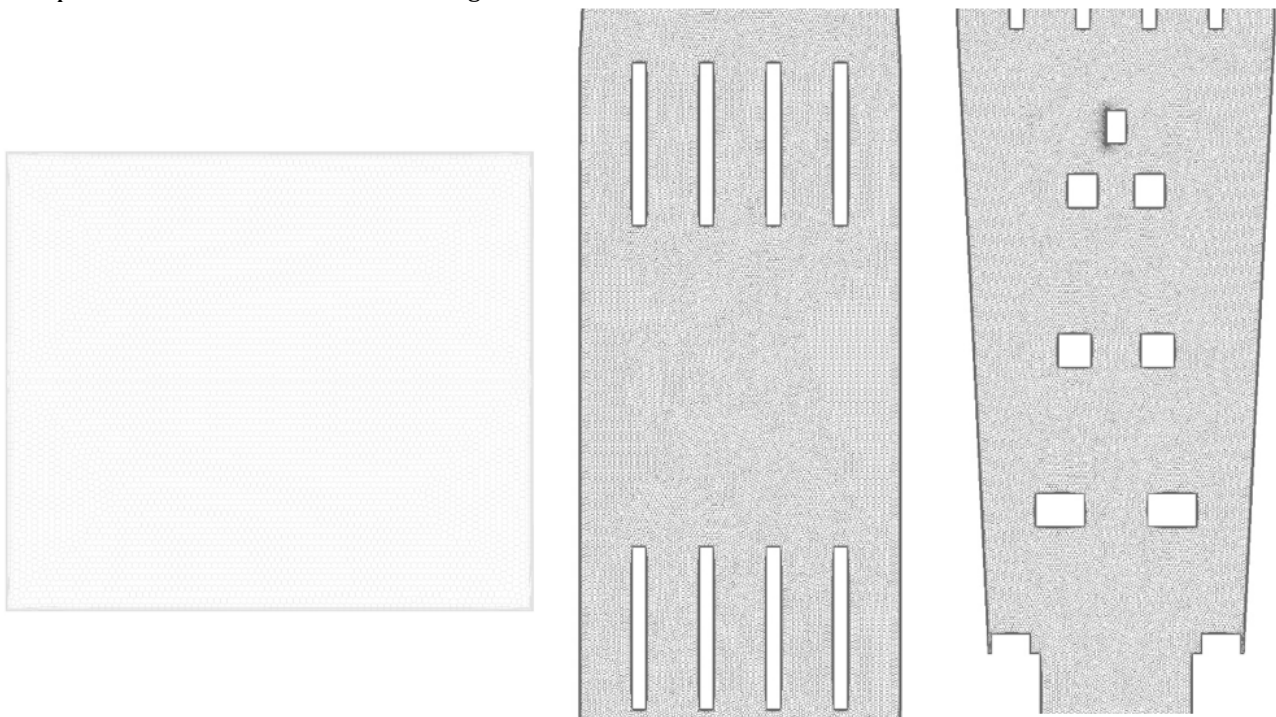
Figure 2-10: Computational mesh (Model 4)

A mesh sensitivity study was carried out with four different mesh sizes (0.94, 1.45, 2.42 and 7.13 M mesh elements). The convergence is obvious especially for results corresponding to the upper part of the test section (Figure 2-11).
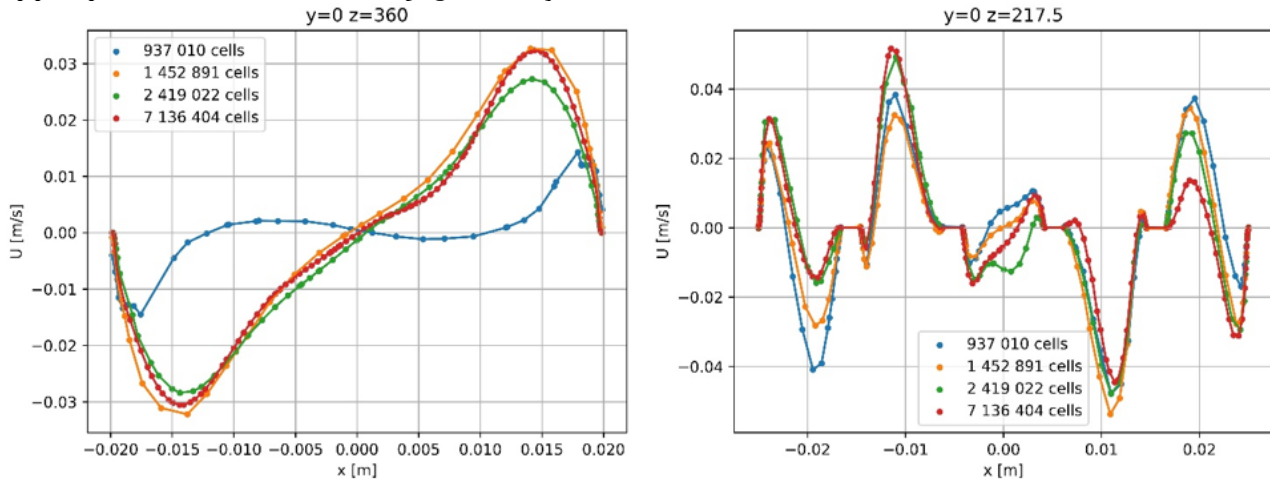
Figure 2-11: Mesh sensitivity study (Model 4)

K-omega SST model of turbulence was used, residuals level below 1e-3 were used after 1000 iterations. Contours of velocity are shown in Figure 2-12.
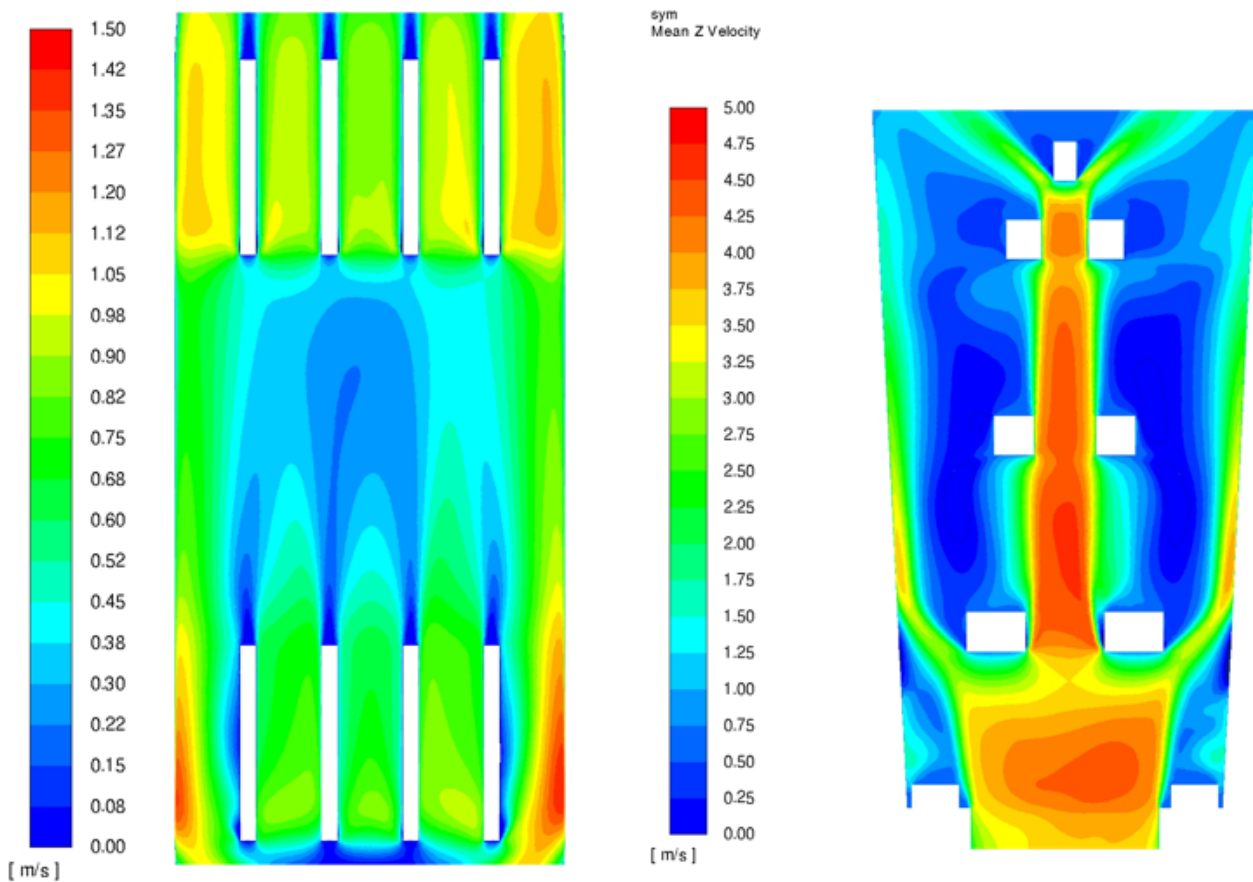
Figure 2-12: Contours of velocity (Model 4)

2.2.1.5 Model 5 – Fluent model of VUJE

A model using ANSYS Fluent 2019 R3 was prepared by VUJE. Combination of hexahedral and tetrahedral mesh with hexa core was created. The final mesh has 11.7 M mesh elements. Three

meshes were tested within the mesh sensitivity study. The coarse was meshed with mosaic mesh (polyhedral mesh with hexahedral core). Total number of cells 6 788 631. Improved mesh was split to tree parts (inlet, central and outlet). Simple geometrical parts (inlet, outlet) was meshed with hexahedral mesh in Gambit. Geometrically complicated central part was meshed in Fluent Meshing with tetrahedral mesh with hexahedral core. Total number of cells 11 447 634. The final mesh was developed from improved mesh. The final mesh was refined by adaption. Mesh was refined in places where the largest gradients of velocity, pressure, turbulence parameters and cell's volume occur. Also cells with high y+ where refined. The final mesh is shown in Figure 2-13.
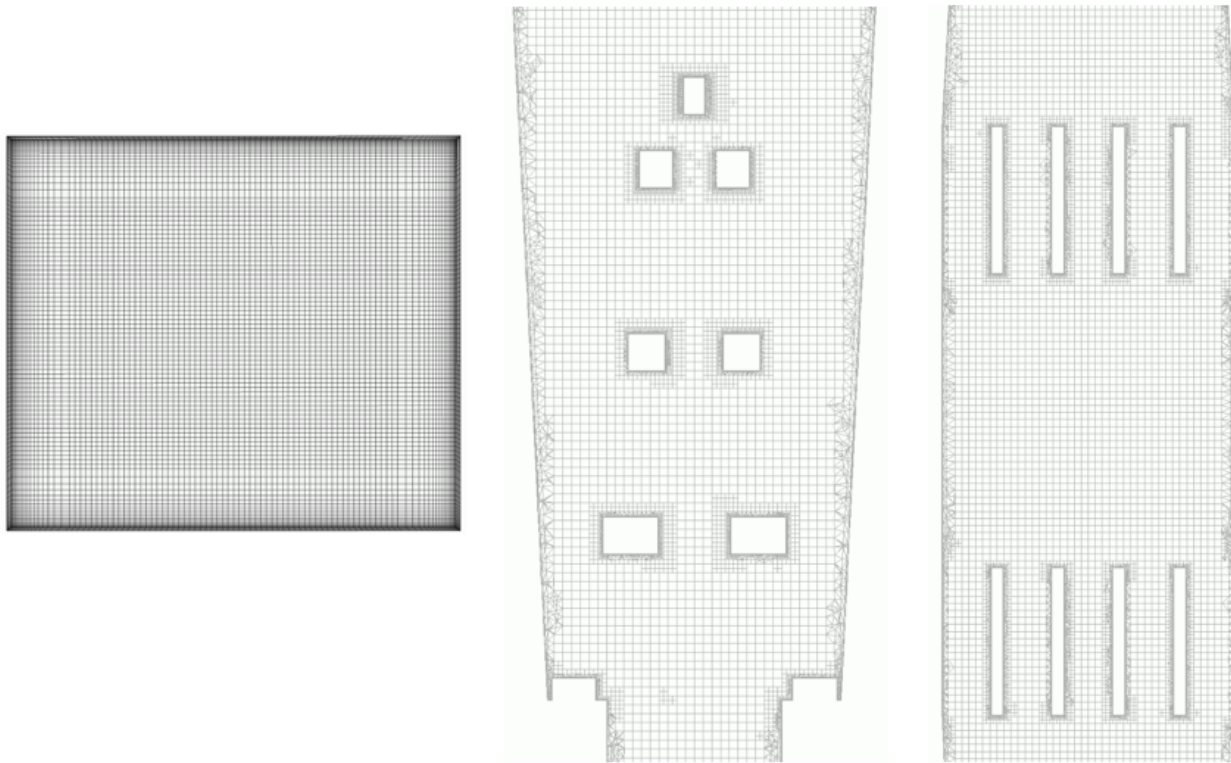
Figure 2-13: Computational mesh (Model 5)

RSM model with linear pressure strain and non-equilibrium wall functions was used. The spatial discretization of second order was set. The case was simulated for 1000 iterations until residuals were below 1e-3 (residual of continuity equation was 0.035). Contours of velocity are shown in Figure 2-14.
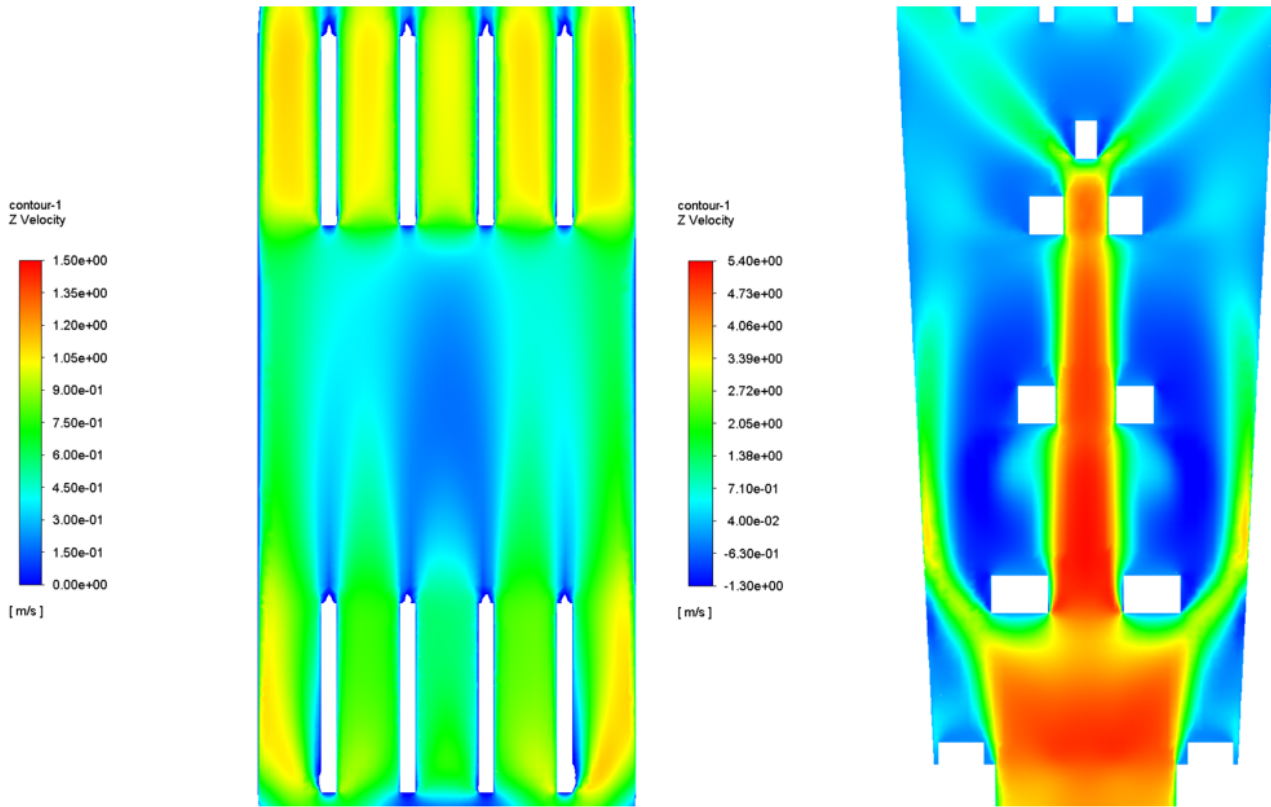
Figure 2-14: Contours of velocity (Model 5)

2.2.1.6 Model 6 – CFX model of BME

A model using ANSYS CFX R19.2 CFD code was prepared by BME. A combined computational mesh was prepared with hexahedral structural mesh in the straightener grids and outlet region. Tetrahedral mesh was made in the lower pipes and deflector cone region. The final mesh has 20.2 M mesh elements. The final mesh is shown in Figure 2-15.
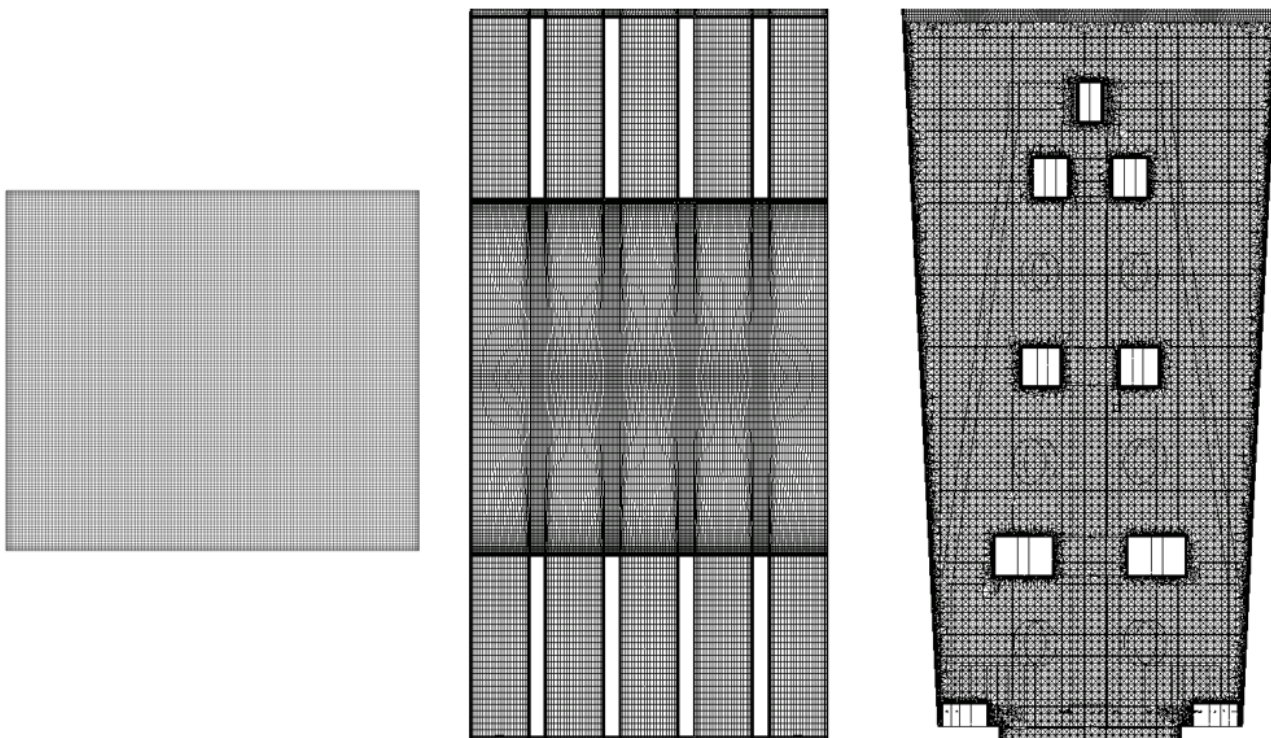

Figure 2-15: Computational mesh (Model 6)

The mesh sensitivity study was carried out with seven different grids with various number of the mesh elements in the region of the straightener grids. Average axial velocity on the outlet plane was compared. The results are shown in Figure 2-16. Mesh
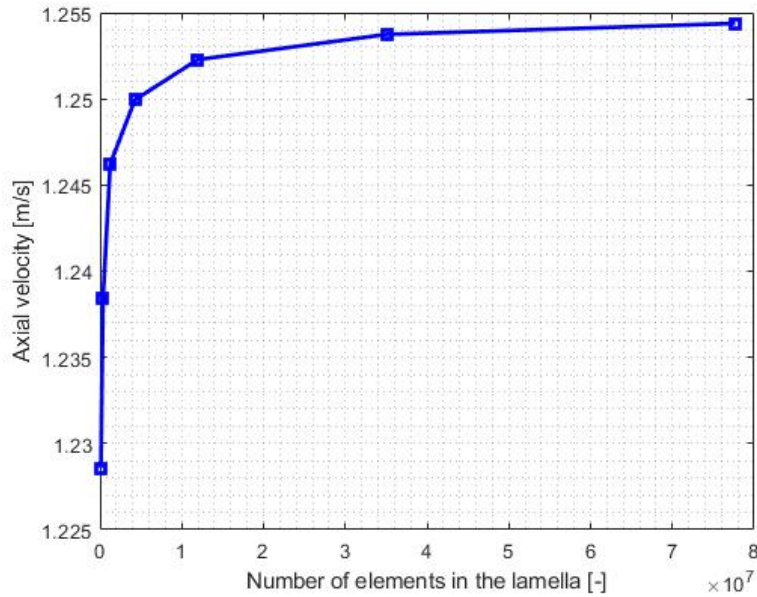
Figure 2-16: Mesh sensitivity study (Model 6)

The Shear Stress Transport model of turbulence was used with High Resolution Advection Scheme and Turbulence Numeric Fluid Timescale control with Auto Timescale and Conservative options. The simulation was run until the residuals were below 1e-4.
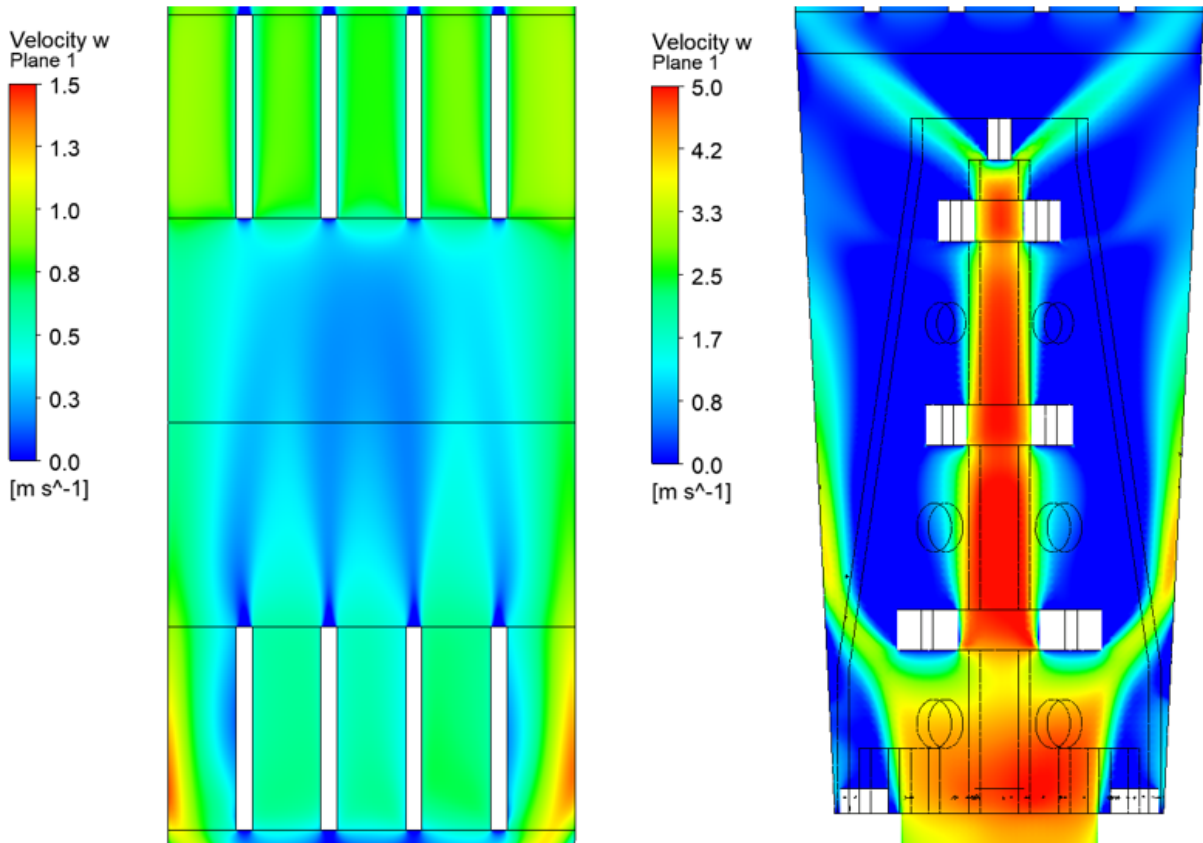
Figure 2-17: Contours of velocity (Model 6)

2.2.2 Comparison of models – flow straightener

In this section, the main characteristics of the CFD models is summarized. The numerical results are also compared code-to-code as well with the experimental data.

### 2.2.2.1 Comparison of the models characteristics

The main characteristics of the CFD models are summarized in Table 2-2.

Table 2-2: Main characteristics of the models

	Model 1	Model 2	Model 3	Model 4	Model 5	Model 6
Partner	CVR	CTU	CTU	UJV	VUJE	BME
CODE	OpenFOAM	StarCCM+	Fluent	Fluent	Fluent	CFX
Mesh type	Poly	Poly	Poly	Poly	Comb. Hex/Tet	Comb. Hex/Tet
Mesh size	0.38 M	3.3 M	0.28 M	7.1 M	11.7 M	20.2 M
Max. AR	229	NA	110	262	404	77
Min. OQ	0.06	NA	0.25	0.14	0.03	3.38e-5
Avg. Y+	12.6	19.4	3.7	0.94	1	3.22
Max. Y+	24	81	177	48	45.5	9.54
Turb. Model	k-epsilon realisable	k-epsilon st., all y+ WT	k-omega SST	k-omega SST	RSM	SST
Residuals	< 1e-4	< 1e-6 1000 iter.	< 2.3e-3	< 3.7e-4 1000 iter.	< 3.5e-2	< 1e-4
Marker for figures below	orange	purple	red	green	cyan	blue

2.2.2.2 Results comparison

The results on the individual lines corresponding to the PIV measurement (black continuous line) are depicted for all CFD models and compared with the experimental measurement. There are 18 measuring lines (9 in the inlet domain, 9 in the outlet domain) and two velocities (z-direction and x-direction) are measured, thus results are evaluated in 36 positions (Figure 2-18, Figure 2-19, Figure 2-20, Figure 2-21).
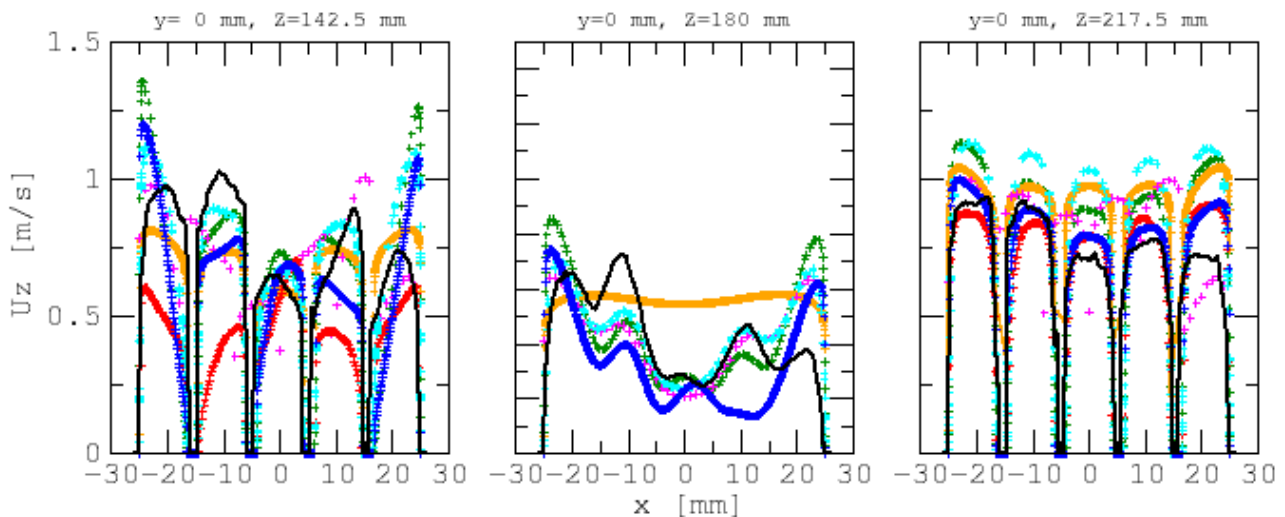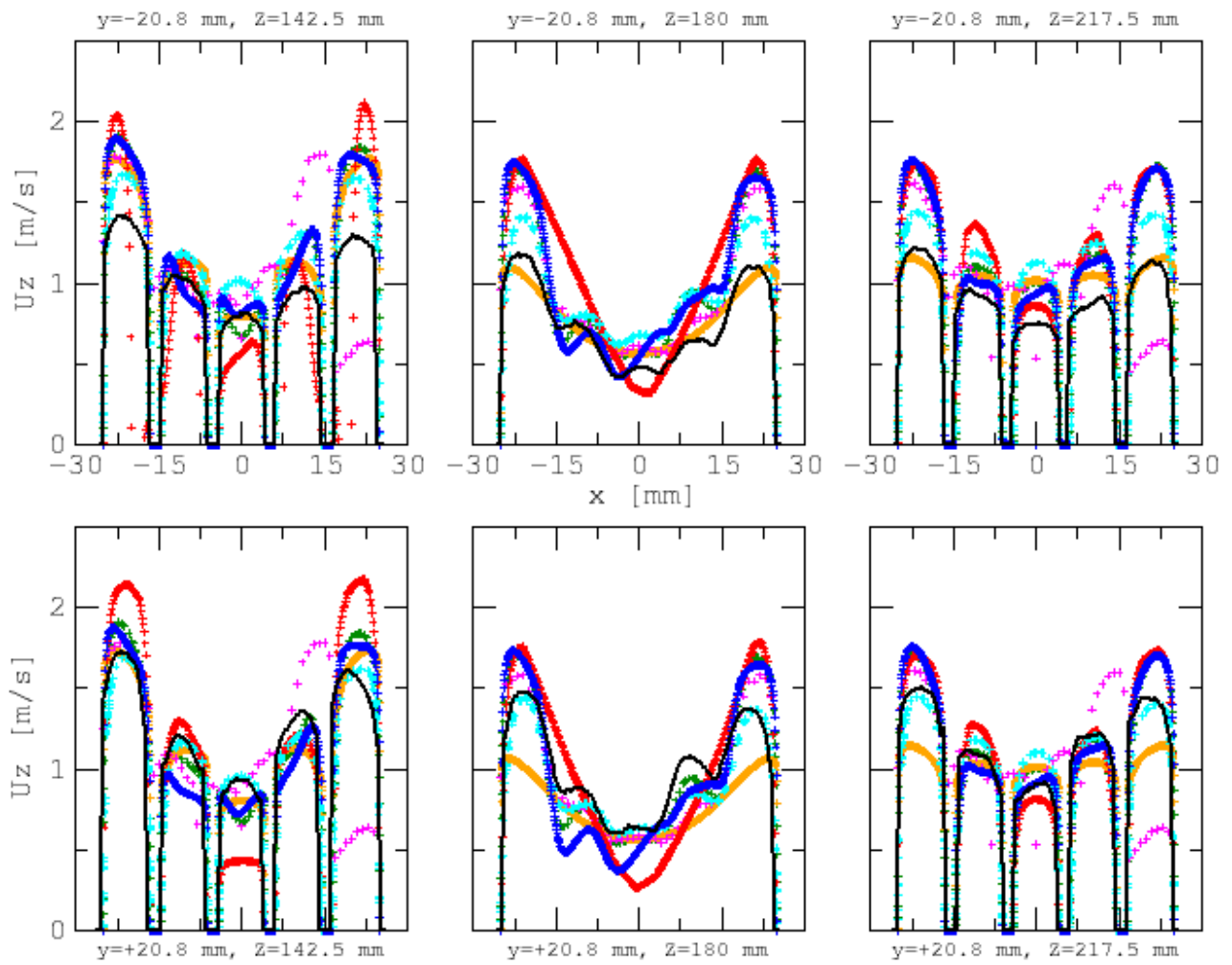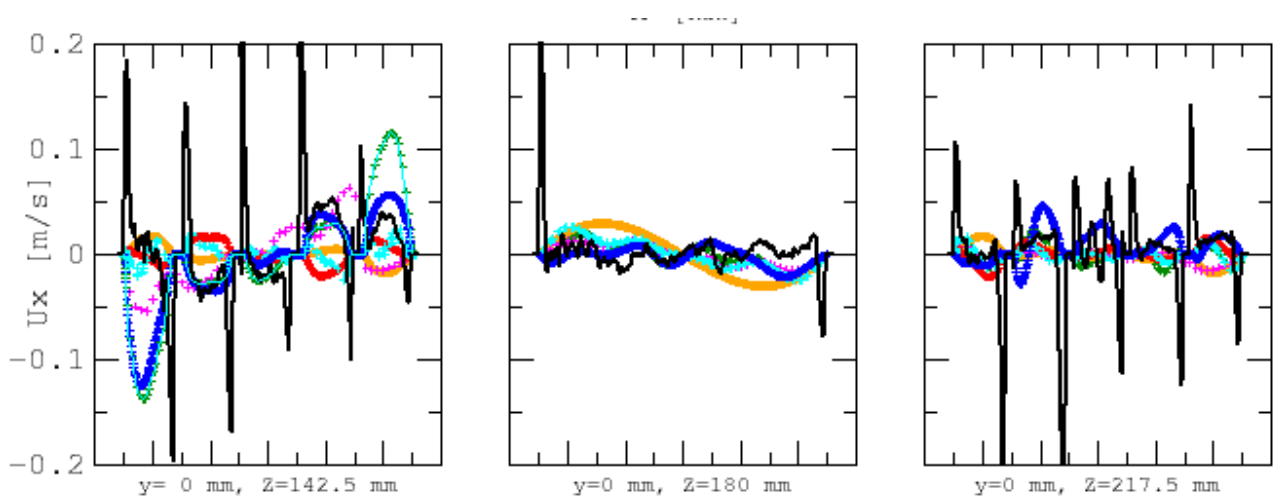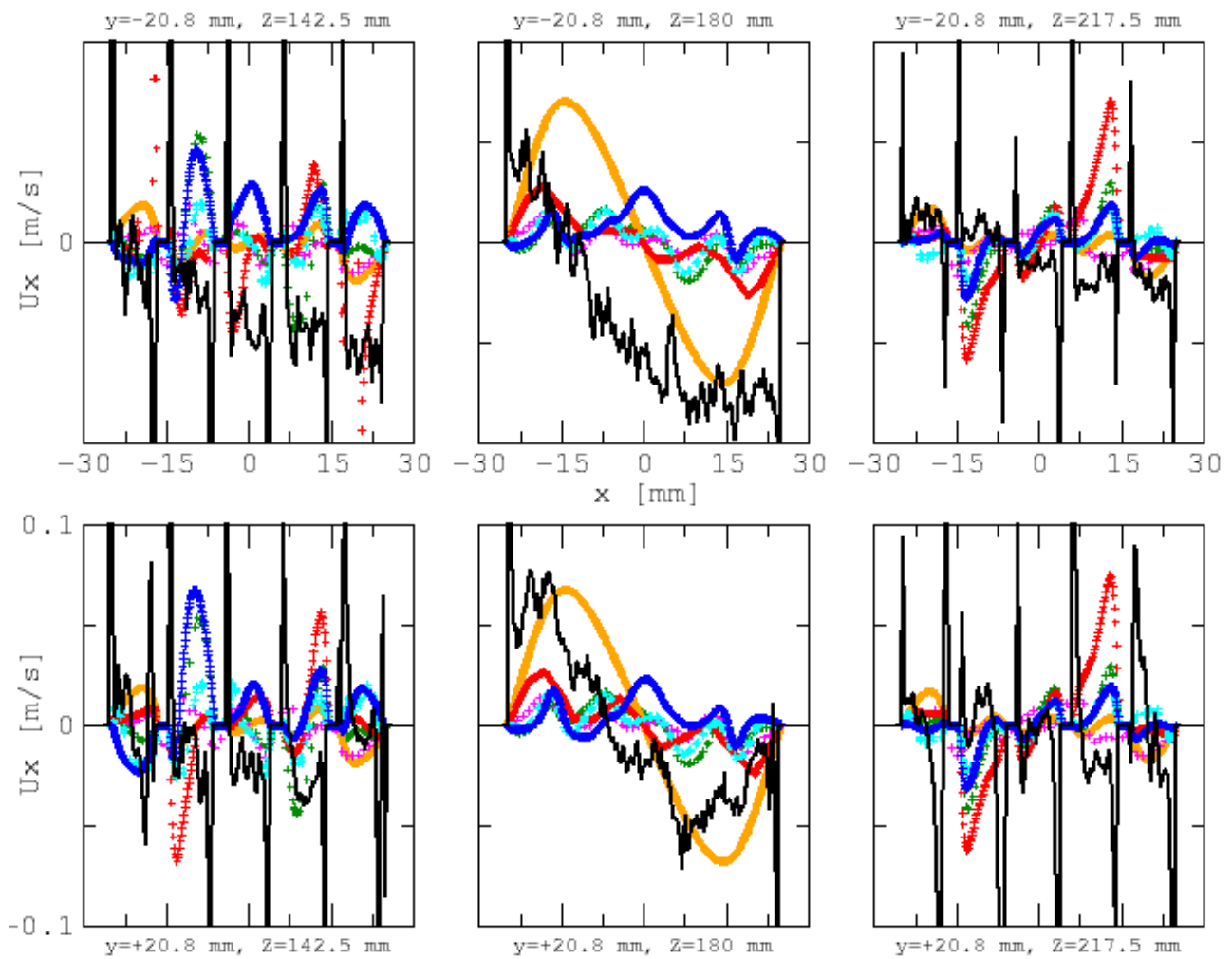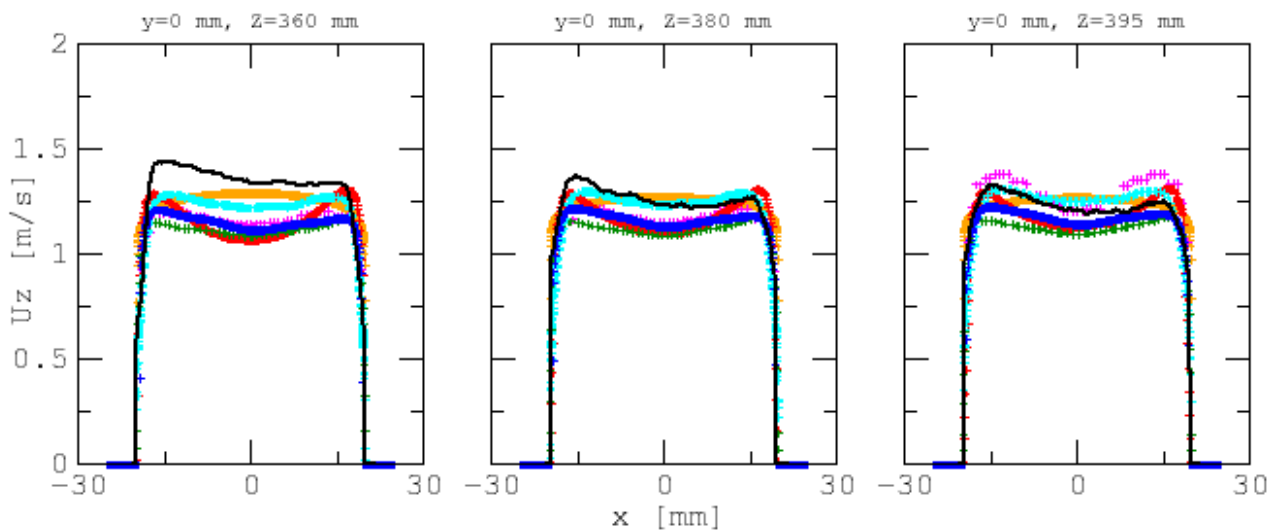
Figure 2-18: z velocity (inlet domain)

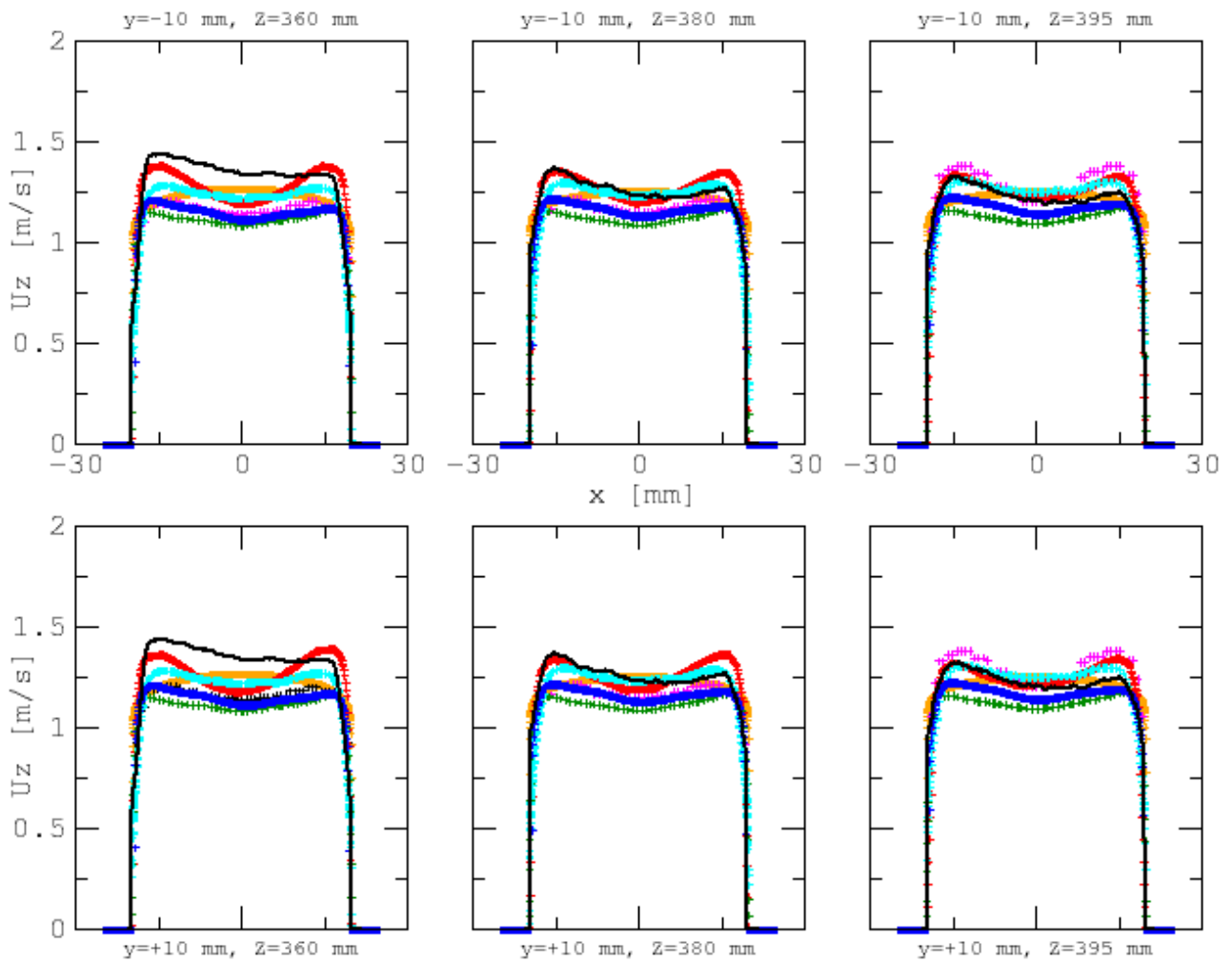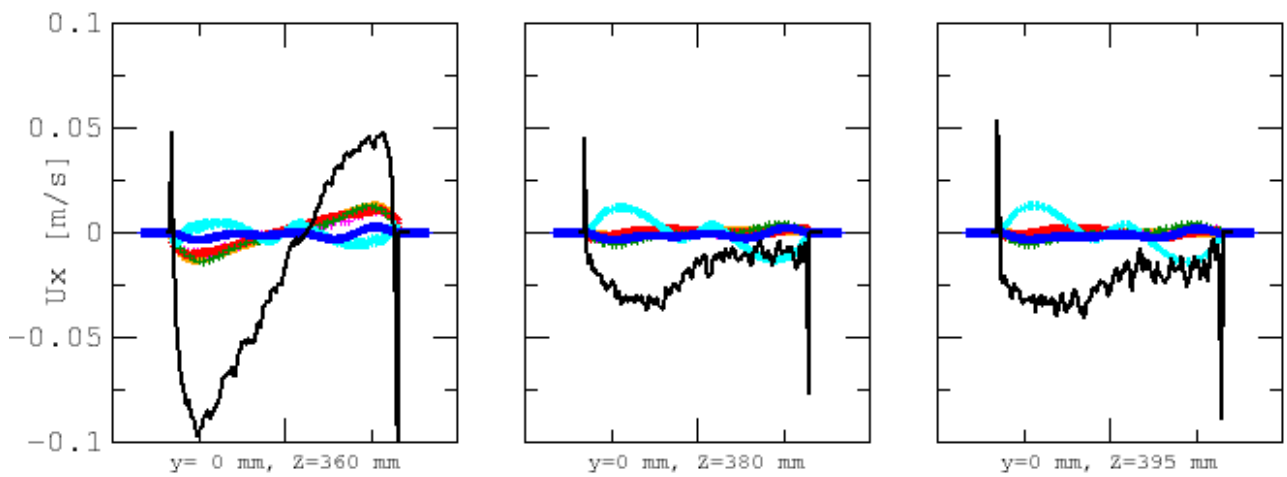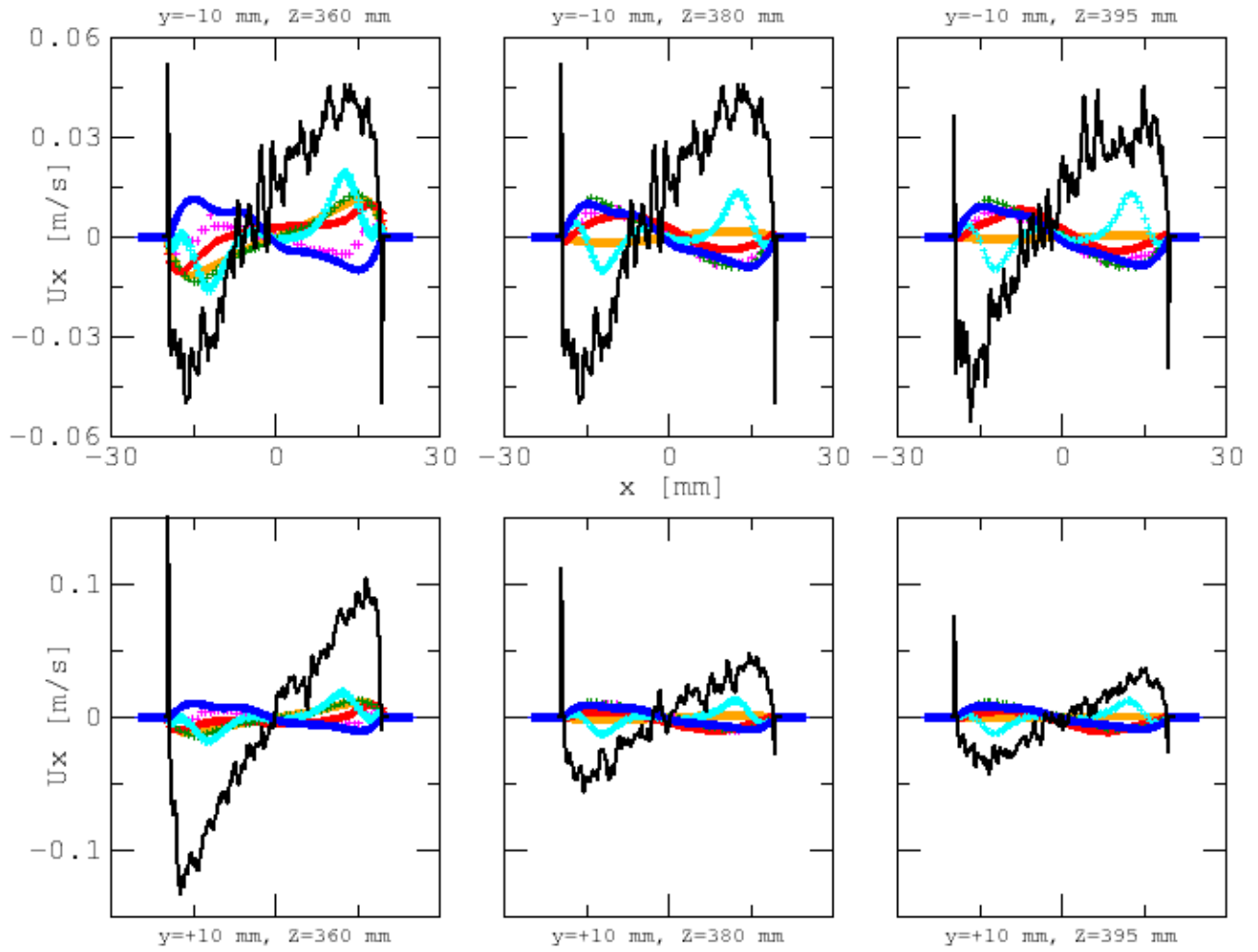**Figure 2-19: x velocity (inlet domain)**

Figure 2-20: z velocity (outlet domain)

Figure 2-21: x velocity (outlet domain)

For better clarity, selected graphs are presented in Figure 2-22 and Figure 2-23 in larger scale.
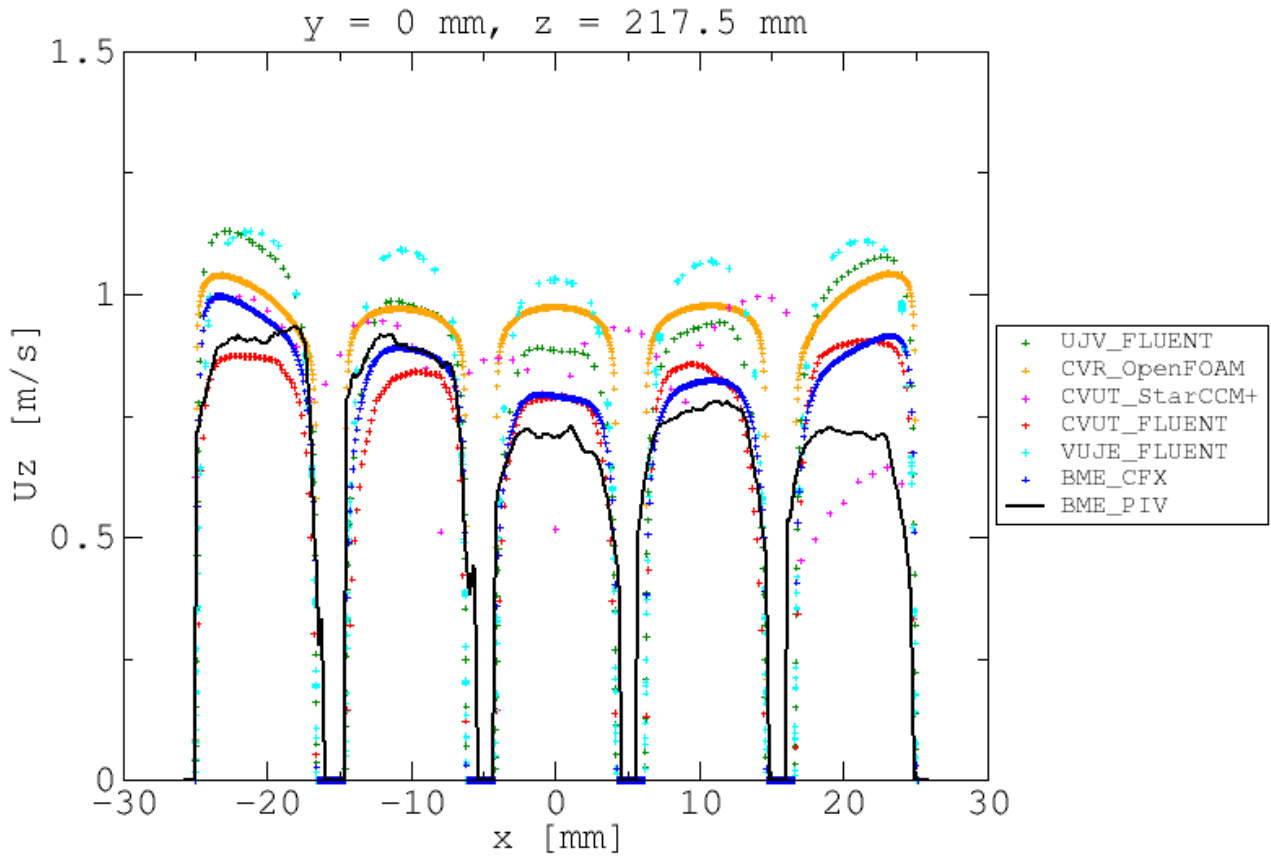
Figure 2-22: Uz, y = 0 mm, z = 217.5 mm

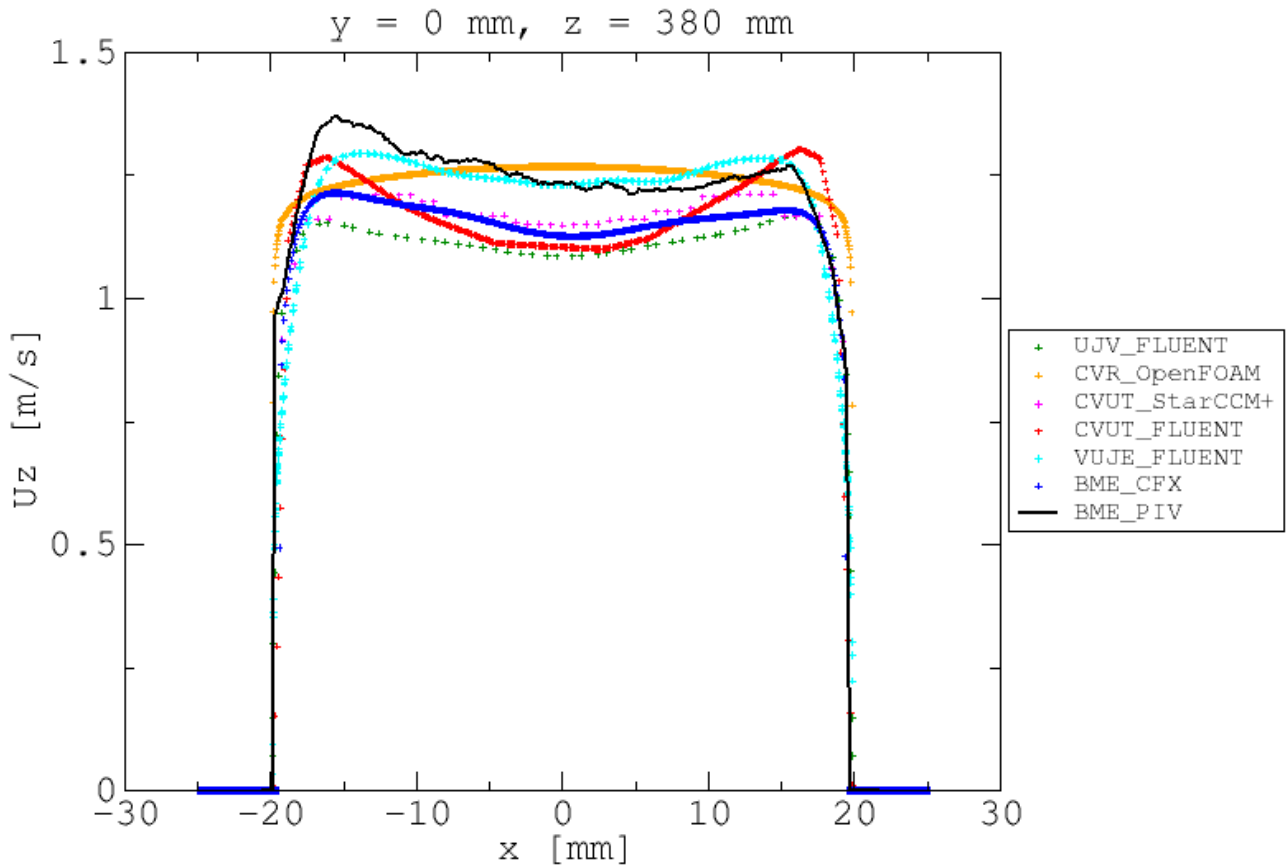**Figure 2-23: Uz, y = 0 mm, z = 380 mm**

2.2.3 Conclusions – flow straightener

The first part of the CFD benchmark was successfully completed, in which all participants were able to correctly describe the line-along profiles recorded by the measurements in the outlet domain. The aim of the current phase was to be able to obtain a sufficiently detailed inlet velocity distribution boundary condition for the full-length rod bundle models, to be found in the second phase. In the meantime, useful experience was gained by the participants.

Six models with completely different mesh structures and simulation approaches were created. Polyhedral, tetrahedral and hexagonal meshes were constructed, ranging from 0.28 M to 20.2 M elements. It can be said that differences of the model´s results are relatively low despite significant differences in the meshing and model´s setup.

A deeper understanding of the results is beyond the scope of this project, but we can see that, the complicated geometry of the lower part of the flow straightener challenged all models involved. Unfortunately, it is not possible to say with absolute certainty, which modelling technique produced the results that best approximate the measurements. There were positions where one model performed better and positions where another model performed better. Most models in the outlet region approximate the measured axial velocity profiles within a margin of error, which was the main purpose of this section. For the transversal velocity profiles, there are larger deviations, but in this case the relative uncertainty of the measured results is also much larger, due to the small absolute values of the velocities. It can be also said that the flow behavior might be affected by secondary flows that cannot be captured by RANS models that were used by all participants. However, modelling of the test section using more advanced model such LES would be too expensive and out of the scope of this activity. Perhaps in the future, in the framework of another research project, these discrepancies can be resolved.

2.3 CFD Benchmark – Part 2

The second part of the CFD benchmark followed the first part. The data for the part 2 were collected from the same PIROUETTE facility of BME. The subject of interest is "rod bundle" section, that is located upstream the flow straightener. The test section was designed to investigate the emerging flow conditions in various nuclear fuel assembly rod bundles. The measurement method is based on Particle Image Velocimetry (PIV) with Matching of Index of Refractory (MIR) method. Despite the coolant will be helium in ALLEGRO, the working fluid is water in the measurements, but both fluids are in the same Reynolds-number range.

2.3.1 Test description

The test section is designed to includes the measurement section, the associated confuser, and diffuser connectors. These parts are easily interchangeable to perform measurements for different nuclear reactor rod bundles. The cross-section of the measuring channel is a little bigger than the ALLEGRO, but on the basis of the similarity theory, the hydraulic parameters are exactly the same. The 1-meter-long test bundle is made of FEP (Fluorinated Ethylene Propylene) to meet the refractory index of water. The FEP polymer has a refractory index of 1.33 which is nearly the same as of the working fluid (water). The outer and inner diameter of the rods are 10/6 mm, and the inside of the rods was filled with ultrafiltrated water. The diameter of the ALLEGRO refractory fuel rod is 9.1 mm. Therefore, the upscaling ratio of the channel was 10/9.1=1.0989. The rods are connected with pins into the first and fourth spacer grids, and the spacer grids are connected to the wall of the channel with groove fitting.
The distance between the spacers is 296 mm in axial direction. The spacers were designed according to the ALLEGRO GFR assembly spacers, with slight modifications to fit the

measurement requirements. The wall thickness of the spacers is 0.8 mm. The grids were made by a high resolution 3D printing method (SLA) with special rigid composite resin (see in Figure 2-24).
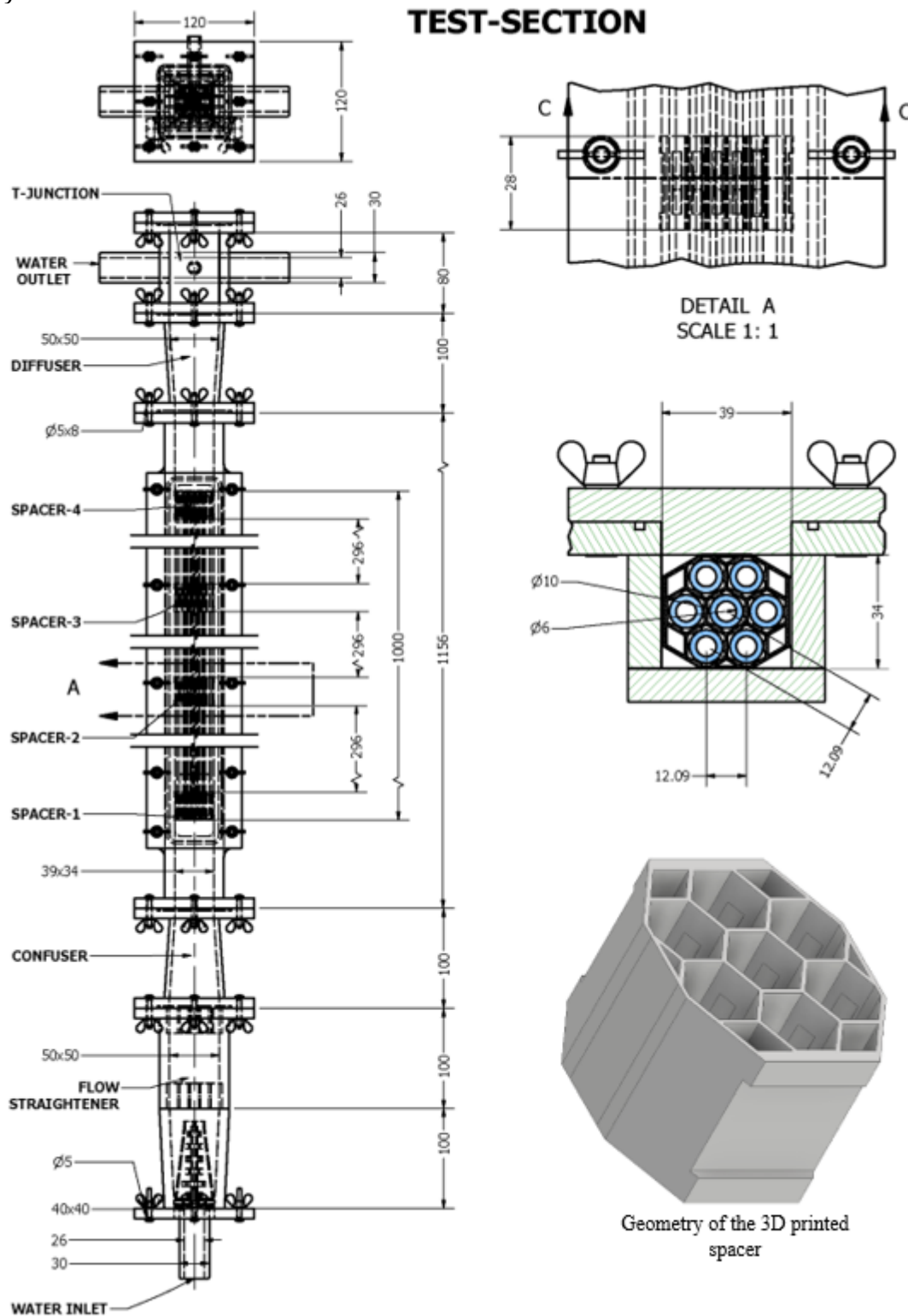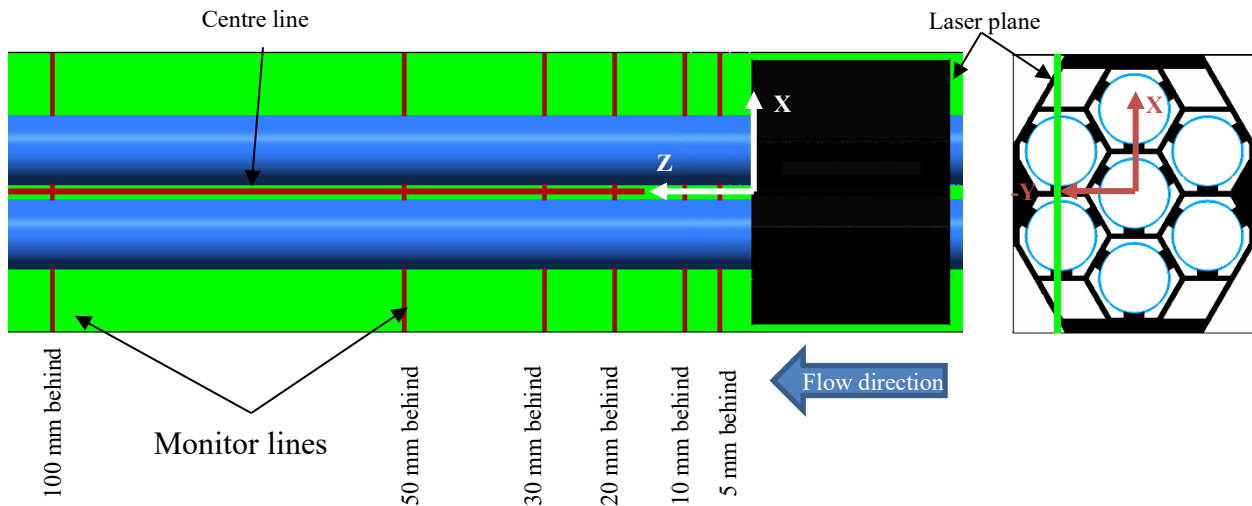

Figure 2-24: Test section geometry

The data were collected using the PIV method, similarly as in the previous case. 7 lines and two different directions were observer, thus flow velocity in 14 linear positions was captured and used for comparison with the numerical models. Layout of the measuring positions is shown in Figure 2-25.

Figure 2-25: Measuring positions in the rod bundle

The input data are coming from measurements of PIROUETTE test facility. The volumetric flow rate is set to 6 m³/h and is maintained under control thanks to the ultrasonic flow meters. The temperature of the water is 30°C and is maintained constant thanks to a heat exchanger, where at the second side there is mains tap water. Thanks to the heat exchanger, the model can be considered adiabatic in all its parts. The pressure of the water can be considered to be atmospheric at the outlet since the water is discharged in an open water tank. The properties of the water, such as density and dynamic viscosity, have to be computed considering the previously mentioned conditions, and the mass flow rate can be calculated considering these properties. The walls are considered smooth. The input data are summarized in Table 2-3.

Table 2-3: Input data

|	Volumetric flow rate [m³/h]	Temperature [°C]	Pressure [bar]	Density [kg/m³]	Dynamic viscosity [Pas]	Mass flow rate [kg/s]
Input value	6	30	1	995.6515	7.9735 E-4	1.6594

2.3.2 Models description

Four models were carried out for this part of the benchmark. The main properties will be described in this section.

2.3.2.1 *CFX model of BME*

CFX code was used by BME. The inlet boundary condition is given as a mass flow rate of 6 m3/h (1.6594 kg/s). The relative pressure at the outlet is defined as 0 Pa. The channel walls, spacers, rods, and straightening elements were assumed to be smooth walls (Smooth Wall). The velocity on the walls is zero (No Slip Wall). Flow is adiabatic and water properties were determined at 30 °C and atmospheric pressure. All the calculations were carried out using ANSYS CFX 19.2 code.

A mesh sensitivity study was carried out to select a proper mesh for this case. Mesh structure on the rod bundle cross-section is shown in .
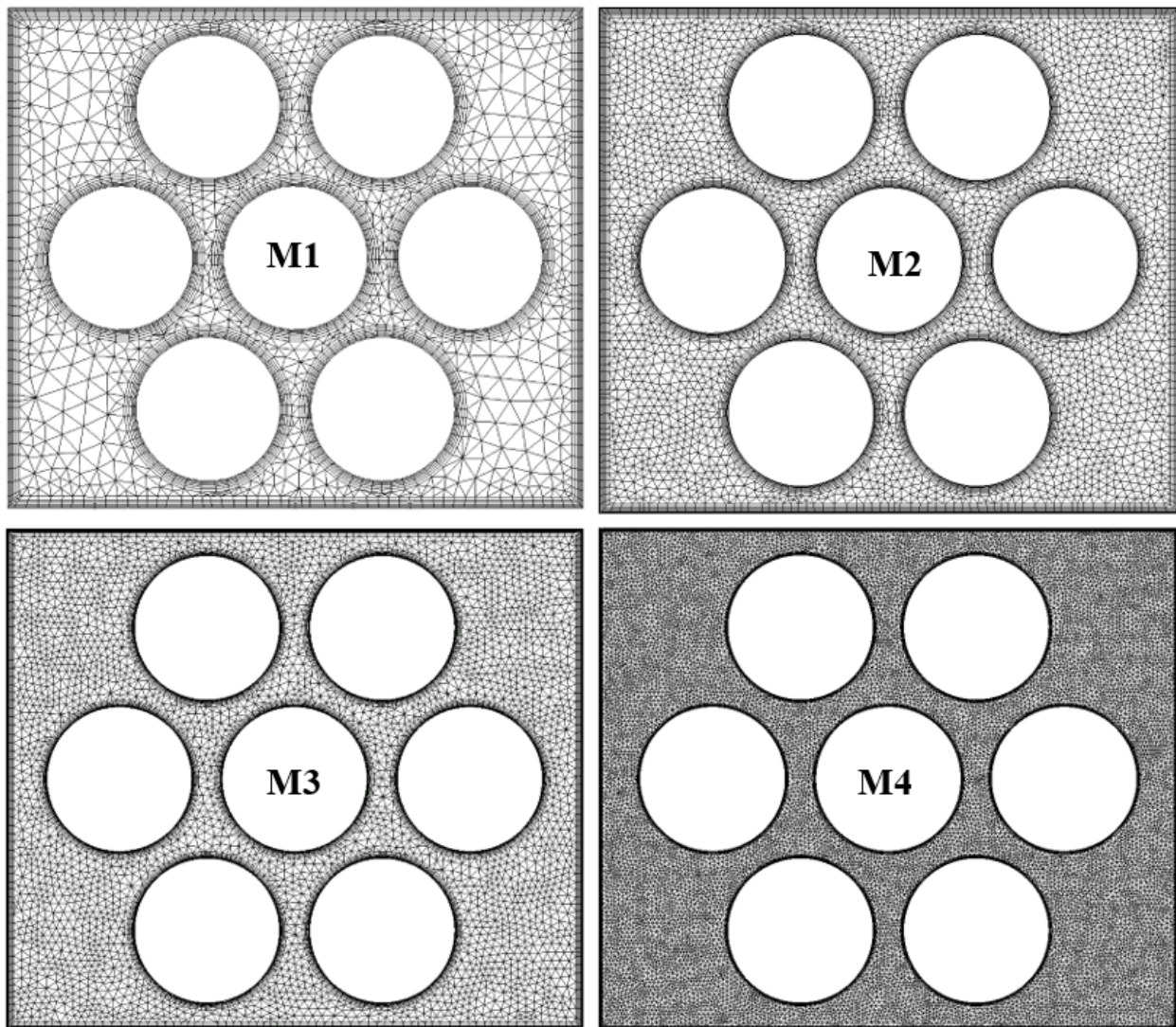
Figure 2-26: Meshes considered in the BME model

The parameters of all four meshes are shown in Table 2-4, velocity profile comparison is shown in Figure 2-27.
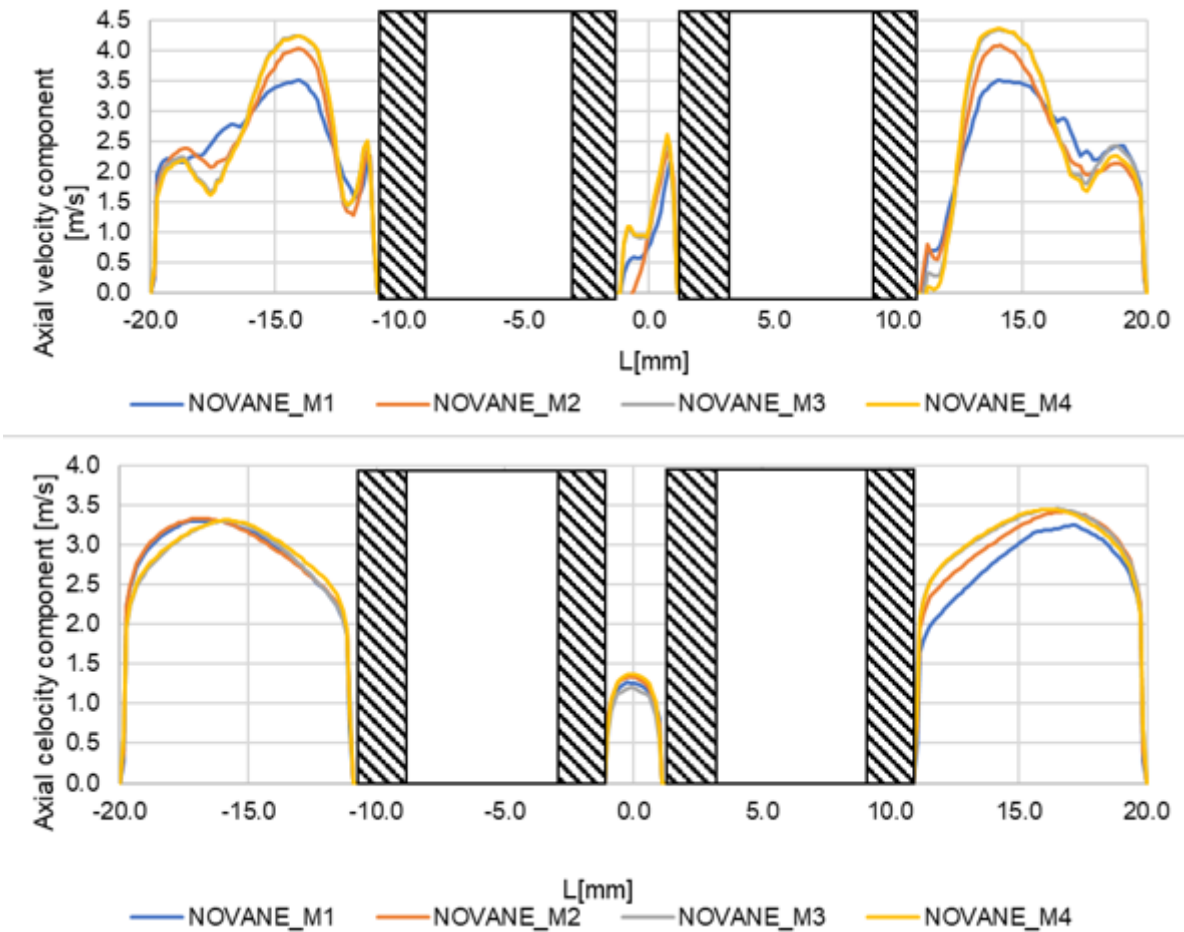
Figure 2-27: Mesh sensitivity study – velocity comparison

Table 2-4: Mesh sensitivity study

	M1	M2	M3	M4
Number of elements in the rod bundle test section	6 914 604	17 999 798	35 74 973	103 436 982
Maximal element diameter [mm]	3	2	0,7	0,5
Properties of the mesh near the walls				
High of the first layer [mm]	0,1	0,08	0,02	0,01
Number of layers [-]	5	6	8	8
Height ratio [-]	1,2	1,2	1,3	1,3
Y+ on rod wall [-]	9,91	3,57	2,69	1,37
Y+ on spacer wall [-]	16,47	10,6	4,06	2,56

Based on the line along profile comparisons, it can be concluded that the M1 and M2 meshes have different results than the finer meshes. Thus the M3 mesh was chosen for further investigations, which also avoids the excessive computational demands of the M4 mesh.

2.3.2.2 FLUENT Model of UJV

A polyhedral mesh with almost 20 M mesh elements was prepared for the FLUENT model prepared by cooperation of UJV and CTU. Standard k-epsilon model of turbulence was used. The minimum orthogonal quality of the mesh is 0.15, the maximum aspect ratio is 210. The inlet velocity profile was imported from the flow straightener model.
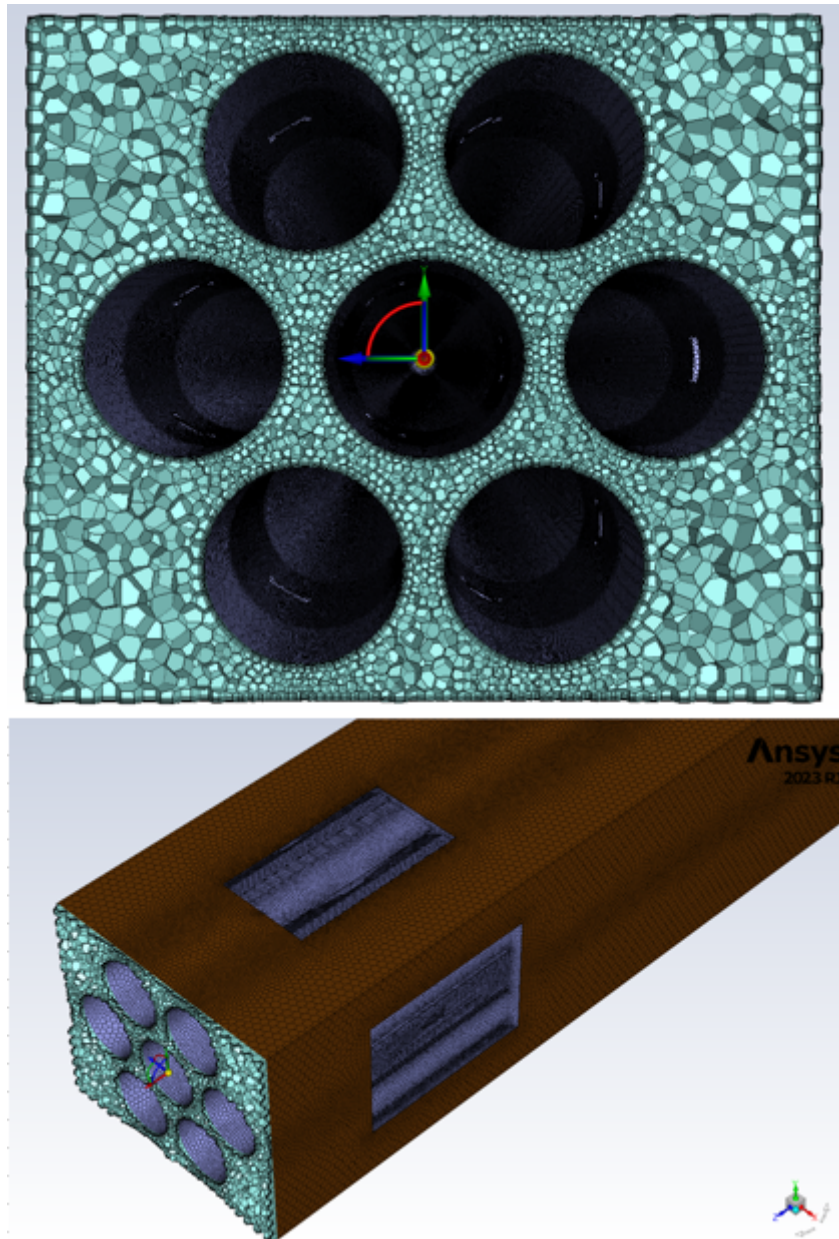
Figure 2-28: Mesh of the UJV model

2.3.2.3 FLUENT model of VUJE

An ANSYS FLUENT model was prepared by VUJE. Combined polyhedral and hexahedral mesh was prepared with 9.2 M mesh elements. Maximum aspect ratio in the mesh is 128, minimum orthogonal quality is 0.25. K-omega SST model of turbulence was used.
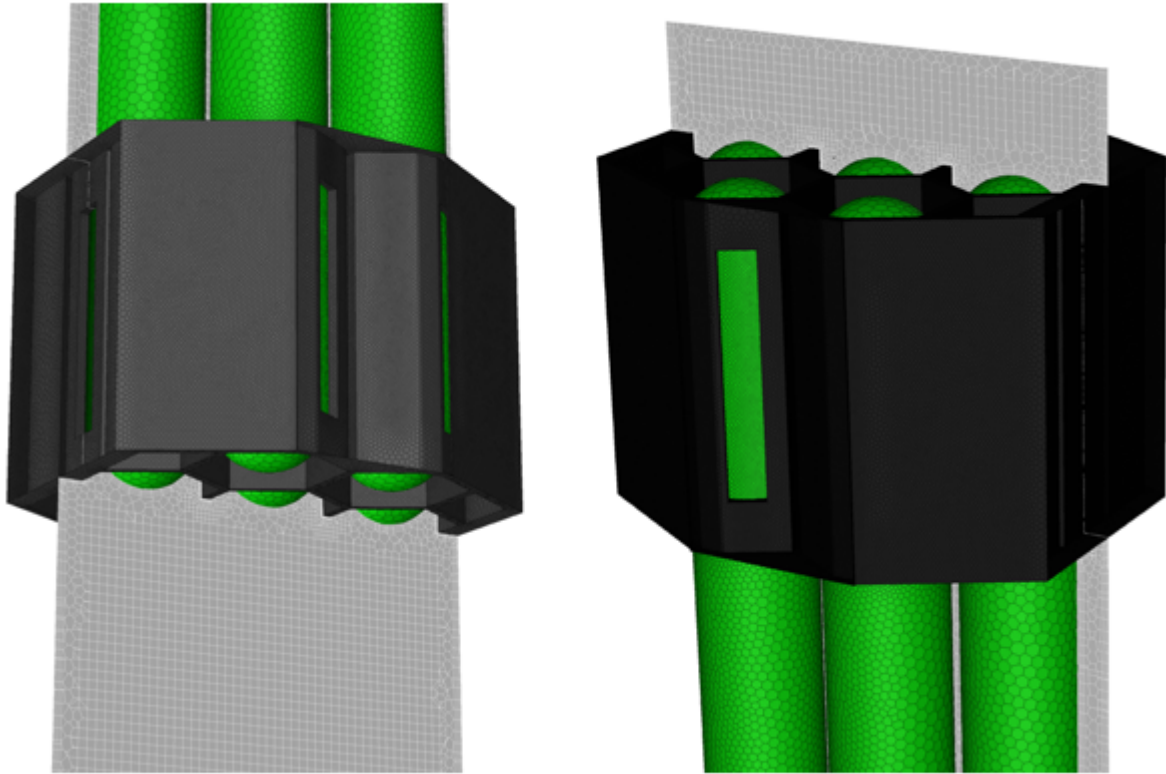
Figure 2-29: Mesh of the rod bundle of VUJE model

2.3.2.4 OpenFOAM Model of CVR

Polyhedral computational mesh was prepared using ANSYS tool, but OpenFOAM was used as a solver. K-omega SST model of turbulence was used. The computational mesh has approx. 5.5 M elements, avg. y+ 2.6 and max. y+ 11.3. Constant velocity is applied on the inlet face. The computational mesh is shown in **Figure 2-30**.
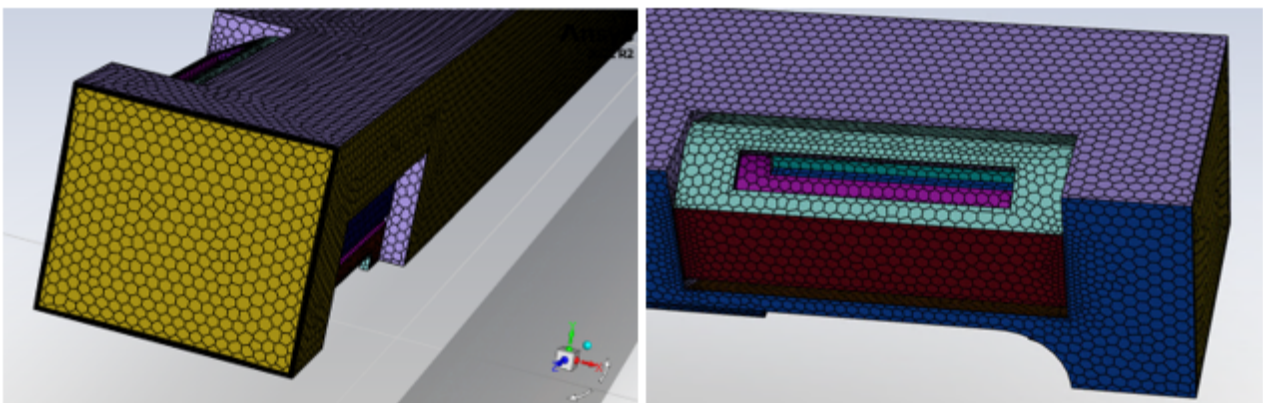

Figure 2-30: Mesh of the rod bundle of CVR model

2.3.3 Data evaluation

In this section, the numerical data from all models were compared with the experimental results. For all measuring positions, graphs with spatial distribution of velocity at observed positions were generated. Corresponding positions are shown in Figure 2-25. The axial velocity profiles are shown in Figure 2-31, the transversal velocities are in Figure 2-32.
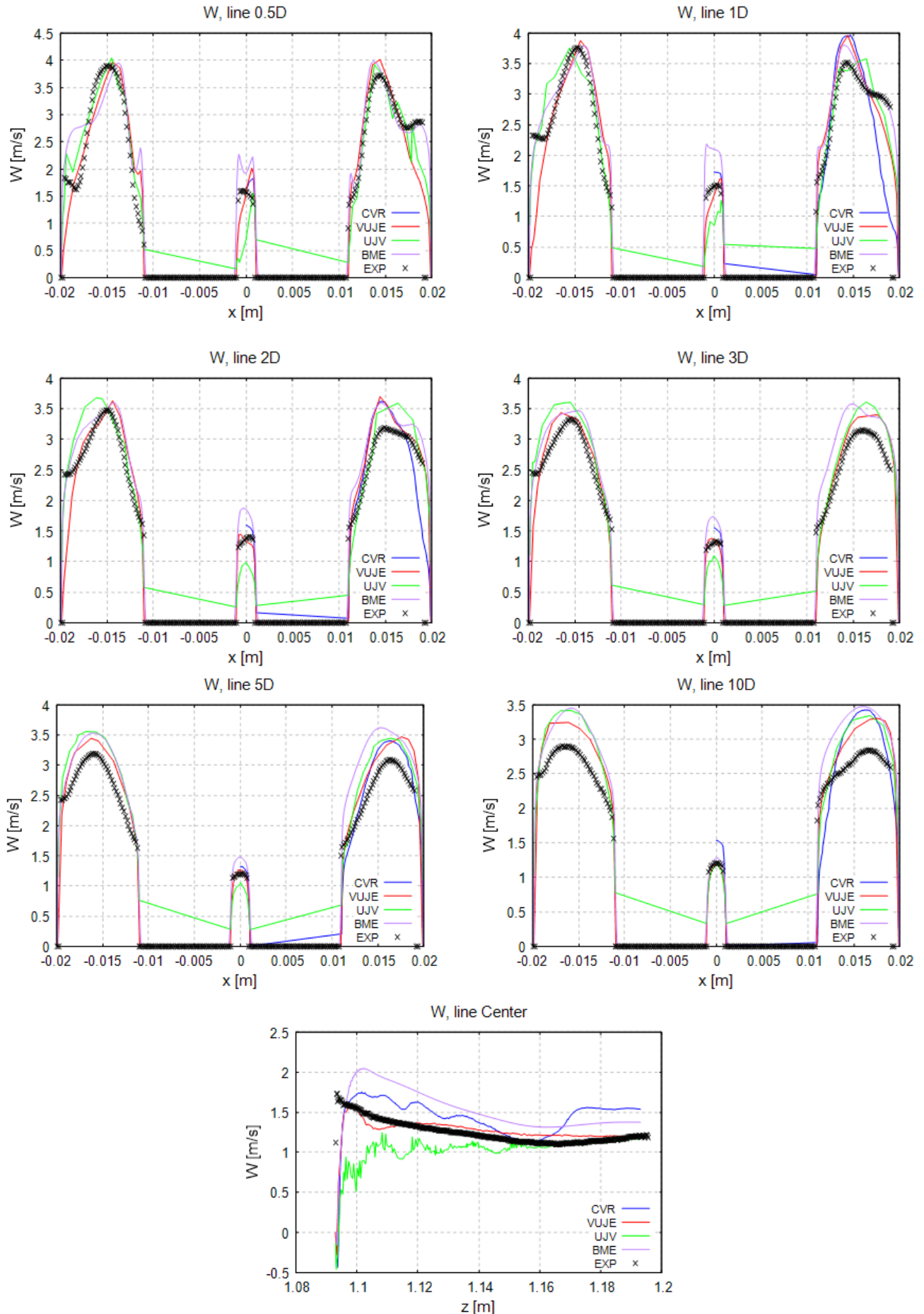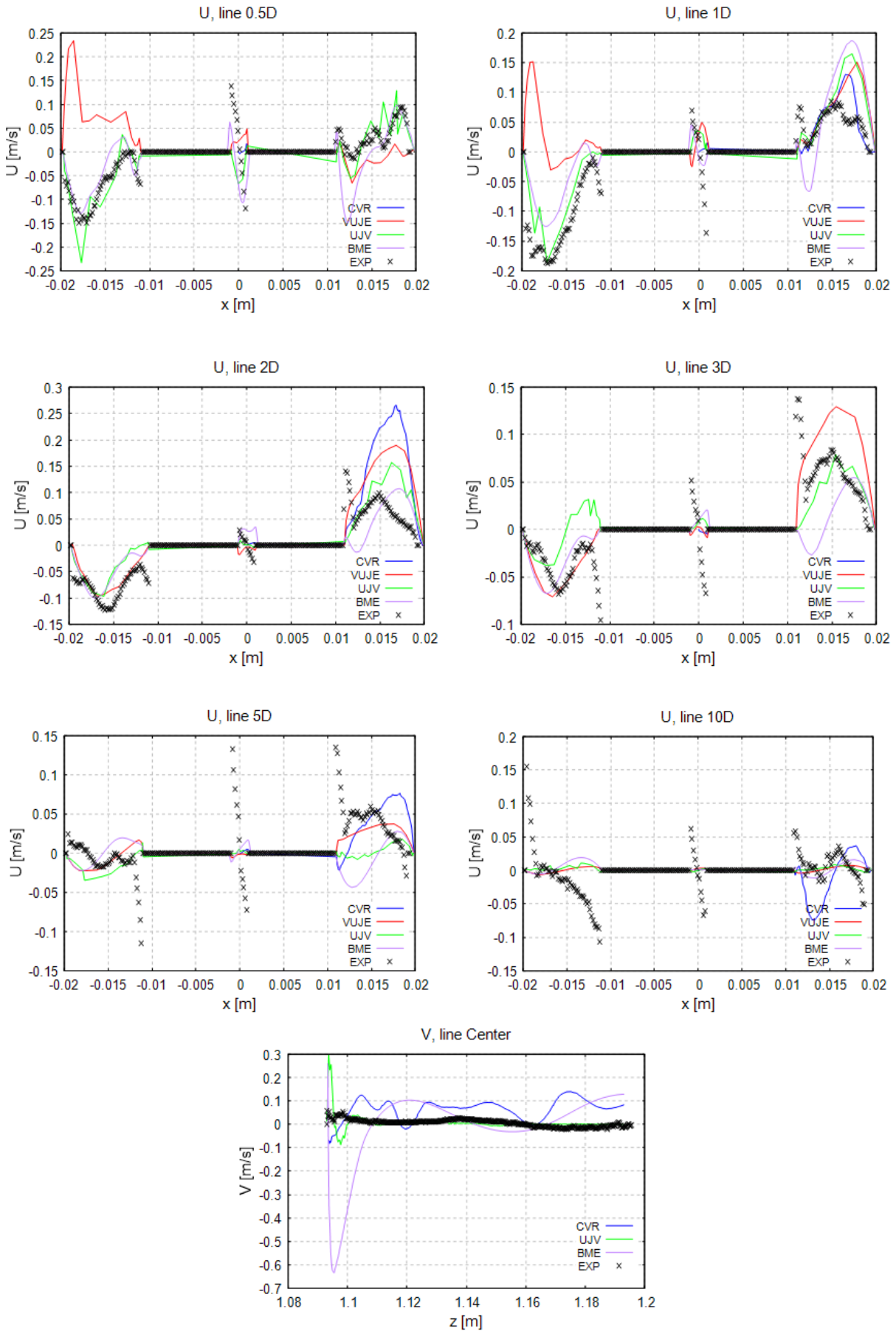
Figure 2-31: Axial velocity at monitoring lines

Figure 2-32: Transversal velocity profile at monitoring lines

2.3.4 Conclusions – rod bundle

The second part of the CFD benchmark focused on the flow through rod bundle geometry under GFR fuel-relevant conditions. Velocity profiles obtained using the PIV method at selected positions in both axial and transversal directions were compared with numerical data from four CFD models. Two models were prepared using ANSYS FLUENT, one using ANSYS CFX, and one with OpenFOAM. Despite the educational nature of the activity, significant effort was dedicated to preparing all models to ensure high quality. The results from all models are comparable and show good agreement with the experimental data, particularly regarding axial velocity profiles. However, higher discrepancies were observed when comparing the transversal data. This may be attributed to the limited capabilities of the RANS models used by all participants. The use of advanced models such as LES, however, was beyond the scope of this activity. Overall, the outcomes meet and likely even surpass the expected objectives of the SafeG project WP5.

REFERENCES

[1]   RELAP5-3D© Code Manual. RELAP5-3D© Code Development Team, Idaho National Laboratory, rev. 2.4. June 2005.

[2]   Apros development team, HOMOGENEOUS MODEL OF APROS, VTT Technical Research Centre of Finland Ltd. Espoo, 2015.

[3]   A. Zukauskas: Heat transfer from tubes in crossflow, vol. 8 of Advances in Heat Transfer, Elsevier, 1972, pp. 93 – 160.

[4]   Joona Leskinen: Constitutive Equations for Helically Coiled Tubes, Apros user-manual, VTT Technical Research Centre of Finland, Espoo, 2020.

[5]   Tomáš Melichar, Jan Šefl, Daniel Kříž: Definition of the Thermal-Hydraulic Benchmark, DELIVERABLE D5.3, SafeG project No. 945 041, Centrum výzkumu Řež, 2023.

[6]   Miriama Lacková, Boris Kvizda: S-Allegro RELAP5-3D model Engineering handbook, SafeG project No. 945 041, VUJE, a.s. Trnava, Slovakia, 2023.

[7]   A. Petruzzi, F. D'Auria: Thermal-Hydraulic System Codes in Nulcear Reactor Safety and Qualification Procedures, UNIPI, Science and Technology of Nuclear Installations Volume 2008, Article ID 460795, 16 pages.

[8]   ASME (1998) 'Performance Test Code on Compressors and Exhausters: An American National Standard'. New York: ASME.

[9]   VDI (2010) VDI Heat Atlas. Berlin, Heidelberg: Springer Berlin Heidelberg. Available at: https://doi.org/10.1007/978-3-540-77877-6.

[10]   WMU, without date: Shell-and-Tube Heat Exchangers [online] [27.03.2024] Dostupné z: https://pdf4pro.com/amp/download?data_id=6e6fa8&slug=5-1-shell-and-tube-heat-exchangers-homepages-at-wmu

[11]   XRG Simulation GmbH (2022) 'ClaRaPlus'. Hamburg: XRG Simulation GmbH.

[12]   Modelica® Language specifiacation. Modelica Association. Version 3.6, March 9, 2023. Available at: https://specification.modelica.org/maint/3.6/MLS.html

[13]   Bc. Tomáš Křivský, Termohydraulický model smyčky S-Allegro, Thesis, ČESKÉ VYSOKÉ UČENÍ TECHNICKÉ V PRAZE, Fakulta strojní, Ústav procesní a zpracovatelské techniky, Prague, 2020.